

**Orientation-Independent Optically Pumped Magnetometers:  
Total Field Sensors Without Dead Zones**



FINAL REPORT

Prepared Under  
Contract No. N00014-93-C-0272

For

The Office of Naval Research  
800 North Quincy Street  
Arlington, Virginia 22217-5660

April 28, 1994

**DISTRIBUTION STATEMENT A**  
Approved for public release  
Distribution Unlimited

19950925 020



Quantum Magnetics, Inc.  
11578 Sorrento Valley Road  
San Diego, CA 92121

~~THIS COPY IS UNCLASSIFIED~~

~~04 5 02 081~~

## Table of Contents

EXECUTIVE SUMMARY .....	ii
1 INTRODUCTION .....	1
2 TECHNICAL BACKGROUND .....	4
2.1 Operating Principles of Existing OPMs .....	4
2.2 The Free-Precession Magnetic Detector (FPMD) .....	5
2.3 The Orientation-Independent Potassium Magnetometer .....	6
3 SUMMARY OF OBJECTIVES AND RESULTS FOR PHASE I .....	9
4 TASK 1: MODIFY EXISTING POTASSIUM MAGNETOMETER .....	11
5 TASK 2: DEMONSTRATE ORIENTATION-INDEPENDENT MEASURE- MENT PROCESS .....	15
5.1 Preliminary Experiments on Optical Pumping .....	15
5.2 Optical Pumping with Field Cycling .....	16
5.3 Refinements for Future Work .....	25
6 TASK 3: DESIGN INSTRUMENT FOR PHASE II .....	27
6.1 Analysis of Performance and Design Issues .....	28
6.1.1 Optical Pumping Technique: Tradeoffs of Sensitivity, Sensor Size, and Gradient Tolerance .....	28
6.1.1.1 Basic Sensitivity Model .....	29
6.1.1.2 Key Parameters and Fundamental Performance Tradeoffs .....	29
6.1.1.3 Sensitivity Estimates: Sensor Size and Optical Pumping Tech- nique .....	33
6.1.1.4 Sensitivity-Size Tradeoff: Compact Unit with Moderate Sensi- tivity .....	35
6.1.1.5 Sensitivity-Size Tradeoff: Maximum-Sensitivity Configuration ....	37
6.1.2 Tolerance for Magnetic-Field Gradients .....	38
6.1.3 Drifts and Heading Errors .....	40
6.1.4 Motional Noise Due to Gyroscopic Effects .....	43
6.1.5 Pumping with Laser Diodes .....	43
6.1.6 Fluorescence Detection and Laser Pumping .....	47
6.1.7 Low-Power Operation of the OIOPM .....	48
6.1.8 Interfacing the OIOPM to a Sensor System .....	50
6.1.8.1 Rugged Packaging .....	50
6.1.8.2 Voltage Requirements .....	51
6.1.8.3 Temperature Requirements .....	51
6.1.8.4 Magnetic Environment .....	51
6.2 Design of Prototype Instrument .....	52
6.2.1 Configuration of the Optical Pumping Unit. ....	53
6.2.2 Measurement Algorithm and Electronics for the OIOPM. ....	56
7 REFERENCES .....	60

## EXECUTIVE SUMMARY

This report presents our SBIR Phase-I results demonstrating the feasibility of an improved optically pumped magnetometer without dead zones, with improved sensitivity, reduced heading errors, and reduced power consumption.

Optically Pumped Magnetometers (OPMs) are among the most sensitive magnetometers available. In addition, OPMs are total-field sensors; they measure the magnitude of the ambient magnetic field rather than its vector components. The total-field measurement greatly reduces noise when the magnetometer is deployed on a moving platform such as an aircraft, towed body, or diver's hand. This reduced motional noise is a crucial advantage over competing technologies such as fluxgates, magnetoresistive sensors, and SQUIDs (Superconducting QUantum Interference Devices).

One major disadvantage of existing OPMs is that they have "dead zones"; the noise in the magnetic measurements deteriorates badly when the OPM is oriented in the wrong way with respect to the ambient magnetic field. This orientation-dependent performance restricts the way the OPM can be deployed. In some applications, multiple sensor units are required to cover the full range of platform orientations. The dead zones thus impair the utility and increase the cost of OPMs.

In Phase I, we established the feasibility of an OPM without dead zones: an Orientation-Independent Optically Pumped Magnetometer (OIOPM). We achieved three main objectives:

1. We demonstrated in the laboratory the innovative optical pumping technique that makes the OIOPM possible. These experiments are the most important step in establishing the feasibility of the OIOPM.
2. We investigated a range of engineering issues. We evaluated the key tradeoffs between sensitivity, sensor size, and tolerance for magnetic gradients. We verified the feasibility of low-power operation with solid-state light sources for the pump beam. In addition, we estimated the heading error of the instrument, and considered some of the practical issues involved in interfacing the OIOPM to a sensor package.
3. On the basis of this analysis, we designed a prototype instrument for development during Phase II.

Our analysis indicates that, in addition to eliminating dead zones, the OIOPM can provide improved sensitivity and much lower heading errors. We envision this new sensor being developed in a variety of forms, each optimized for specific applications in terms of sensitivity, sensor size, and gradient tolerance. A compact sensor, appropriate for hand-held sensors and remotely deployed sensor arrays, would provide noise below the fluctuations of the ambient magnetic field, with an optical pumping unit roughly one inch in diameter and two inches long. A high-sensitivity version, appropriate for sensitive magnetic gradient measurements, would use a larger sensor unit to measure magnetic gradients with sensitivities approaching

those of SQUIDs (Superconducting QUantum Interference Devices). Either instrument would provide heading errors 10 to 1000 times lower than those of conventional OPMs. The optically pumped sensors would consume less than 1/3 watt of electric power, and could potentially be designed for even lower-power operation.

These improved capabilities would be useful in a variety of military systems such as remotely deployed sensor arrays; handheld magnetometers for detecting buried ordnance; and airborne, towed, or floating sensors for detecting mines and submarines. Dual-use applications would include geophysics, oil and mineral exploration, and public security.

Accession For	
NTIS CRA&I	<input checked="" type="checkbox"/>
DTIC TAB	<input type="checkbox"/>
Unannounced	<input type="checkbox"/>
Justification _____	
By <i>per tti</i>	
Distribution /	
Availability Codes	
Dist	Avail and/or Special
A-1	

## 1 INTRODUCTION

The Navy has long used optically pumped magnetometers (OPMs) for detecting mines, submarines, concealed bombs, and buried ordnance. Thirty years after their initial development, OPMs are still among the most sensitive magnetometers available; in this respect, they are surpassed only by superconducting quantum interference devices (SQUIDs) which operate at cryogenic temperatures. Perhaps more importantly, OPMs are total-field sensors; they measure the magnitude of the total magnetic field, rather than the projection of the field onto a specific axis. The total-field measurement remains nearly constant as the instrument is rocked back and forth in the presence of the earth's magnetic field. When the magnetometer is deployed in an airplane, towed body, floating buoy, or diver's hand, this insensitivity to sensor motion gives OPMs a crucial advantage over vector magnetometers such as SQUIDs, fluxgates, or magnetoresistive sensors.

Although the measured total field varies only weakly with orientation, OPMs are orientation dependent in a different sense: the noise in the magnetic measurement varies strongly with the angle between the ambient magnetic field and the optical axis of the instrument. For a given OPM in a given application, there will be a range of solid angle in which the noise level is unacceptable. This range of angles is called a dead zone.

These dead zones create restrictions that reduce the usefulness of the OPM. In a handheld instrument, the dead zones force the operator to orient the instrument in a particular way with respect to the ambient magnetic field. If the OPM is mounted on an airplane or towed vehicle, the dead zones force the sensor platform to avoid certain directions of travel. To accommodate the dead zones, some magnetometer systems actually use three independent sensors oriented along three orthogonal axes. This approach eliminates restrictions on platform heading, but increases the weight, cost, complexity, and power consumption of the OPM. Eliminating the dead zones altogether would make it possible to avoid orientational restrictions without using multiple sensor units. OPMs would be made smaller, lighter, less expensive, and easier to use.

The dead zones in conventional OPMs arise inherently from the optical technique that is used to measure the ambient magnetic field. In this technique, a special optical absorption process, called optical pumping, is used to align the atomic spins of alkali atoms with the ambient magnetic field. The atomic spins are then manipulated by using a radio-frequency (RF) field to stimulate the Larmor precession of the atomic spins about the ambient field. The change in spin alignment is observed by monitoring the optical absorption. By combining these processes, it is possible to determine the Larmor precession frequency, which is proportional to the intensity of the ambient magnetic field. OPMs using this approach have dead zones because the optical pumping is only effective when the optical pump beam has a sufficient component along the ambient field.

Our goal is to develop a new OPM with no dead zones. This Orientation - Independent Optically Pumped Magnetometer (OIOPM) will use a new optical pumping technique that does not depend on the orientation of the optical axis with respect to the ambient field. In essence, this new technique separates the optical pumping from the actual magnetic measurement. We do the optical pumping in the presence of an applied magnetic field, which we adjust so that it lies along the pump beam. We remove this applied field adiabatically, in such a way that the optically pumped atoms end up aligned with the ambient magnetic field. We then manipulate the atomic spins as in a conventional OPM, using an RF field to stimulate the Larmor precession of the atoms. We finally observe the effect of the RF field by adiabatically restoring the applied field and repeating the optical pumping process. Thus, by making optical measurements in an applied field that is aligned with our optical apparatus, we can observe a physical process which depends on the Larmor frequency of the atoms in the ambient earth's field.

During Phase I, we achieved three main objectives in order to establish the feasibility of the orientation-independent optically pumped magnetometer:

1. Our most important achievement was to observe the new, orientation-independent optical pumping technique in the laboratory. These experiments demonstrated the key physical process that makes possible the orientation-independent OPM.
2. In addition to these experiments, we have analyzed the potential performance of the new instrument. Our models indicate that, in addition to eliminating the dead zones, the OIOPM can provide significantly improved sensitivity and reduced heading errors.
3. We also investigated the enabling technologies that might have to be developed to produce the new instrument. The OIOPM can be developed using essentially the same technologies that are used in conventional OPMs. However, we can considerably improve the cost, reliability, and power consumption if we use solid-state laser diodes instead of the traditional electrodeless discharge lamps to produce the spectral light for optical pumping. Light sources very similar to those required are already being used in optically pumped frequency standards.

Our Phase-I studies confirm that we can develop a new type of OPM with improved performance and no dead zones. Based on these results, we hope to build and demonstrate a prototype instrument during Phase II.

Our analysis so far indicates that the OIOPM can be produced in a number of forms, tailoring its performance for different applications. The simplest form, based on optical pumping of cesium or rubidium vapor, would provide noise levels and heading errors comparable to those of existing OPMs. A slightly more advanced version using potassium vapor can potentially provide heading errors 10 to 1000 times lower than those of conventional OPMs. Optimized for sensitivity, the same potassium instrument can potentially provide noise levels below 100 femtotesla per root hertz, more than ten times better than the previous generation of OPMs. With modern CMOS electronics and solid-state light sources, the potassium, cesium, or

rubidium sensor could operate on less than 1/3 watt of electric power. This power consumption would permit the instrument to operate for seven months on five kilograms of lithium oxyhalide batteries.

The remainder of this report describes in more detail our Phase-I feasibility study. Section 2 reviews the technical background on which this program is based. Section 3 then summarizes our achievements in relation to the original program objectives. Sections 4, 5, and 6 describe in detail our work under each of the main tasks in the statement of work. Finally, an appendix presents a series of performance models for the OIOPM, which we developed during a separate research contract. As anticipated in our original proposal, we were able to draw upon this related work in our performance analysis during Phase I.

## 2 TECHNICAL BACKGROUND

In this section, we present the technical basis of our proposed orientation-independent optically pumped magnetometer. We first review the operating principles of existing optically pumped magnetometers (Sec. 2.1), and briefly review our own prior work in this field (Sec. 2.2). We then describe the operating principle of the new instrument, and show how this new system will overcome some of the limitations of existing technology (Sec. 2.3).

### 2.1 Operating Principles of Existing OPMs

Optically pumped magnetometers (OPMs) determine the intensity of the ambient magnetic field by measuring the Larmor precession frequency of paramagnetic atoms. This precession-frequency measurement involves three basic processes [1,2]. First, the atomic spins in a vapor of paramagnetic atoms are aligned with the ambient magnetic field. This spin alignment is achieved by optical pumping, a process in which atoms acquire angular momentum by repeatedly absorbing and reemitting circularly polarized light [1,3]. Second, a resonant, radio-frequency magnetic field, or tipping field, stimulates the atomic spins to precess about the ambient magnetic field. Finally, the Larmor precession is observed by detecting modulations in the absorption of circularly polarized light.

This measurement scheme works only when the pump beam has a sufficient component in the direction of the ambient magnetic field. As the axis of the pump beam deviates more and more from the direction of the ambient field, the optical pumping becomes less and less effective in aligning the atomic spins. No net spin alignment is produced when the pump beam is perpendicular to the direction of the earth's field. With a reduction in spin alignment comes a reduction in the signal-to-noise ratio of the optical absorption measurement, and hence a reduction in the precision with which the Larmor precession frequency can be measured. Consequently, the noise in the magnetic measurements depends on the angle between the pump beam and the ambient field. The noise goes to infinity when the pump beam is perpendicular to the ambient field and the spin alignment produced by optical pumping goes to zero. This orientation dependence of the optical pumping is responsible for the dead zones in conventional OPMs.

The measurement process in an OPM also subtly perturbs the atomic precession, producing a slight shift in the measured Larmor frequency. This perturbation gives rise to subtle long-term drifts and orientational errors in the magnetic measurements. The low-frequency drifts arise because the perturbation of the Larmor frequency depends on experimental parameters such as the intensity of the pump beam, the amplitude of the RF field, and the density of the atomic vapor. The perturbation of the Larmor resonance also depends on the orientation of the RF field and pump beam with respect to the ambient magnetic field. This orientational effect gives rise to heading error, a slight variation of the magnetic measurement according to the angle of instrument with respect to the ambient magnetic field. The heading error creates motional noise when the instrument rocks back and forth in the earth's field [1,2,4-6].

In magnetometers based on cesium or rubidium vapor, the heading errors and long-term drifts are compounded by the composite structure of the Larmor resonance. In alkali metals, the Larmor precession involves a manifold of quantum-mechanical spin transitions. Each of these transitions has a slightly different frequency, and the measured precession frequency is effectively a weighted average over the entire manifold of transitions. The relative weights of the different states, and hence the center of gravity of the lineshape, vary according to the orientation of the instrument, the amplitude of the tipping field, and the intensity of the pump beam [1,7].

Because of this composite-line effect, cesium and rubidium OPMs have total heading errors in the neighborhood of one nanotesla. That is, the magnetic measurement varies over a range of roughly one nanotesla as the instrument is rotated through the full range of orientations with respect to the ambient magnetic field [1,2,4-6]. If such an instrument is mounted on a moving platform, rocking motions of one degree will produce measurement fluctuations on the order of 10 picotesla.

The heading errors and drifts in an OPM can be reduced significantly by using potassium instead of cesium or rubidium [1,7-9]. With potassium, the individual atomic spin transitions are well separated in frequency, and the magnetometer can operate using only a single spin transition. As a result, the errors produced by the composite lineshape are eliminated altogether. The remaining drifts and heading errors, produced by slight perturbations of this single spin transition, are much smaller than those in cesium and rubidium magnetometers (Sec. 6.1.3) [1,10].

## 2.2 The Free-Precession Magnetic Detector (FPMD)

In previous work, we demonstrated an optically pumped magnetometer that avoids some of the noise problems in conventional OPMs [8,9]. This free-precession magnetic detector (FPMD) uses a pulsed measurement process analogous to that used in nuclear magnetic resonance. The measurement sequence consists of an optical pumping phase, a tipping phase, and an optical observation phase. During the pumping phase, a strong, circularly polarized light beam aligns the atomic spins of a potassium vapor with the ambient magnetic field. During the tipping phase, an RF pulse rotates the spins into the plane perpendicular to the ambient field, and causes them to precess about the ambient field at the Larmor frequency. During the observation phase, both the pumping light and the RF field are turned off. The free precession of the potassium atoms is then observed by monitoring the transmitted intensity of a weak, circularly polarized probe beam that is oriented perpendicularly to the ambient field. Because of the angle-dependent absorption of circularly polarized light, the probe-beam signal contains an oscillatory component at the atomic precession frequency.

This system improves performance in two main ways. First, using the principle described in the previous section, the FPMD minimizes drifts and heading errors by working with a single spin transition of potassium. In addition, since each step of the optical pumping process is performed separately, it is possible to optimize each step for maximum sensitivity

and minimum systematic errors. During the pumping phase, an intense pump beam is used to produce maximum spin alignment. The RF pulse is also adjusted in duration and intensity to create the maximum precessing atomic spin. During the observation phase, however, only the weak probe beam is present, so that perturbing effects are minimized. At the same time, the sensitivity of the optical measurement is maximized by choosing the probe-beam intensity to achieve an optimum balance between the strength of the optical signal and the lifetime of the precessing atomic spins [8,9].

### **2.3 The Orientation-Independent Potassium Magnetometer**

Based in part on our experience with the FPMD, we proposed a new type of OPM that has no dead zones, and provides the same high sensitivity regardless of its orientation in the ambient magnetic field. This Orientation-Independent OPM (OIOPM) is based on a new optical pumping technique, which we call optical pumping with field cycling (OP/FC). In this technique, the optical pumping is performed in a applied field that is always aligned with the pump-beam, while the actual atomic precession measurement is made in the ambient magnetic field. Demonstrating this process was our most important achievement during Phase I.

In the following paragraphs, we describe the field-cycling technique in fundamental terms. Sec. 6.2 presents our specific plans for implementing this measurement process in the Phase-II prototype instrument. Our presentation below assumes that the direction and magnitude of the ambient magnetic field is approximately known at the outset. We anticipate using a set of inexpensive auxiliary sensors, probably Hall probes, to determine the approximate ambient field in our prototype OIOPM.

The magnetic measurement is performed in two repeated phases, optical pumping, and RF depolarization. Between these two steps are brief intervals in which we change the applied magnetic field.

During optical pumping, the instrument uses a set of three orthogonal coils to supply its own magnetic field. The currents in these field coils are adjusted so that the net magnetic field, the vector sum of the applied field and the ambient earth's field, is oriented along the axis of the pump beam. The pump beam is turned on for a short period, placing most of the alkali atoms in the spin state corresponding to maximum polarization along the net field. Since the pump beam and net magnetic field are always aligned with each other, this process guarantees maximum spin polarization.

After optical pumping, the applied field is removed, leaving only the ambient field. The field is removed adiabatically, over a time long in comparison with the Larmor precession frequency of the alkali atoms, so that the atomic spins smoothly follow the magnetic field as it changes. The spins, which were originally lined up with the pump beam, end up aligned with the ambient magnetic field.

During the depolarization phase of the measurement, a radio-frequency magnetic field is applied in a direction perpendicular to the ambient field, at a frequency close to one of the atomic spin transitions of the potassium vapor. This excitation changes the populations of the atomic spin states, decreasing the net polarization of the spins in the direction of the ambient field. The amount of depolarization depends on the amplitude and duration of the RF field pulse, as well as how close the RF frequency is to the center of the atomic spin resonance. The pulse duration and intensity are chosen so that the maximum depolarization occurs when the RF field is exactly in resonance with the spin transition.

At end of the RF pulse, the applied field is adiabatically reapplied, so that the net magnetic field once again becomes aligned with the pump beam. Since the field is reapplied adiabatically, the alkali spins again smoothly follow the changing field, so that the entire atomic spin population, now partially depolarized as a result of the RF pulse, rotates smoothly and ends up aligned with the net magnetic field.

Then, the pump beam is turned on again to restore the atomic spins to their original state of maximum alignment. During this repumping process, the depolarized state of the alkali atoms is reflected in an increased absorption of the pumping beam. The absorption of the pump beam is thus a measure of how close the RF frequency was to the center of the Larmor precession line.

On successive optical pumping cycles, this information is used to adjust the applied RF frequency, maintaining a constant pump-beam absorption and hence a constant relationship between the RF frequency and the atomic precession frequency. The precession frequency, and thus the intensity of the ambient magnetic field, is determined from the RF frequency required to maintain this constant pump-beam absorption.

With field cycling, then, we perform the optical absorption measurement in an applied field under our experimental control, and use it to observe the effect of an RF depolarization experiment whose result depends on the Larmor frequency of the alkali atoms in the ambient earth's magnetic field. This process allows us to measure the intensity of the ambient field, no matter how that ambient field is oriented with respect to the optical axis of our instrument.

In practice, we would alternate in successive optical pumping cycles between two RF frequencies on opposite sides of the Larmor lineshape. Maintaining a constant separation between the two RF frequencies, we would adjust their average so that the pump-beam absorption was the same for both. This approach, commonly used in other optically pumped magnetometers, would nullify the effects of drift in the pump-beam intensity and the Larmor linewidth. As a result, the long-term drifts in the magnetic measurement would be determined only by the slight perturbation of the atomic spin states by the depolarizing RF field. This small source of drift is analyzed in Sec. 6.1.3.

In addition to eliminating dead zones, the field-cycling measurement scheme retains some key advantages from our previous free-precession magnetic detector. As in the FPMD, the pulsed measurement process separately optimizes the different phases of the optical-pumping experiment, maximizing the signal-to-noise ratio in the optical measurement. The field-cycling scheme also allows us to work with a single spin transition of potassium, eliminating drifts and heading errors due to the composite line shape of the Larmor precession.

In fact, the measurement process in the OIOPM is equally compatible with cesium, rubidium, or potassium. We anticipate using cesium and rubidium in the earliest versions of the instrument, since laser-diode light sources have already been developed for optical pumping in these elements. With a slight extension of the laser-diode technology, we can then develop a version based on potassium. This version will provide the optimum combination of high sensitivity, low heading errors, and low drifts. As discussed in Sec. 6.1, our analysis indicates that the OIOPM can potentially achieve much greater performance than conventional OPMs.

### 3 SUMMARY OF OBJECTIVES AND RESULTS FOR PHASE I

In our proposal for Phase I, we identified three specific objectives, which we felt were crucial in establishing the feasibility of the orientation-independent OPM. In the following paragraphs, we restate these three objectives, and summarize briefly how we have achieved them during Phase I.

*"1. Demonstrate operating principle. Using a modification of an existing apparatus, we will experimentally demonstrate all the basic processes required for the orientation-independent operation of an optically pumped magnetometer."*

We met this objective by observing in the laboratory the technique of optical pumping with field cycling. We performed optical pumping in an applied field, along an axis perpendicular to the ambient earth's magnetic field. We then removed the applied field, and depolarized the spins by applying a radio-frequency field at approximately the Larmor resonance of the alkali atoms in the ambient field. We observed this depolarization by restoring the applied field and repeating the optical pumping. As expected, the results of this experiment were dependent on the agreement between the RF frequency used and the atomic Larmor resonance in the ambient field.

This experiment verified the crucial principle behind the orientation-independent OPM: Optical pumping can monitor the results of a physical process reflecting the Larmor frequency of the atoms in the ambient earth's field, even though the optical pumping itself is performed in an applied field, along an axis completely different from that of the ambient field itself.

These experiments are described more completely in Sec. 5.

*"2. Analyze engineering and physics issues. We will analyze the sensitivity limits, engineering tradeoffs, physical configuration, and power consumption of the new instrument."*

We met this objective, as proposed, by applying previously developed models to analyze a variety of fundamental and engineering issues. These issues included

- (1) the fundamental tradeoffs of sensitivity, sensor size, and tolerance for magnetic gradients,
- (2) the prospects for improved performance through modifications of the optical measurement technique,
- (3) the low-frequency drifts and heading errors due to perturbations introduced by the measurement process,
- (4) the motional noise due to gyroscopic effects,
- (5) the feasibility of using solid-state devices to produce the pump beam,
- (6) the power requirements of the instrument, and

- (7) several practical issues involved in interfacing the OIOPM with the rest of a sensor platform.

Our analysis of these issues is described in detail in Sec. 6.1.

*In preparing the conceptual design, we will take into account a number of practical and fundamental issues:*

- (1) *We will estimate of the power consumption of the instrument, including the light source, cell heaters, magnetic-field coils, and associated electronics.*
- (2) *We will refine our models of low-frequency drift and heading error, so as to define stability requirements for the electronics.*
- (3) *We will investigate improved optical pumping techniques to maximize sensitivity.*
- (4) *We will estimate the optimum size of a practical sensor, taking into account the tradeoff between sensitivity and cell size.*
- (5) *We will investigate the feasibility of using laser diodes instead of vapor discharge lamps for the optical pumping. Laser diodes may use less power and have greater lifetimes than the potassium-vapor electrodeless discharge lamps now used. However, tuning the laser diodes to the potassium spectral lines may be a problem.*
- (6) *To make use of laser diodes, we will evaluate an alternative method for monitoring the absorption of the pump beam. Since the light from the laser diode has a much broader spectral width than the absorption lines of potassium, a large amount of pump light will pass through the optical pumping cell without interacting with the potassium vapor. This additional light will add to the noise in measuring the transmission of the pump beam. However, instead of monitoring the transmitted beam, we can measure the pump-beam absorption by detecting the light reemitted by optically excited atoms. This fluorescence would be detected using photodiodes that were mounted at the sides of the optical pumping cell, out of the path of the transmitted pump beam.*

*"3. Design full-scale instrument. We will produce a conceptual design identifying all major system components and their performance requirements."*

Our conceptual design for the full-scale instrument is described in Sec. 6.2.

In order to meet the three technical objectives of the program, our Phase-I work statement included the following three tasks:

1. Modify Existing Potassium Magnetometer.
2. Demonstrate Orientation-Independent Measurement Process.
3. Design Instrument for Phase II.

The next three sections describe in detail our work under each of these three tasks.

#### 4 TASK 1: MODIFY EXISTING POTASSIUM MAGNETOMETER

The first task in the Phase-I work statement was described as follows in the original proposal:

*"Our experiments during Phase I will make use of the existing apparatus that was used during our work on the Free-Precession Magnetic Detector. For Phase I, we install a new set of coils in order to generate the applied magnetic field that is used in the OIPM during the optical pumping process. We will also add a set of three orthogonal RF coils, so that we can adjust the orientation of the RF field with respect to the earth's magnetic field."*

During Phase I, we determined that this extensive modification of the apparatus was unnecessary to meet the goals of the project. In particular, we found that we could apply the necessary DC and RF magnetic fields using two existing sets of Helmholtz coils on the original optical pumping unit. As shown in Fig. 1, one set of coils, with a diameter much larger than that of the alkali vapor cell, produces a field transverse to the ambient earth's magnetic field. This coil set was used to produce the RF tipping field in our previous experiments with the Free-Precession Magnetic Detector (FPMD) [8,9]. The second, smaller, set of Helmholtz coils is oriented along the ambient field, and was used in the FPMD to null out the difference in magnetic field between two optical pumping units in a first-order magnetic gradient measurement. In our experiments during Phase I, we used the smaller coils to cancel out the earth's magnetic field, and the larger coils to produce an applied field along the pump beam (Fig. 1).

We had to consider a number of factors in deciding to use these two coil sets for our Phase-I experiments. First, we determined that, in spite of the small diameter of the windings in these coils, we could produce fields as large as the earth's field without excessive resistive heating in the coils. Second, we devised an electronic circuit that allowed us to use one set of coils, the set transverse to the ambient field, both to produce a DC field during optical pumping and to produce an RF field during the spin depolarization phase of the experiment. Third, we verified with a simple calculation that, in spite of the small size of the longitudinal coils, they would produce a field adequately uniform for optical pumping. To the extent that the field produced by these coils is not uniform, the net magnetic field in some portions of the optical pumping cells will deviate from the axis of the pump beam. This deviation will reduce the spin alignment produced by optical pumping.

Although we did not modify the optical pumping units themselves, we did significantly add to the electronics that control the applied RF and DC magnetic fields. The timing electronics in our existing apparatus had been designed for the transverse optical pumping process used in the Free-Precession Magnetic Detector (FPMD) (Sec. 2.2). The overall repetition rate of optical pumping experiment was controlled by a master oscillator, which was triggered synchronously with the electric power lines. This master oscillator was used directly to gate the pump beam on and off. The timing circuit was constructed so that we could independently adjust the on time and off time of the pump beam. An additional timing pulse, triggered at

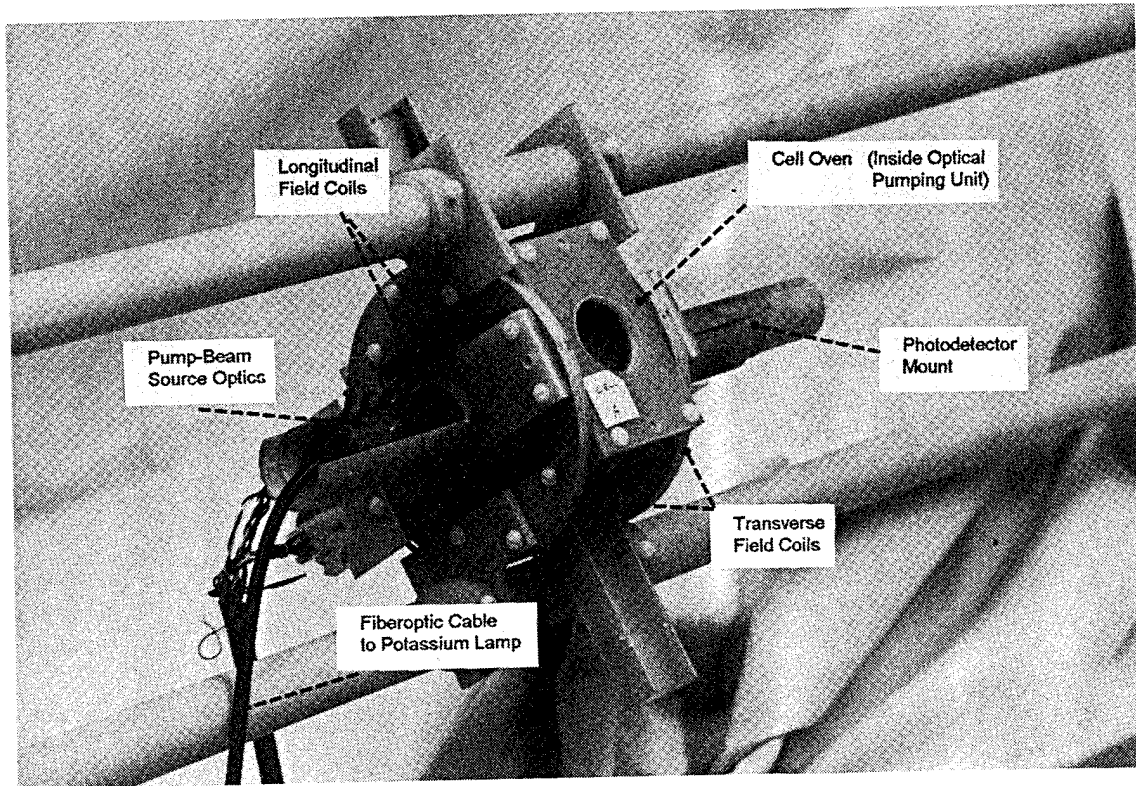


**Fig. 1. Optical pumping apparatus configured for field cycling experiment. The earth's magnetic field is perpendicular to the pump beam, along the axis of the unused optics holders that protrude diagonally from the optical pumping unit.**

the point where the pump beam was turned off, was used to gate the RF tipping field. In the FPMD, the transverse optical measurements were made during the dead time after the end of the tipping pulse and before the pump beam was turned back on.

The FPMD timing electronics also included adjustable voltage supplies for the resistive heaters that maintained the vapor pressure of potassium in the optical absorption cell. These heaters were gated on and off with the pump beam, so that no current was flowing in the heaters during the transverse optical measurements. This practice ensured that no magnetic gradients were present to reduce the transverse spin relaxation time of the precessing atomic spins.

For our field-cycling experiments, we have added several new functions to the electronics. In these experiments, we need to switch an applied magnetic field on and off, changing the field slowly enough so that the atomic spins adiabatically follow the changing field. To control the field cycling, we take the output of the existing master oscillator, and pass it through an analog integrator. We use Zener diodes to clip the output of the integrator, thus converting the square-wave timing signal into a trapezoidal signal with a sloped rise and fall. By varying the time constants in the analog integrator, we control the rate at which the trapezoidal wave switches between its high and low values.

Since the DC field coils in our existing apparatus contain only a few turns of wire, we need to supply them with currents slightly greater than half an ampere in order to produce fields comparable to the ambient earth's field. To supply these currents, we pass the trapezoidal signal from the integrator through two linear power amplifiers. We use one amplifier to drive the longitudinal coils that cancel the earth's field, and the second amplifier to drive the transverse coils that provide the applied field along the axis of the pump beam. We adjust the currents in the two sets of coils independently by adjusting the gain of the amplifiers. The time spent in developing these power amplifiers was, in effect, the price we paid for not adding additional field coils to the optical pumping apparatus.

One of the crucial requirements in the field cycling experiment was to turn off the DC current to the field coils completely during the phase of the experiment when the RF pulse was used to excite the Larmor resonance of the alkali atoms. In an effort to minimize any leakage currents during this period, we added a diode to the output of each power amplifier. We arranged the circuit so that, when the output voltage of the amplifier dropped below zero, the diode was reversed-biased and had a very large effective resistance.

We will reexamine during Phase II this system for turning off the applied field. In our initial optical pumping experiments, we found that the Larmor frequency was slightly different (by approximately 0.3%) in the field-cycling mode than in a simpler optical pumping experiment with no applied field. This result may indicate that there was some residual current in the applied-field coils during the period when the RF pulse was applied. The result may, however, reflect only the fact that the two experiments differed slightly in the timing of the RF pulse with respect to the background noise from the electric power lines. These initial experiments were performed inside the laboratory, where the 60-Hz power-line fields could well be as much as 1% of the earth's field. We did, in fact, observe a variation in the optical pumping

signal when we varied the trigger point of the master oscillator with respect to the phase of the signal from the power lines. This change in signal indicated that the RF pulse was depolarizing the atomic spins to differing degrees according to the timing of the experiment. This effect presumably reflected a change in the Larmor precession frequency during the RF depolarizing pulse.

In addition to these modifications involved in ramping the applied DC field, we also added one more timing signal to the control electronics. This additional timing signal allowed us to delay the RF field pulse until well after the applied magnetic field had finished ramping down.

## 5 TASK 2: DEMONSTRATE ORIENTATION-INDEPENDENT MEASUREMENT PROCESS

The most important part of Phase I is described as follows under Task 2 of the statement of work:

*"Using the modified apparatus, we will demonstrate each phase of the measurement process .... This demonstration will include:*

- (1) polarizing the atomic spins in an applied field that is aligned with the pump beam,*
- (2) adiabatically removing the applied field,*
- (3) depolarizing the atomic spins by the application of an RF field,*
- (4) adiabatically restoring the applied field,*
- (5) repolarizing the atomic spins, while monitoring the absorption of the pump beam to determine the degree of spin depolarization, and*
- (6) repeating the measurement cycle at different RF frequencies to determine the precession frequency of potassium atoms in the ambient magnetic field."*

This task amounts to a demonstration of our proposed field-cycling technique, the one new measurement process required to operate the OPM without dead zones. The following paragraphs describe the experiments we performed to demonstrate this key process.

### 5.1 Preliminary Experiments on Optical Pumping

In preparation for the field-cycling experiments, we first performed a simple longitudinal optical pumping experiment. In this experiment, we pass a circularly polarized beam of potassium  $D_1$  light through a cell of potassium vapor, in a direction parallel to the ambient earth's magnetic field. In absorbing and reemitting this circularly polarized light, the potassium atoms on average acquire a net angular momentum in the direction of the pump beam. As a result, the atomic spins become polarized along the ambient magnetic field. When the spins are nearly completely polarized, we apply a radio-frequency magnetic field at the Larmor precession frequency of the potassium atoms in the ambient field. This RF field excites transitions among the atomic spin states, reducing the polarization of the spins along the ambient field. After we remove the RF field, the spins gradually regain their polarization through optical pumping.

We observe these changes in spin alignment by using a photodiode to monitor the transmission of the pump beam through the potassium vapor. This observation is possible because absorption of the circularly polarized light depends on the angle between the atomic spin and the polarization axis of the light. In the case of  $D_1$  light, the absorption is maximized when the spins are antiparallel to the polarization axis, and minimized when the spins are aligned with the polarization axis.

Figure 2 is a timing diagram which summarizes this sequence of events. As shown in the figure, the atomic spin polarization dips sharply when the RF pulse is applied, and then recovers slowly, in an exponential fashion. Correspondingly, the transmitted pump beam dips during the RF pulse, and then recovers to a maximum value.

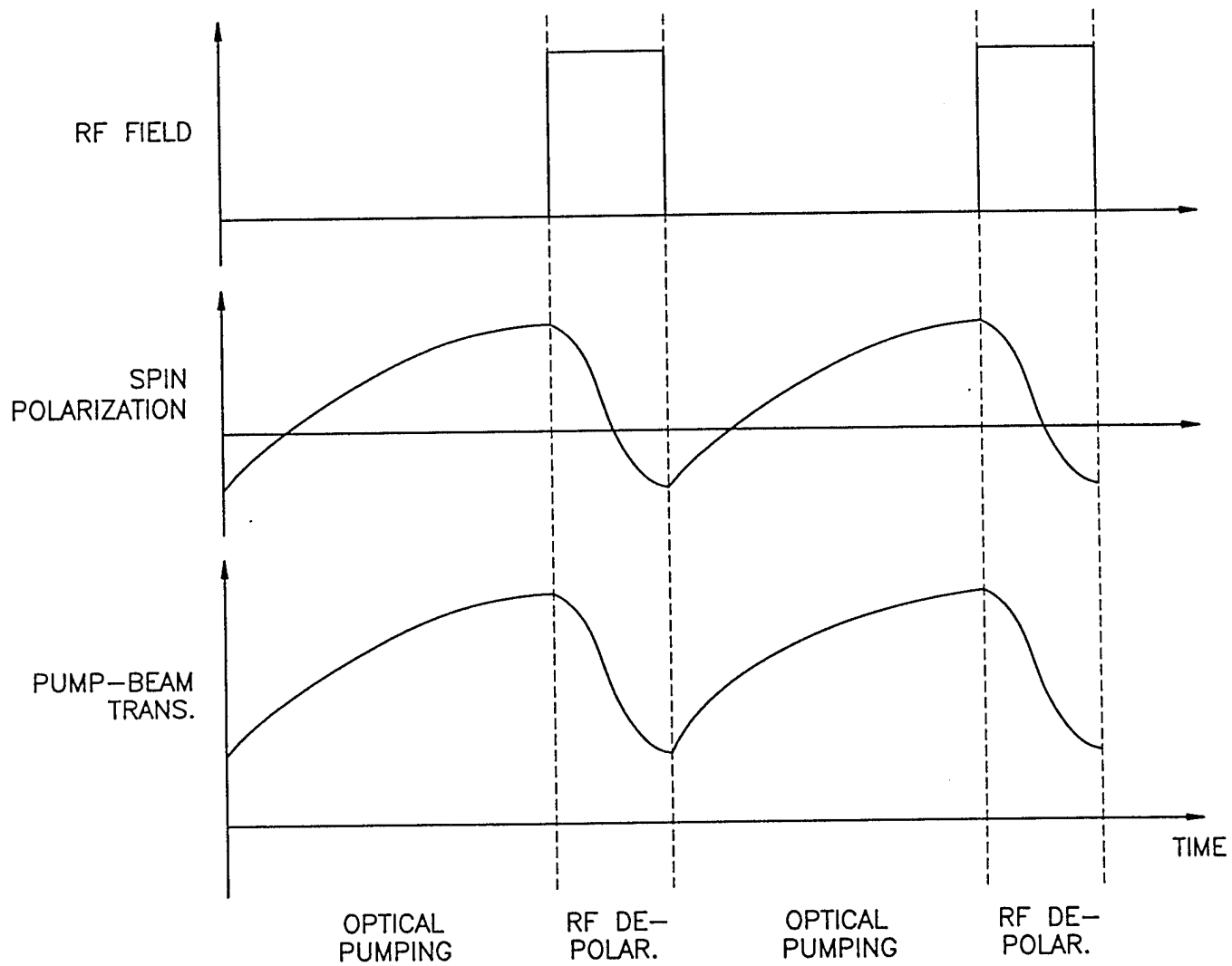
Since the RF field depolarizes the atomic spins only when it matches the Larmor frequency of the atoms, this spin depolarization experiment can be used to measure the Larmor frequency, and hence the magnitude of the ambient magnetic field. This principle is, in fact, used in a type of OPM called the locked-oscillator magnetometer (LOM). The LOM uses a feedback loop to adjust the RF frequency while monitoring the optical absorption signal. By maintaining a constant optical absorption, the feedback loop keeps the RF frequency at a constant point on the peaked lineshape that characterizes the degree of spin depolarization as a function of the RF frequency.

Figure 3 shows the configuration of the optical pumping apparatus for this spin-depolarization experiment. The pump beam is generated by an electrodeless discharge lamp, in which an RF field is used to excite an electrical discharge inside a small glass bulb containing potassium metal and low-pressure xenon gas. The light from the lamp is focused by a lens, passed through a filter to separate the  $D_1$  line from the nearby  $D_2$  line, and then refocused into a fiberoptic cable. Exiting the fiberoptic, the  $D_1$  light is passed through a collimating lens, and then through a circular polarizer formed by a linear polarizer followed by a quarter-wave plate. The circularly polarized light then passes through the potassium vapor cell, and is finally focused by a lens onto a photodiode.

In this experiment, the pump beam is passed through the cell in the direction of the earth's magnetic field, upward at a slight angle in Fig. 3. The RF field is applied transversely to the earth's field (horizontally in Fig. 3), and is produced by the large Helmholtz coils shown in the figure.

## 5.2 Optical Pumping with Field Cycling

Our orientation-independent optical pumping technique is essentially a spin-depolarization experiment in which the optical pumping is performed in an applied DC magnetic field, while the spin-depolarizing RF field is applied in the absence of this applied field. Figure 4 is a timing diagram for this experiment. In this experiment, unlike the simple spin depolarization experiment, we have the pump beam perpendicular to the ambient magnetic field. During the initial phase of the experiment, we apply our own magnetic field to the alkali-vapor cell. We adjust the magnitude and direction of this applied field so that the net magnetic field, the sum of the applied and ambient fields, is approximately parallel to the pump beam. Since the net magnetic field in the cell is parallel to the pump beam, the pump beam acts to align the atomic spins with this net magnetic field. When the spins are nearly completely aligned, we remove the applied field over a time long compared with the Larmor frequency of the atoms. Under these conditions, we expect that the atomic spins will adiabatically follow the changing direction of the instantaneous net magnetic field. By the time the applied field has been removed com-



**Fig. 2. Timing diagram of spin depolarization experiment.**

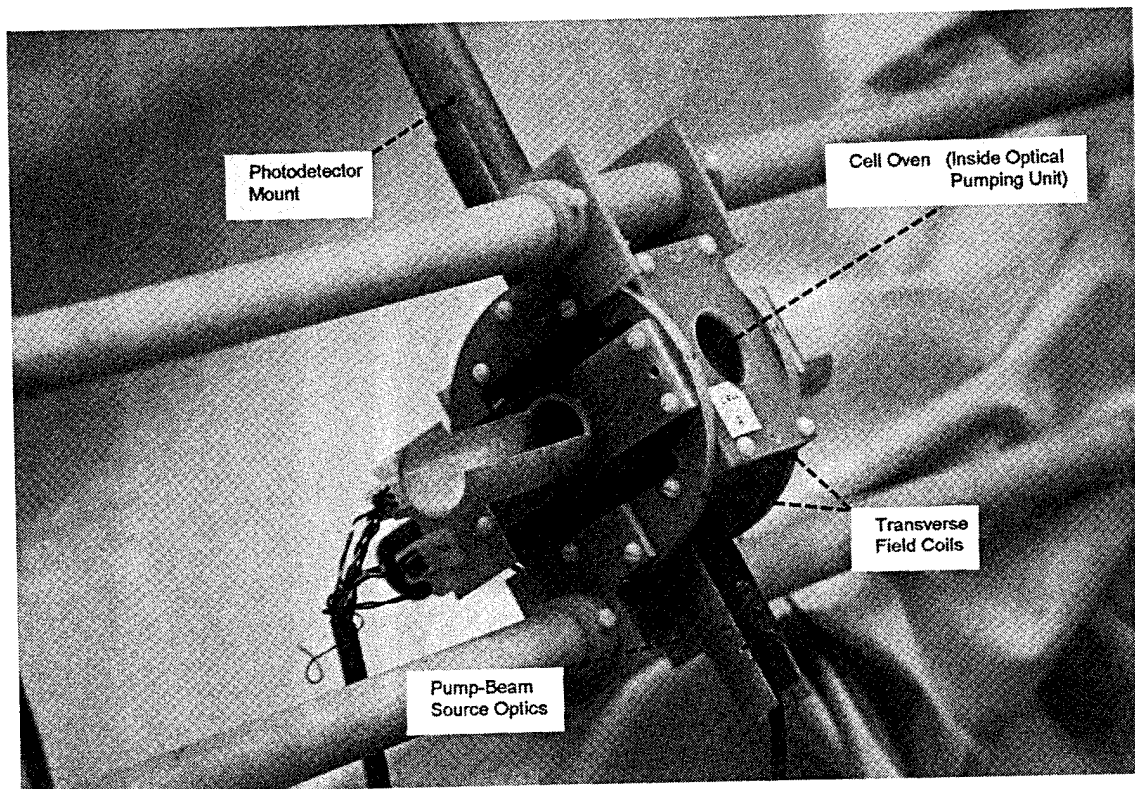


**Fig. 3. Optical pumping apparatus configured for spin depolarization experiment. The earth's magnetic field is parallel to the pump beam.**

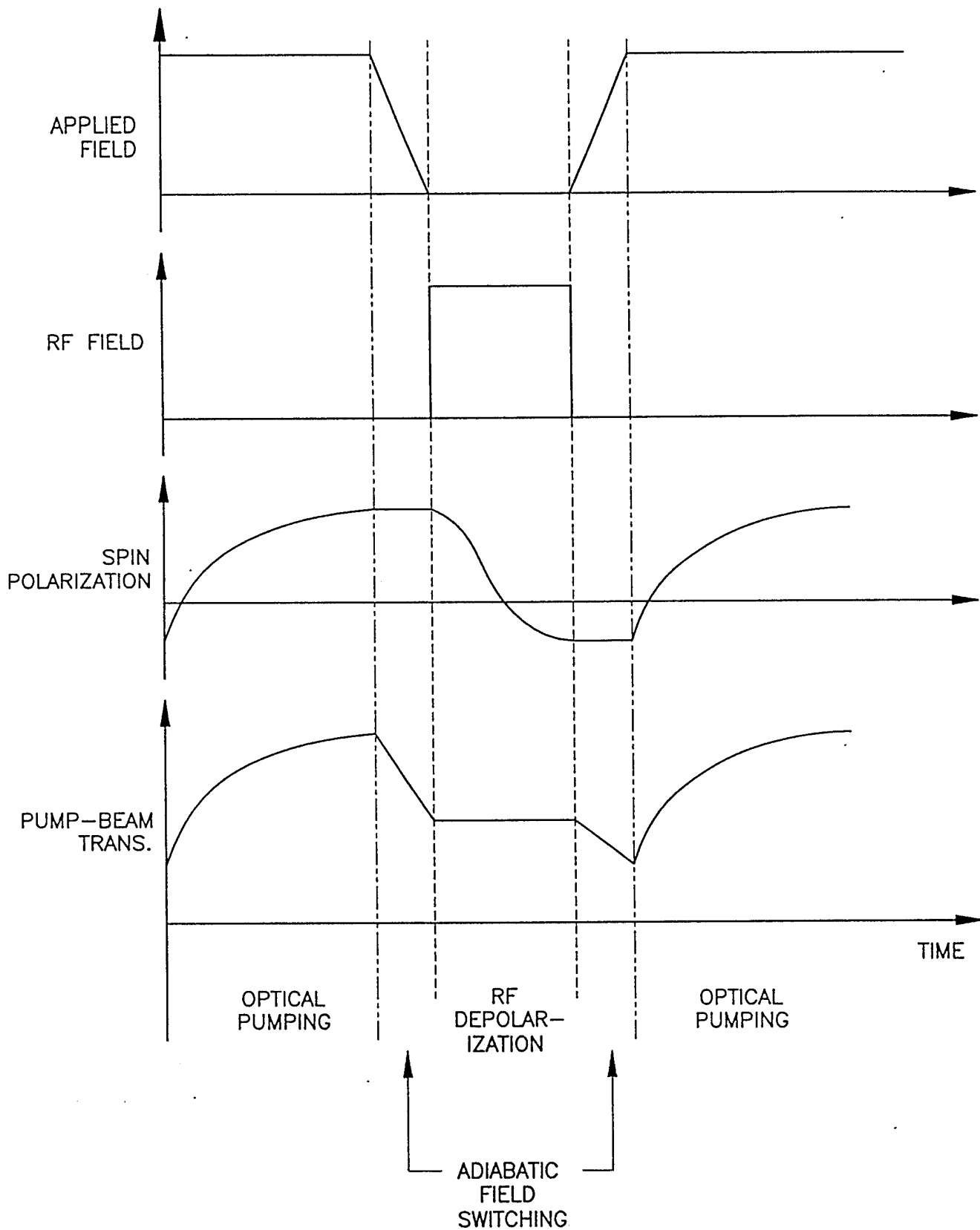


Fig. 4. Timing diagram of optical pumping experiment with field cycling.

pletely, the atomic spins will have rotated so that they are aligned with the ambient magnetic field. After removing the applied field, we depolarize the atomic spins by applying the RF field at the frequency corresponding to the Larmor precession of the atomic spins in the ambient magnetic field. To observe the results of the RF field pulse, we adiabatically restore the applied field, and monitor the transmission of the pump beam as the atomic spins recover back toward their maximum polarization along the net field.

Fig. 4 shows how we expect the atomic spin polarization and optical transmission to vary during the experiment. In the figure, we assume that the pump beam is perpendicular to the ambient magnetic field and that the pump beam is left on continuously during the experiment. The transmission of the pump beam is at a maximum just before we remove the applied field, when the atomic spins have their greatest polarization. As we remove the applied field, the spins remain polarized along the changing net magnetic field. However, the transmission of the pump beam decreases, since the spins follow the direction of the net field and end up no longer aligned with the pump beam. When we apply the RF pulse, the spins become less polarized along the net field. This fact is not immediately reflected in the optical absorption measurement because the spins were already aligned in a direction crosswise to the pump beam before the RF pulse. However, when we restore the applied field, the effect of the RF pulse becomes apparent, as the transmission of the pump beam remains low, indicating that the atomic spins are no longer aligned with the net magnetic field. Starting from this low value, the transmission of the pump beam increases as the spins are repumped back to their maximum polarization along the net field. In the figure, we actually show a decrease in the pump-beam transmission when the applied field is restored. This result corresponds to a case in which the RF field actually rotates the atomic spins so that their net polarization is antiparallel to the net magnetic field.

Fig. 1 shows how we set up our apparatus for this field-cycling experiment. Instead of aligning the pump beam with the ambient magnetic field (diagonally upward in the figure), we have moved the fiberoptic beam source and photodetector so that the pump beam is perpendicular to the ambient field (horizontal in the figure). We generate the DC magnetic field using the two sets of Helmholtz coils shown in the figure. We use the smaller set to produce a field that approximately cancels the earth's magnetic field, and the large set to produce an additional field in the horizontal direction. The net applied field then lies approximately parallel to the pump beam in our experiment. When the applied field is removed, we use the larger coils apply the RF depolarizing field in a direction perpendicular to the ambient magnetic field.

As shown in Fig. 5, our observations with this apparatus follow the expected pattern very well. The figure shows, as a function of time, the photodiode signal corresponding to the transmission of the pump beam. (The time scale in the figure is 100 milliseconds per division.) The signal starts at a maximum, then decreases rapidly as we remove the applied field. The photodiode signal remains approximately constant for approximately 40 milliseconds (except for a slight glitch which we have shown to be an artificial effect of our

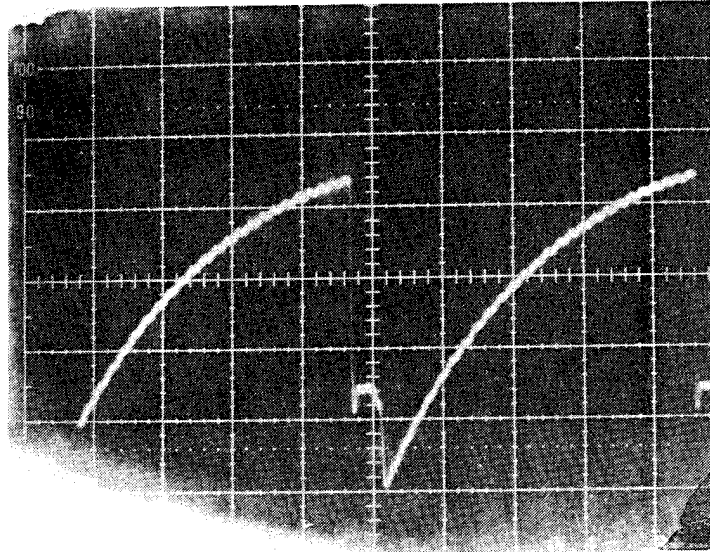


**Fig. 5. Pump-beam transmission as a function of time during field cycling experiment. RF field at Larmor resonance. Time scale is 100 milliseconds per division.**

electronics). At the end of this interval, we restore the applied field, and the transmission decreases, indicating that the spins are partially aligned in the direction opposite to the pump beam. The photodiode signal then recovers exponentially toward its maximum value, as the pump beam repolarizes the atomic spins along the net magnetic field. Table 1 gives some of the experimental parameters used to obtain this result.

Table 1. Timing Parameters for Field-Cycling Experiment

Applied field on time	440 msec
Applied field off time	40 msec
Applied field ramp-down time	5 msec
Applied field ramp-up time	5.5 msec
RF pulse duration	0.44 msec
RF pulse delay (from beginning of applied-field down-ramp)	10.0 msec

This example shows the significant loss of spin polarization that we observe with the RF frequency adjusted to match the Larmor resonance of the atomic spins in the ambient field. We obtain a much different signal if we do not apply the RF field (Fig. 6), or if we apply the RF field at a frequency far from the peak of the Larmor resonance (Fig. 7). Under these conditions, the pump-beam transmission after restoring the applied field is only slightly less than that observed before removing the field. These results indicate that the atomic spins retain most of their initial polarization while the applied magnetic field is adiabatically cycled off and then back on, unless we deliberately depolarize them by applying an RF field in resonance with their Larmor precession in the ambient field.

The contrasting results observed with the RF field on and off resonance confirm the essential premise behind the orientation-independent optically pumped magnetometer: With adiabatic field cycling, we can make our optical pumping measurements in a net magnetic field that is aligned with the pump beam, and still observe the results of a physical process, RF spin depolarization, that depends on the Larmor frequency of the atomic spins in the presence of the ambient magnetic field alone.

As explained in Sec. 2.3, we can exploit this measurement process to determine the Larmor frequency, and hence the magnitude of the ambient magnetic field. In essence, on successive cycles of the measurement process, we would vary the RF frequency while using the pump beam signal to monitor the degree of spin depolarization produced by the RF pulse. By adjusting the RF frequency to maintain a constant spin depolarization, we would maintain the RF frequency at a constant point on the lineshape corresponding to the Larmor resonance.

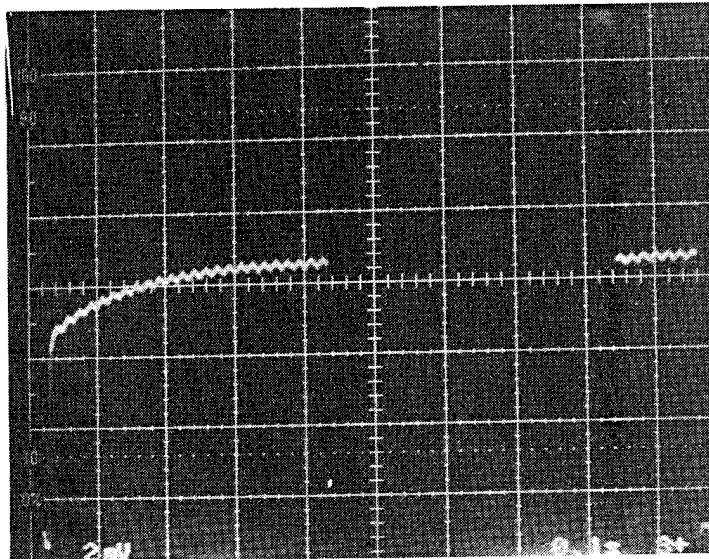
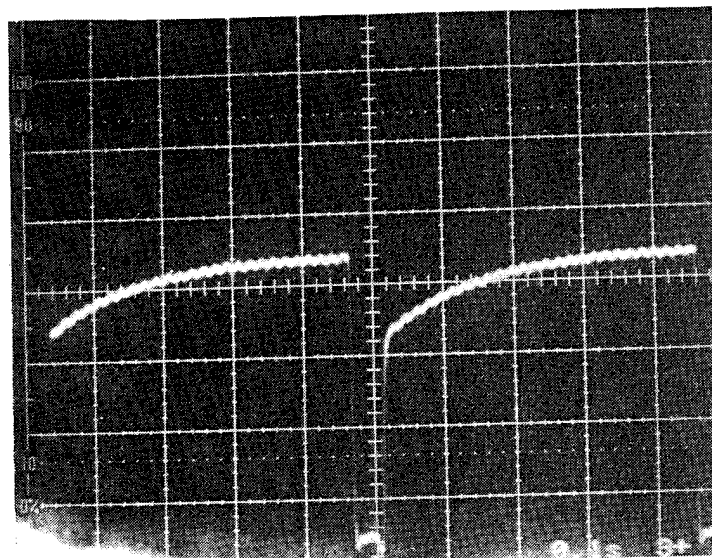


Fig. 6. Pump-beam transmission as a function of time during field cycling experiment. No RF field applied.



**Fig. 7. Pump-beam transmission as a function of time during field cycling experiment. RF frequency 10 kHz above Larmor resonance.**

### 5.3 Refinements for Future Work

Our experiments in the previous section represent our first demonstration of the basic field-cycling technique. In the next few paragraphs, we describe some of the ways these initial results will be refined as we work toward an actual magnetometer based on this technique:

a. **Investigate Field Shift.** In both our field-cycling experiment and our preliminary longitudinal spin-depolarization experiment, we measured the Larmor frequency of the potassium atoms by adjusting the applied RF frequency to obtain the maximum degree of spin depolarization. In the simple spin-depolarization experiment, we found an optimum RF frequency of approximately 23.8 kHz. In the field-cycling experiment, we found a slightly shifted optimum frequency of approximately 24.5 kHz. This shift presumably indicates a slight difference between the two experiments in the magnetic field that was present in the optical pumping cell at the time of the RF pulse. This difference could conceivably indicate that, in the field-cycling experiment, some small residual current was still present in the applied-field coils at the time of the RF pulse. As explained in Sec. 4, however, it also appears quite likely that the slight shift simply reflects a difference in the timing of the RF pulse with respect to the 60-Hz background fields produced by nearby electric power lines.

We plan to investigate this issue in more detail early in Phase II. The first step in this investigation will be to repeat the field-cycling and spin-depolarization experiments in a lower-noise magnetic environment. If these experiments indicate that there is still a field shift, we will redesign the electronics for the prototype instrument to guarantee that there is no residual current in the applied-field coils when the RF field is applied. One possible method would be to replace the diode-blocking circuit now used with a mechanical reed switch. This method would effectively increase the resistance of the field-coil circuit to infinity during the RF field pulse. Another approach would be to use a series of FET switches, connected in a ladder configuration with bypass resistors to ground between the stages. This arrangement would effectively attenuate any residual voltage at the input to the ladder by  $r^n$ , where  $n$  is the number of stages and  $r$  is the ratio of the blocking resistance in the FET switch to the bypass resistance to ground.

b. **Optimize Field Cycling Rate.** In these initial experiments, we switched the applied field on and off in a linear fashion, with a switching time of 5 milliseconds. Since this time is long in comparison with the 320-kHz Larmor frequency of the potassium atoms in the earth's field, we expect that the atomic spins should follow the change of the applied field rather well. However, our results in Figs. 6 and 7 do indicate that some polarization is lost in removing and then restoring the applied field, even when we do not deliberately depolarize the spins using the RF field. Some of this polarization loss is presumably due to the fact that we left the pump beam on while the applied field was off. During this off time, the pump beam would have tended to spoil the spin polarization since the atomic spins were aligned with the ambient field, that is, transverse to the pump beam. Our

calculations, based on the observed optical pumping time constant when the net field is aligned with the pump beam, indicate that this pump-beam effect accounts for roughly half the observed loss of spin polarization.

We plan to investigate further, to determine any remaining effects that spoil the spin polarization during adiabatic field cycling. One part of this investigation will be to vary the rate at which we remove and restore the field, as well as the interval over which the applied field is left off. During Phase II, we will also be able to investigate the possible advantages of more homogeneous applied fields on the effectiveness of the adiabatic field cycling. An additional part of our investigation during Phase II will be to determine what, if any, effect this slight loss of polarization would have on the accuracy of the Larmor frequency measurement in the ambient field. At this stage of the program, we expect that imperfections in field cycling will only decrease the sensitivity of the instrument slightly. However, Sec. 6.1.3 does provide a worst-case analysis of the possible heading errors that might arise from the loss of polarization during field cycling. This analysis indicates that the heading error, if any, will be much smaller than that in conventional OPMs.

c. **Reduced RF Intensity.** Our initial experiments were performed inside the laboratory, in the presence of large magnetic field gradients and 60-Hz background noise. Under these conditions, the instantaneous magnetic field varies both with time and with position within the alkali-vapor cell. We therefore have to use a rather short, intense RF pulse containing a relatively wide spectrum of frequencies, to make sure that we excite the Larmor resonance of all the atomic spins in the cell. Our initial experiments used an RF pulse duration of only 0.4 millisecond, and a corresponding RF field intensity of roughly  $1.7 \times 10^{-7}$  tesla. In an actual magnetometer, we would work in a much cleaner magnetic environment. We would then reduce the RF intensity and use an RF pulse length of roughly 0.1 seconds or more, a value comparable to the intrinsic  $T_2$  of the potassium atoms in the cell. This longer, weaker RF pulse would narrow the Larmor resonance to roughly its intrinsic width, allowing us to measure the Larmor frequency and the corresponding magnetic field with maximum precision. In a potassium-vapor magnetometer, the long RF pulse would also allow us to work with a single quantum-mechanical spin transition, eliminating any heading errors or drifts due to the composite structure of the Larmor resonance (Sec. 6.1.3).

We hope to perform our field-cycling experiments with long RF pulses during the early portion of Phase II. The key to these experiments will be to eliminate any magnetic gradients created by residual currents in the applied-field coils. As noted above, there are ways that we can completely open-circuit the applied-field coils during the RF pulse. This approach would eliminate any residual field gradients. We plan to incorporate these improved electronic switching techniques during Phase II.

## 6 TASK 3: DESIGN INSTRUMENT FOR PHASE II

Our final main task for Phase I was described as follows in the statement of work:

*We will produce a conceptual design for a full-scale OIOPM, specifying the overall configuration of the instrument, identifying the major system components and their performance requirements, and detailing the main engineering tradeoffs.*

*In preparing the conceptual design, we will take into account a number of practical and fundamental issues:*

- (1) We will estimate of the power consumption of the instrument, including the light source, cell heaters, magnetic-field coils, and associated electronics.*
- (2) We will refine our models of low-frequency drift and heading error, so as to define stability requirements for the electronics.*
- (3) We will investigate improved optical pumping techniques to maximize sensitivity.*
- (4) We will estimate the optimum size of a practical sensor, taking into account the tradeoff between sensitivity and cell size.*
- (5) We will investigate the feasibility of using laser diodes instead of vapor discharge lamps for the optical pumping. Laser diodes may use less power and have greater lifetimes than the potassium-vapor electrodeless discharge lamps now used. However, tuning the laser diodes to the potassium spectral lines may be a problem.*
- (6) To make use of laser diodes, we will evaluate an alternative method for monitoring the absorption of the pump beam. Since the light from the laser diode has a much broader spectral width than the absorption lines of potassium, a large amount of pump light will pass through the optical pumping cell without interacting with the potassium vapor. This additional light will add to the noise in measuring the transmission of the pump beam. However, instead of monitoring the transmitted beam, we can measure the pump-beam absorption by detecting the light reemitted by optically excited atoms. This fluorescence would be detected using photodiodes that were mounted at the sides of the optical pumping cell, out of the path of the transmitted pump beam.*

*We anticipate addressing many of these issues as part of an ongoing analytical study which evaluates a variety of innovative magnetometer designs. During Phase I, we will build on this prior work in order to define the potential applications of the OIOPM, and produce the best design for the demonstration prototype in Phase II."*

As was anticipated in the statement of work, we did develop models that address many of the points listed above, as part of another program that was in progress at the time we submitted our proposal for Phase I (Appendix A) [10]. We have used the results of this prior work wherever possible in our design study for the Phase-II prototype instrument. However, we took a second look at one key issue, the feasibility of using laser diodes to produce the

potassium, cesium or rubidium spectral light for the pump beam (point 5 above). This second look indicates that developing the diode light sources may be much simpler than we had anticipated. This reinvestigation also affected our assessment of fluorescence detection (point 6).

This parallel work also addressed two other issues not mentioned in our Phase-I statement of work: the OPM's ability to tolerate environmental magnetic gradients, and the gyroscopic noise produced by the rocking motion of the sensor platform. We have included the results of this work in our design study as well.

In the following subsections, we first present the results of our engineering analysis. We then present our conceptual design for the prototype magnetometer to be developed in Phase II. Appendix A presents the models that we developed in the previous study, and have applied in our Phase-I analysis.

## **6.1 Analysis of Performance and Design Issues**

### **6.1.1 Optical Pumping Technique: Tradeoffs of Sensitivity, Sensor Size, and Gradient Tolerance**

*"We will investigate improved optical pumping techniques to maximize sensitivity."*

*"We will estimate the optimum size of a practical sensor, taking into account the tradeoff between sensitivity and cell size."*

These two statements from the Phase-I proposal both relate to the same larger topic: the interrelationships between the basic measurement technique, the specific operating conditions used in the instrument, and the tradeoffs between different performance characteristics. Our analysis indicates some basic tradeoffs between measurement sensitivity and sensor size, and also between measurement sensitivity and tolerance for magnetic-field gradients. These performance tradeoffs are most affected by three basic measurement strategies: (1) the choice of potassium, rubidium, or cesium as the optically pumped species, (2) the method we use to detect the optical absorption signal, and (3) the method we use to suppress spin relaxation at the walls of the optical absorption cell. These basic measurement strategies combine with operating parameters such as the intensity of the pump beam and the dimensions of the optical absorption cell to determine the performance characteristics of the instrument.

In the following subsections, we first summarize the basic mathematical model that we use to relate the sensitivity of the OPM to the other experimental variables (Sec. 6.1.1.1). Using this model to identify the key factors that affect the sensitivity, we show how each key factor plays a role in the tradeoffs between sensitivity, sensor size, and magnetic gradient tolerance (Sec. 6.1.1.2). Then, combining our sensitivity model with data from our previous work on potassium-vapor magnetometers, we estimate the sensitivity of the OIOPM, and show how the sensitivity can be improved by changing the optical pumping technique (Sec. 6.1.1.3). Finally, we use the model to examine the

tradeoff between sensor size and sensitivity. To illustrate this tradeoff, we estimate the sensor size necessary for two different applications with different sensitivity requirements (Secs. 6.1.1.4 and 6.1.1.5).

#### 6.1.1.1 Basic Sensitivity Model

Sec. 6.1.3 below will discuss the low-frequency noise and heading errors arising from instrumental effects that perturb the Larmor frequency of the optically pumped atoms. In the present discussion of performance tradeoffs, we are mainly concerned with a more basic sensitivity limit, the one determined by the statistical noise, or shot noise, in the optical measurement that is used to determine the Larmor frequency of the alkali atoms. Our analysis of this shot noise (Appendix A2.1) yields the following expression for the noise in the magnetic measurement:

$$\delta B \cong \left( \frac{0.649}{\Gamma n_k L (P_2^0 - P_1^0)} \right) \left( \frac{\Delta f_{bw}}{T_2 A b_r \sigma_0} \right)^{1/2} \quad (1)$$

In this expression,  $\Gamma$  is the gyromagnetic ratio of the atomic spins,  $n_k$  is the density of the alkali atoms in the optical absorption cell,  $L$  is the length of the cell in the direction of the pump beam,  $P_1^0$  and  $P_2^0$  are the fraction of the alkali atoms in the  $m=1$  and  $m=2$  spin states,  $\Delta f_{bw}$  is the bandwidth in the magnetic measurement,  $T_2$  is the transverse relaxation time of the atomic spins,  $A$  is the cross-sectional area of the optical cell in the plane perpendicular to the pump beam,  $\sigma_0$  is the cross section for absorption of the pump light by the alkali atoms (in the absence of any net spin polarization), and  $b_r$  is a constant of order unity, representing the average number of pump-beam photons required to pump an atom from the  $m=1$  spin state to the  $m=2$  spin state. This analysis applies to an optically pumped magnetometer that works with a single atomic spin transition, that between the  $m=2$  and  $m=1$  spin states. The analysis also assumes that the optical measurements are made by monitoring the transmitted current in the pump beam.

#### 6.1.1.2 Key Parameters and Fundamental Performance Tradeoffs

In our shot-noise calculation, the useful signal in the optical absorption measurement is essentially the total number photons that the alkali atoms remove from the pump beam while they are being repumped toward their state of maximum spin polarization. The noise in the optical measurement is essentially the square root of the total number of photons that reaches the photodetector during a time comparable to the repumping time. These two basic quantities are related to the physical parameters of the OPM, and these relationships give rise to some fundamental tradeoffs between the different performance characteristics of the instrument. In the next few paragraphs, we enumerate the key parameters, and discuss the role they play in these fundamental performance tradeoffs:

1. **Density of the vapor and degree of spin polarization.** In Eq. (1) above, the shot-noise limit of the OPM is inversely proportional to  $n_k$ , the density of the alkali vapor in the optical absorption cell. This dependence on density reflects two underlying trends. First, increasing the vapor density increases the total number of alkali atoms in the cell, thus increasing the total optical absorption signal. Increasing the density also makes the cell optically thicker, so that the number of unabsorbed photons reaching the photodetector is smaller in relation to the optical absorption signal. The smaller current of unabsorbed photons reduces the noise in the optical measurement.

The optical absorption signal depends not only on the total number of alkali atoms, but also on the degree to which the pump beam is able to polarize the atomic spins. The importance of spin polarization is apparent in Eq. (1), where the noise in the magnetic measurements is inversely proportional to the population difference  $P_2^0 - P_1^0$  between the  $m=2$  and  $m=1$  spin states.

2. **Sensitivity and gradient tolerance.** The need to maintain the spin polarization can lead to constraints on the density of the alkali vapor, depending on whether we use an inert buffer gas in the alkali-vapor cell. The use of the buffer gas, in turn, affects the ability of the magnetometer to operate in the presence of magnetic gradients. As a result, there is a basic tradeoff between gradient tolerance and sensitivity.

In most optical pumping experiments, an inert gas, the buffer gas, is included with the alkali vapor in the optical absorption cell. As discussed in Sec. 6.1.2, eliminating this buffer gas allows the alkali atoms to move freely about the cell, averaging out the effects of magnetic gradients, and improving the gradient tolerance of the optically pumped magnetometer.

With an unbuffered cell, however, the density of the alkali atoms is constrained by a problem called radiation trapping [3]. When an alkali atom absorbs light from the pump beam, it will release its energy either by emitting another photon, or by colliding with another atom. With no buffer gas, the atoms suffer few collisions, and almost every atom that absorbs a photon from the pump beam will re-emit another photon. When the density of atoms becomes too great, a photon can be absorbed and reemitted several times before escaping the cell. Under these conditions, a significant fraction of the light in the cell is reemitted light, rather than light from the pump beam itself. This reemitted light is randomly polarized, and spoils the atomic spin alignment produced by the circularly polarized pump beam. As a result, an OPM with an unbuffered cell must use a relatively low vapor density determined by a compromise between the polarization of the atomic spins and the fraction of the pump beam absorbed by the atoms.

In spite of this constraint on the atom density, we observed noise less than one picotesla per root hertz with an unbuffered cell, in our previous experiments with a potassium-vapor magnetometer [8,9]. This noise is several times lower than that in conventional cesium or rubidium OPMs [1,2,4,5]. Furthermore, by using fluorescence detection to monitor the optical absorption (Sec. 6.1.1.3), we can compensate for the low atom density and achieve sensitivities near 0.1 picotesla per root hertz. With this approach, we can potentially achieve both high sensitivity and high gradient tolerance.

To achieve maximum sensitivity in a low-gradient environment, we would use a conventional buffer gas in the alkali-vapor cell. With a buffer gas, radiation trapping is suppressed because optically excited atoms decay through collisions with the buffer gas, and not by radiation. The lack of radiation trapping allows us to use much higher vapor densities without spoiling the alignment of the atomic spins.

**3. Length of the optical absorption cell.** In Eq. (1), the noise limit of the OPM is inversely proportional to the length of the optical absorption cell. As in the case of the vapor density  $n_k$ , this dependence reflects two underlying trends. Increasing the cell length both increases the total number of alkali atoms, thus increasing the optical absorption signal, and also makes the cell optically thicker, reducing the noise produced by unabsorbed photons. Because of the role played by the length of the cell, there is a basic tradeoff between sensor size and measurement sensitivity. For any given application, the optimum size of the cell will vary according to the requirements for sensitivity and the constraints on sensor size.

The length of the cell also affects the performance of the magnetometer in the presence of magnetic gradients (Sec. 6.1.2). This effect is one of several factors involved in the basic tradeoff between sensitivity and gradient tolerance.

**4. Diameter of the optical cell.** In Eq. (1) above, the noise limit of the OPM is proportional to  $A^{-1/2}$ , where  $A$  is the cross-sectional area of the optical absorption cell. In the case of a cylindrical cell, the noise limit becomes inversely proportional to the cell diameter  $D$ . This dependence reflects the fact that the increasing cell diameter increases the cell volume, and hence the total number of alkali atoms in the cell. In a buffered optical absorption cell, this apparent diameter dependence is a real one; we can increase the cell diameter without affecting the other experimental parameters, thus improving the sensitivity of the magnetometer.

For an unbuffered cell, however, we cannot increase the cell diameter without decreasing the density of the alkali atoms. In the absence of a buffer gas, radiation trapping will tend to spoil the polarization of the atomic spins. The effects of radiation trapping will scale roughly according to an optical thickness parameter  $n_k d_{char}$  where  $n_k$  is the density of the alkali vapor and  $d_{char}$  is a characteristic distance from a typical point in the cell to the outside walls of the cell. The maximum sensitivity, defined by the best compromise between vapor density and spin

polarization, will occur at a certain optimum value of this optical thickness parameter. For a cell whose diameter is much less than its length, the characteristic distance  $d_{char}$  will be proportional to the cell diameter. As a result, the optimum vapor density will be inversely proportional to the cell diameter. As a result, since the SNR in the optical measurement is proportional to the product of the cell diameter and the vapor density, the sensitivity of the magnetic measurements will be roughly constant as a function of the cell diameter, for an OPM using an unbuffered alkali vapor cell.

**5. Spin relaxation time: Sensitivity, frequency response, gradient tolerance, and choice of alkali species.** In Eq. (1), the noise in the magnetic measurement depends on  $T_2^{-1/2}$ , where  $T_2$  is the transverse relaxation time of the precessing atomic spins. This dependence reflects two competing trends: As  $T_2$  decreases, the Larmor resonance becomes broader, reducing the precision with which we can measure the Larmor frequency. At the same time, however, a shorter  $T_2$  allows us to repeat the measurement cycle more often, increasing the SNR in the optical measurement that we use to determine the Larmor frequency. This increased repetition rate partially compensates for the broader linewidth. The net effect is the square-root dependence shown in Eq. (1). (In order to increase the repetition rate of the measurement cycle, we would increase the intensity of the RF field and shorten the RF pulse in proportion to  $T_2$ .)

$T_2$  plays a key role in the tradeoffs between sensitivity, frequency response, and magnetic gradient tolerance. It is also crucial in deciding which alkali element to use in the magnetometer.

The spin relaxation time depends on such factors as the homogeneity of the magnetic field, the spin relaxing effects of wall collisions, and the intrinsic width of the atomic Larmor resonance. In cesium and rubidium OPMs, the effective spin relaxation time is determined by the width of the entire manifold of atomic spin transitions that make up the Larmor resonance. As a result, the effective spin-relaxation times for these elements are rather short, on the order of 10 milliseconds for cesium and 2 milliseconds for rubidium. With potassium, we use only a single spin transition, and the spin relaxation time is determined mainly by such effects as wall collisions and inhomogeneities in the magnetic field. We have observed spin-relaxation times longer than 100 milliseconds in our own experiments on optical pumping in potassium.

Because of this narrow Larmor resonance, OPMs based on potassium vapor are inherently more sensitive than those based on cesium and rubidium. A Russian group has demonstrated a potassium-vapor OPM with a noise floor of 0.1 picotesla per root hertz [1]. The advantage of using potassium is greatest when the environmental magnetic gradients are low, and the requirements for frequency response are modest. Under these conditions, we can take advantage of the long spin

relaxation time by using a weak, long RF pulse to measure the Larmor frequency with maximum resolution. Our sensitivity estimates below indicate an ultimate sensitivity limit below 0.1 picotesla per root hertz, with a repetition rate of roughly 10 hertz for the magnetic measurement cycle.

The advantage of potassium becomes less important in the presence of magnetic gradients. As the magnetic gradient increases, the spin relaxation time decreases. Eventually, we reach the point where the spin relaxation time is determined primarily by the gradient effects, and not by the intrinsic line width of the atomic spin resonance. In this regime, potassium, cesium, and rubidium OPMs become similar in sensitivity.

A similar trend arises as we increase the requirements for frequency response. To make the magnetometer respond more rapidly, we would use a shorter RF pulse so that we could increase the repetition rate of the magnetic measurement. The shorter RF pulse would reduce the resolution of the Larmor frequency measurement. In the mathematical description presented above, we would take this trend into account by replacing the spin relaxation time  $T_2$  by an effective value. In the limit where the RF pulse is short compared with the intrinsic  $T_2$ , this effective value of  $T_2$  would be proportional to the pulse length, and hence inversely proportional to the repetition rate of the measurements. In this limit, potassium, cesium, and rubidium will again produce roughly similar sensitivity limits.

#### 6.1.1.3 Sensitivity Estimates: Sensor Size and Optical Pumping Technique

In this section, we use the results of our sensitivity model to explore the tradeoffs between sensitivity, sensor size, and gradient tolerance. Our approach here is to start with the actual noise levels from our previous experiments with potassium magnetometers, and then use Eq. (1) to predict how the sensitivity will vary according to the experimental parameters and measurement technique.

1. **Baseline Sensitivity Estimate.** In previous work, we developed a potassium-vapor OPM, the free-precession magnetic detector (FPMD). We measured the noise in this instrument by taking the standard deviation of the individual magnetic readings taken on successive repetitions of the measurement cycle. The standard deviation of the individual measurements was roughly 0.85 picotesla, and each measurement represented approximately 100 milliseconds of data averaging. Assuming that the noise spectrum was white, these data indicate a noise spectral density of 0.5 picotesla per root hertz. The FPMD used a measurement technique somewhat different from that in the OIOPM. However, the basic physical parameters affecting the sensitivity were the same as those in the OIOPM, and we expect that the OIOPM's sensitivity, using the same experimental conditions, would be within a factor of two of the levels we measured with the FPMD.

The FPMD used potassium vapor in an unbuffered, wall-coated spherical cell 5 cm in diameter. It made its optical absorption measurements by monitoring the transmission of a probe beam through the alkali vapor cell. In the next few paragraphs, we estimate how the sensitivity of the instrument will be affected by changes in cell size and measurement technique.

**2. Lower Noise through Better Optical Pumping.** For some applications, it may be desirable to achieve noise levels well below 0.5 picotesla per root hertz. The noise floor in the FPMD was limited by the fact that we used an unbuffered alkali vapor cell. With this unbuffered cell, the atomic spin polarization deteriorated as we increased the vapor density in the cell. As a result, our best noise measurements were made at the rather low potassium vapor density of  $6 \times 10^9 \text{ cm}^{-3}$ . At this low density, the optical absorption signal, represented by the change in pump-beam transmission as the atomic spins rotated through 180 degrees, was only 1/30 of the total photon current in the probe beam. As a result, we had to measure a relatively small optical absorption signal in the presence of the shot noise produced by this much larger probe-beam current.

One way to improve the sensitivity of the OIOPM would be to introduce a buffer gas into the alkali vapor cell, suppressing radiation trapping and allowing us to use much greater vapor densities without compromising the spin polarization. With this approach, we might expect to see an optical absorption signal 1/3 as great as the total throughput of the pump beam. This increased optical signal would translate into a ten-fold improvement in the sensitivity of the OIOPM. That is, using an optical cell 5 cm in diameter, we would expect a shot-noise limited sensitivity of 50 femtotesla per root hertz. This expectation is supported by recent experiments in which a noise floor of 100 femtotesla per root hertz was observed in a potassium-vapor magnetometer [1].

**3. Better Sensitivity through Fluorescence Detection.** One advantage of unbuffered cells is that they increase the magnetometer's tolerance for magnetic gradients. This advantage is lost if we use a buffer gas to improve the optical pumping and increase sensitivity.

An alternative way to improve the sensitivity of the OIOPM is to change the way we monitor the absorption of the pump beam. In our previous experiments with potassium magnetometers, we measured the optical absorption by monitoring the transmitted pump beam. However, since we could use only a limited density of potassium vapor, most of the pump beam passed through the alkali vapor cell unabsorbed by the potassium atoms. These unabsorbed photons produced a large background current in the optical transmission measurements. The statistical fluctuation of this background current was the main source of noise in the optical measurement.

We can eliminate this background flux by fluorescence detection. In this technique, we place photodetectors around the periphery of the optical absorption cell, out of the path of the transmitted pump beam. With this arrangement, the photodetectors do not collect the large flux of unabsorbed pump-beam photons. However, the peripheral photodetectors do detect the fluorescence photons emitted by atoms that have absorbed light from the pump beam. In an unbuffered cell, nearly every optically excited atom will decay by fluorescence, and there will be roughly one fluorescence photon for every pump-beam photon that is absorbed. We can reasonably expect to collect as much as half of these fluorescence photons. As a result, our optical absorption signal will be comparable to that in the transmission measurement. In contrast with transmission detection, however, there will be no large background current due to the unabsorbed portion of the pump beam.

To estimate the resulting improvement in sensitivity, we note that the shot noise in the optical absorption measurement is proportional to the square root of the total number of photons collected. In our previous transmission measurement, the total number of photons was approximately thirty times the number of photons corresponding to the optical absorption signal [8,9]. If the alkali vapor removed a total of  $N$  photons from the pump beam, the photodetector would have collected a total of  $30N$  photons in the transmitted beam. Measured in terms of photons, the optical absorption signal would have been  $N$ , the total statistical noise would have been  $\sqrt{30N}$ , and the signal-to-noise ratio in the optical absorption measurement would have been  $N/\sqrt{30N} = \sqrt{N/30}$ . With fluorescence detection, the number of fluorescence photons produced would be essentially equal to the number of photons absorbed by the alkali vapor. If we collected half these fluorescence photons as they emerged from the cell, the optical absorption signal would be  $N/2$ . Since there would be no additional background flux due to the unabsorbed pump beam, the total number of photons collected would also be  $N/2$ , and the statistical fluctuation in the total photon count would be  $\sqrt{N/2}$ . The signal-to-noise ratio in the optical absorption measurement would be  $\sqrt{N/2}$ . This example suggests that, with fluorescence detection, we could improve the signal-to-noise ratio of the optical measurements by a factor of  $\sqrt{30/2} \sim 4$ . Using the 5-cm cell diameter from our previous examples, the resulting noise in the magnetic measurements would be roughly 0.1 picotesla per root hertz. This noise is more than an order of magnitude lower than that in the standard types of OPM.

#### 6.1.1.4 Sensitivity-Size Tradeoff: Compact Unit with Moderate Sensitivity

Our sensitivity model (Eq. 1) indicates that the sensitivity of the OIOPM will improve in proportion to the length and cross-sectional diameter of the alkali vapor cell. This trend indicates that we can trade sensitivity for sensor size, according to the demands of a given application. To illustrate this flexibility, we consider the cell dimensions and sensor size for two types of applications.

OPMs are most commonly used as simple magnetometers. That is, a single sensor is used to measure the magnetic field at one location in space. With a simple magnetometer, there is little reason to reduce the noise in the OPM below the fluctuations in the earth's magnetic field. In the vicinity of one hertz, these earth's field fluctuations have a spectral density in the vicinity of 3 picotesla per root hertz.

With this observation in mind, we anticipate that many applications of the OIOPM will require a noise floor of 3 picotesla per root hertz. In Sec. 6.1.1.3, we predicted that the OIOPM would have a noise of approximately 0.5 picotesla per root hertz, using potassium vapor, with an unbuffered spherical cell 5 cm in diameter. If all other parameters remain constant, our sensitivity model indicates that the noise in the OIOPM will scale as the inverse square of the cell diameter. Consequently, we would expect a noise floor of 3 picotesla per root hertz with a cell diameter of approximately 2 cm.

However, as we reduce the cell diameter, we may be able to increase the density of the alkali vapor, because the radiation-trapping effects that limit the vapor density should scale as the product of the cell diameter and vapor density. If we increase the vapor density in inverse proportion to the cell diameter, the magnetometer noise should scale only as first power of the diameter. In this case, we might achieve a noise floor of 3 picotesla per root hertz with a cell as small as one cm in diameter. Further research would be required, however, to determine whether some new limiting effect arises as we increase the vapor density by the required factor of five.

The example above assumes that we use an unbuffered alkali-vapor cell to maximize tolerance for magnetic gradients. It also assumes that we measure the optical absorption by detecting the transmitted pump beam. If we used a buffered cell, we could achieve our 3-picotesla sensitivity with a cell diameter of approximately 0.65 cm. If we use fluorescence detection, we could achieve the same performance with an unbuffered cell one cm in diameter.

Based on these estimates of the cell size, we can also estimate roughly the overall size of the sensor unit. An actual sensor would include the alkali vapor cell itself, together with thermal insulation, the DC/RF field coils, and the pump-beam optics. The field coils will be the main factor that determines the outer diameter of the sensor package. To ensure that the field coils produce sufficiently uniform fields, we anticipate that the package will be roughly twice as large in diameter as the cell itself.

The length of the magnetometer package will be determined mainly by the focal length of the pump-beam optics. The focal length will depend on whether or not we use a buffer gas in the alkali vapor cell. If we use a buffered cell, this focal length would be comparable to the cell diameter because we would have to expand the pump beam to sweep out almost the entire volume of the cell. Under these

assumptions, an OIOPM sensor unit would have a diameter of approximately 1.3 cm and a length of approximately 4 cm, using a buffered cell to achieve a noise floor of 3 picotesla per root hertz.

If we use an unbuffered cell, the focal length of the optics can be much less than the cell diameter because the mobility of the alkali atoms allows us to sample all of the atoms using a very narrow pump beam. In this case, both the length and the diameter of the sensor unit might be twice the cell diameter. The sensor unit might then have a diameter and length between 2 and 4 cm, with a sensitivity requirement of 3 picotesla per root hertz.

These sample calculations indicate that a very compact OIOPM can provide a noise floor as low as the fluctuations of the ambient magnetic field. This noise will be adequate for many applications in which a single sensor unit is used to measure the magnetic field.

#### **6.1.1.5 Sensitivity-Size Tradeoff: Maximum-Sensitivity Configuration**

Although the ambient magnetic field fluctuates at the level of a few picotesla per root hertz, magnetic measurements at lower noise levels become possible if one uses magnetic difference measurements to null out some of the background noise. This noise cancellation is possible because the fluctuations of the ambient magnetic field usually arise from sources much farther away than the objects that the instrument is being used to detect. The background field from these distant sources is much more uniform spatially than the signals from the nearby objects of interest. As a result, the background noise can partially be nullified by subtracting the magnetic fields measured at two or more locations.

The simplest form of spatial noise cancellation is the first-order magnetic gradiometer, where the difference between two sensors is used to determine one of the spatial first derivatives of the magnetic field. Such gradient measurements, based on conventional alkali-vapor OPMs, are often used in geophysical magnetic surveys from aircraft. SQUID-based magnetic gradiometers are also being developed for mine detection and other Navy applications.

In magnetic gradient measurements, the magnetic-field difference between the sensors will have much smaller fluctuations than the ambient magnetic field itself. As a result, sensors with noise levels below the ambient-field fluctuations are potentially useful in such gradient measurements. Extremely sensitive sensors are, in fact, necessary in many cases because the magnetic gradients from a source of interest will fall off much more rapidly with distance than the magnetic fields themselves.

In Sec. 6.1.1.3 above, we estimated that the OIOPM could have a noise floor of roughly 50 femtotesla per root hertz, using a buffered potassium-vapor cell 5 cm in diameter. If we increased the cell diameter to 10 cm, the estimated noise floor would drop to 12 femtotesla per root hertz. This noise level is competitive with that achieved using SQUID magnetometers. Two such sensor units, separated by a distance of one meter, would measure magnetic-field gradients with a sensitivity of  $10^{-14}$  tesla per meter per root hertz. This sensitivity is several times better than that achieved using SQUIDs, since existing SQUID gradiometers are limited to baselines of a few inches.

In this particular example, each sensor unit might be 30 cm (12 inches) long, and 20 cm (8 inches) in diameter. Such sensors would be too bulky for some applications, such as remotely deployed, disposable sensor arrays, but might be useful in airborne or towed magnetic gradiometers for detecting mines, submarines, and other magnetic anomalies.

### 6.1.2 Tolerance for Magnetic-Field Gradients

If an optically pumped magnetometer is deployed near the ground or near the ocean bottom, it may be subjected to magnetic-field gradients due to the proximity of magnetic rocks or other magnetic debris. Sufficiently large field gradients will interfere with the operation of an optically pumped magnetometer by increasing the linewidth of the atomic Larmor resonance. The increased linewidth will reduce the precision of the Larmor frequency measurement, reducing the sensitivity of the magnetometer. This gradient problem is a serious one with at least one type of OPM, the helium-3 nuclear magnetometer. When this sensor is deployed on the ocean bottom, special precautions are taken to place the sensor a few feet above the bottom itself. Alkali-vapor OPMs are inherently more tolerant of magnetic gradients than the helium-3 magnetometer [10]. However, in designing the OIOPM for specific applications, we will need to take into account the requirements for magnetic gradient tolerance. These requirements will affect a variety of design parameters including the dimensions of the optical absorption cell, and the intensity of the RF fields and pump beam.

Gradient tolerance also has implications for the method we use to suppress the relaxation of atomic spins at the walls of the alkali-vapor cell. Most OPMs use a buffer gas to impede the diffusion of the optically pumped atoms to the cell walls. This method effectively immobilizes the atoms, so that each atom experiences the magnetic field at a different location within the cell. Under these conditions, the width of the Larmor resonance is directly related to the variation of the magnetic field over the cell. An alternative approach is to apply a special coating to the wall, so that many wall collisions are required on average to flip the spins of the atoms. With the wall coating, we can remove the buffer gas, and allow the alkali atoms can move freely about the cell. The motion tends to average out the effect of a magnetic gradient [7].

We developed a mathematical model for this averaging effect as part of our recent magnetometer study for the Navy (Appendix A3.1). In this model, we consider the contribution to the transverse spin relaxation rate due to the statistical variation of the magnetic fields seen by different atoms in the cell. We then define the maximum tolerable gradient to be that gradient for which this statistical relaxation effect becomes comparable to the intrinsic linewidth produced by all other sources of line broadening.

This analysis indicates that removing the buffer gas can enhance the gradient tolerance of an OPM by as much as a factor of 100, depending on parameters such as the dimensions of the optical absorption cell and the relaxation rate of the atomic spins in the presence of the pump beam. The benefit of motional averaging is especially important when the spin relaxation time is long compared with the time required for an atom to traverse the cell. This condition applies particularly to the most sensitive OPMs, which rely on having a very narrow Larmor linewidth. For example, our previous potassium-vapor magnetometer achieves a noise floor of approximately 0.5 picotesla per root hertz with an unbuffered cell 5 cm in diameter, using the relatively low pump-beam intensity that maximized measurement sensitivity [8,9]. Applying our model to this cell, we find that this sensor's noise would begin to increase substantially at a magnetic gradient of roughly 350 nanotesla per meter. If we used a buffer gas in this cell, the sensitivity would have deteriorated rapidly in gradients above 7 nanotesla per meter.

Our analysis indicates that we can adjust the sensor parameters to trade measurement sensitivity for gradient tolerance. With unbuffered cells, the models in Appendices A2.1 and A3.1 indicate that the maximum gradient varies with the inverse square of the longest dimension of the cell, while the noise floor of the instrument varies only as the inverse first power of the length of the cell. Thus, in the example above, if we reduced the cell diameter to 2.5 centimeters in the example considered above, the noise floor would increase to 1.0 picotesla per root hertz, but the maximum gradient would increase to approximately 1400 nanotesla per meter.

As explained in Sec. 6.1.1.2, the use of unbuffered cells will involve some compromise of sensitivity. In the absence of a buffer gas, radiation degrades the efficiency of optical pumping when the alkali vapor becomes too dense. This effect forces us to use a lower than optimum vapor density, so that the optical absorption signal is only a small fraction of the transmitted pump beam. This weak signal, together with the large background flux of unabsorbed photons, produces a relatively low signal-to-noise ratio in the optical absorption measurement.

In spite of this constraint on the atom density, our Free-Precession Potassium Magnetometer used an unbuffered cell to achieve a noise floor below one picotesla per root hertz. This noise is several times lower than that in conventional cesium or rubidium OPMs [1,2,4,5]. Furthermore, by using fluorescence detection to monitor the optical absorption (Sec. 6.1.1.3), we can eliminate the noise produced by the large flux of unabsorbed photons. This approach partially compensates for the low atom

density, and may achieve sensitivities near 0.1 picotesla per root hertz. This very high sensitivity can be achieved without losing the gradient tolerance of the unbuffered alkali-vapor cell.

Motional averaging becomes less effective in the extremely large gradients, tens of thousands of nanotesla per meter, that may be encountered near large concentrations of iron. In such large gradients, the spin relaxation time becomes so short that the atoms make only a few passes across the cell during the relaxation time. These few passes are ineffective in averaging out the effects of the inhomogeneous magnetic field. Under these conditions, a buffered cell may actually provide slightly better sensitivity than an unbuffered cell, since it permits us to use a higher density of alkali atoms.

With unbuffered cells, however, we can adjust the OPM for different magnetic gradients, without modifying the equipment, simply by electronically adjusting the intensity of the RF field. In low gradients, we would obtain maximum sensitivity by using a weak RF field, and a long RF pulse. This approach would maximize the resolution of our Larmor frequency measurement. As the gradient increased, we would preserve as much sensitivity as possible by increasing the RF intensity and shortening the RF pulse in proportion to the increased Larmor linewidth produced by the inhomogeneous magnetic field. The shorter RF pulses would partially compensate for the increased linewidth by increasing the number of measurements we could make in a given time. In moderately large gradients, the unbuffered cells would provide better sensitivity than buffered cells. In the highest gradients, the unbuffered cells would be somewhat less sensitive, but this penalty would be small if we used fluorescence detection.

Our analysis shows how we can adjust the OIOPM for optimum performance in differing magnetic environments. For the maximum sensitivity in low gradients, we would use a buffer gas to suppress radiation trapping, so that we could use a large density of alkali atoms in the optical absorption cell. For maximum sensitivity in moderately large gradients, we would dispense with the buffer gas, in order to take advantage of motional averaging. With the unbuffered cell, we could optimize the sensitivity in a given gradient simply by adjusting the intensity of the RF field. Finally, for gradients so large that motional averaging becomes ineffective, we would again use a buffer gas to maximize the number of potassium atoms in the cell. In this regime, we would accept the increased Larmor linewidth produced by the field gradient, and regain as much sensitivity as possible by using a very intense RF field.

### 6.1.3 Drifts and Heading Errors

*"We will refine our models of low-frequency drift and heading error, so as to define stability requirements for the electronics."*

One important advantage of OPMs is that they measure the magnitude of the magnetic field in a way that is inherently insensitive to systematic errors. That is, the OPM measures the field not through its direct effect on some electronic device, but by

observing the Larmor frequency of the optically pumped atoms in the presence of the field. The proportionality between this Larmor frequency and the total field is, to a first approximation, an intrinsic property of the alkali atom.

This fundamentally accurate measurement process means that OPMs tend to have very low long-term noise. The measurement process also makes OPMs rather insensitive to errors due to the rocking motion of a moving platform. In essence, since the Larmor frequency of the alkali atoms is determined primarily by their interaction with the ambient field, and not by their interaction with the instrument, the total-field measurement is nearly independent of the orientation of the instrument. (What does vary with orientation in conventional OPMs is the signal-to-noise ratio with which we can observe the Larmor precession. This variation in sensitivity is what produces dead zones. Maintaining full sensitivity at all orientations is the main goal of the present program.)

In contrast, a vector magnetometer, such as a fluxgate, SQUID, or magnetoresistive sensor, measures a component of the magnetic field along an axis that rotates with the instrument. This field component is proportional to the cosine of the angle between the measurement axis and the ambient magnetic field, and the magnetic measurement thus changes substantially as the instrument rocks back and forth. Since the ambient earth's field is much larger than the typical magnetic signals of interest, slight rocking motions of the instrument can create measurement noise much larger than the desired signals.

OPMs are orders of magnitude less subject to motional errors than are vector magnetometers. However, OPMs do have subtler motion effects and low-frequency drifts, arising from the fact that the measurement process slightly perturbs the atomic Larmor precession [1,7]. Cesium and rubidium magnetometers typically have total heading errors near one nanotesla [1,2,4-6]; that is, the reading varies by approximately one nanotesla as the instrument is rotated through an angle of 180 degrees. This total heading error corresponds to a fluctuation of approximately 10 picotesla if the sensor is rocked through an angle of one degree. If implemented using cesium or rubidium, the OIOPM would probably have heading errors comparable to these existing instruments.

The OIOPM can potentially provide much lower heading errors and drifts. This improvement can be achieved by using potassium instead of rubidium or cesium. The heading errors in cesium and rubidium OPMs arise in part from the fact that the Larmor resonance in cesium and rubidium has a complex lineshape involving a manifold of quantum-mechanical spin transitions [1,7]. In effect, the measured Larmor frequency is a weighted average over all these transitions, and this average changes according to the experimental conditions. In potassium, however, the individual spin transitions are so well separated that the magnetometer can work with a single transition. This approach greatly reduces the effects of sensor motion [1,7]. Alexandrov and co-workers

have demonstrated a locked-oscillator magnetometer based on this single-line approach [1]. Our recent potassium-vapor magnetometer also used a single spin transition [8,9], although we have not systematically measured its heading errors.

With a single-line OPM, the heading errors and drifts will arise from subtle perturbations of the spin transition. In our recent Navy sensor study, we analyzed these perturbations in detail (Appendix A2.3). We considered two main sources of error: the collisions between the potassium atoms, and the effects of the applied radio-frequency depolarizing field. We found that the collisional effects would produce measurement drifts less than 0.1 picotesla (100 femtotesla), provided we controlled the temperature of the alkali-vapor cells to within 0.3 K. The RF field would produce drifts less than 0.1 picotesla if we kept the RF power constant to within 10%, or 0.01 picotesla if we kept the RF power constant to 1%. This analysis establishes the stability requirements for the two components of the measurement electronics that have the main effect on the stability of the magnetic measurement.

Of the two effects considered, only the RF field will contribute to the heading error in the OIOPM. Our quantum-mechanical perturbation analysis indicates that the total measurement shift produced by the RF field will be approximately one picotesla. This shift places an upper bound on the magnitude of the total heading error in the OIOPM. We can actually make the heading errors much smaller than one picotesla by adjusting the RF field to keep constant its component transverse to the ambient magnetic field. To adjust the field, we would use inexpensive sensors with, say, 1% accuracy to monitor the orientation of the ambient field. We would then adjust the RF field by varying the currents in a set of three orthogonal field coils. If the transverse RF field is constant to within 1%, the total heading error of the OIOPM will be only 0.01 picotesla (10 femtotesla). The measurement fluctuations due to small rocking motions would be even smaller, well below the intrinsic shot-noise sensitivity limit of the instrument.

During Phase I, we have identified an additional effect that could conceivably produce heading errors in the OIOPM. In our initial experiments, the atomic spins appeared to lose a little bit of their polarization during the adiabatic field cycling. Most likely, this slight polarization loss will only cause a subtle variation in the signal-to-noise ratio of the OPM as a function of heading. However, the polarization loss would contribute to the heading errors of the instrument, if the loss mechanism somehow distorted the lineshape that characterizes the optical pumping signal as a function of the applied RF frequency. That is, the magnetic measurement would only be affected if the loss of polarization were different when the RF frequency was on one side of the Larmor lineshape than when the RF frequency was on the other side of the line. We are not aware of any reason why such a distortion should occur. However, we will have to identify the mechanism that produces the polarization loss before we can confidently rule out the possibility of a heading error due to non-symmetric spin-loss effects during the adiabatic field cycling. We plan to investigate the mechanism of polarization loss during Phase II.

In the meantime, a crude worst-case calculation suggests that this contribution to the heading error will almost certainly be smaller than the heading errors in existing cesium and rubidium OPMs. We suppose that approximately ten percent of the spin polarization is lost due to imperfections in the adiabatic field change. We also assume as a worst case that this loss only occurs when the RF frequency is on one side of the Larmor resonance, and no polarization at all is lost when the RF frequency is on the other side of the resonance. Under these circumstances, the center of gravity of the resonance might shift by roughly one tenth the characteristic width of the line. In accordance with previous experiments with potassium magnetometers, we can assume conservatively that the spin relaxation time  $T_2$  of the potassium atoms is at least 0.2 seconds. In this case, we can adjust the intensity of the RF field so that the characteristic width of the Larmor resonance is roughly  $1/T_2$ , or 5 Hz. The shift of the line due to spin loss would then be at most 0.5 Hz, which is equivalent to a magnetic-field error of roughly 70 picotesla.

In comparison, the outputs of cesium and rubidium OPMs typically vary by roughly 1000 picotesla if the instrument is rotated 180 degrees with respect to the ambient magnetic field. We expect that the actual heading error in the OIOPM will be much smaller than the estimate above, both because we can improve the efficiency of the adiabatic field cycling, and because there is no apparent reason why the loss of spin polarization should be different on the two sides of the Larmor lineshape.

#### **6.1.4 Motional Noise Due to Gyroscopic Effects**

In addition to the heading error produced by the perturbing effect of the measurement process, OPMs are also subject to motional noise produced by gyroscopic effects. These effects arise because the rotational velocity of the measuring instrument changes the apparent precession frequency of the optically pumped species. The importance of this effect is largest where the gyromagnetic ratio of the precessing species is low, and the rotation rate of the platform is a relatively large fraction of the Larmor frequency being measured. Consequently, gyroscopic errors can be significant in the helium-3 magnetometer, where the precessing species is a helium-3 nucleus with a Larmor frequency of only 3 kHz or so in the earth's magnetic field. These errors are much smaller in alkali-vapor magnetometers, including the OIOPM, since the precessing alkali atoms have Larmor frequencies of several hundred kHz in the earth's field. Appendix A3.5 presents a sample calculation that indicates how large the gyroscopic measurement fluctuations might be under typical operating conditions.

#### **6.1.5 Pumping with Laser Diodes**

*"We will investigate the feasibility of using laser diodes instead of vapor discharge lamps for the optical pumping. Laser diodes may use less power and have greater lifetimes than the potassium-vapor electrodeless discharge lamps now used. However, tuning the laser diodes to the potassium spectral lines may be a problem."*

In conventional OPMs, the pump beam is produced by an electrodeless discharge lamp (EDL). The EDL uses a radio-frequency plasma discharge to excite optical emission in a vapor of the same alkali element that is being used in the optically pumped magnetometer. This approach automatically produces light at the spectral wavelengths required for optical pumping. However, the RF discharge requires complex RF electronics, and typically consumes several watts of electrical power. In addition, the lamp bulbs themselves have limited lifetimes which may become a problem in long periods of unattended operation.

To produce a simple, inexpensive sensor that consumes a minimum of power, we plan to use solid-state laser diodes to produce the pump beam for the OIOPM. Laser diodes, used mainly in fiberoptic communications, are ideal light sources for the disposable, air-dropped OPM. They are simple, inexpensive, and mass-produced, they require no complex radio-frequency electronics, and they convert a large fraction of the supplied power into light. They are also inherently rugged, in that the entire laser is integrated onto a single semiconductor chip. Even the laser cavity is integrated; the cleaved edges of the chip act as the mirrors of the cavity. As a result, there is no delicate mirror assembly that would have to be adjusted to within a wavelength of light.

When we first looked into laser pumping, we were concerned with two main problems. The first concern was obtaining laser diodes that would produce light at the very specific wavelengths absorbed by the alkali atoms. Laser diodes are only available in narrow wavelength bands that are fixed by the basic characteristics of the materials used in the diode itself. The output wavelength can be adjusted by varying the temperature of the diode, but only over a limited range. Furthermore, many laser diodes tune discontinuously with temperature; that is, the output wavelength changes smoothly with temperature over some range, and then skips abruptly to a new value. This discontinuous tuning means that, for a given batch of diodes, there may not be any temperature at which the output wavelength actually matches the spectral absorption line of the alkali atoms.

Our second concern was that the output wavelength distribution of the laser diode might be much broader than the absorption lines of the alkali atoms. This broad linewidth would be a problem in measuring the transmission of the pump beam, since a great deal of light would reach the photodetector at wavelengths outside the absorption band of the alkali atoms. This additional light would increase the statistical noise in the optical measurement, without providing any useful information about the spin state of the alkali atoms.

During Phase I, we reexamined both potential problems. We discovered that laser diodes are available, at the rubidium  $D_2$  (780 nm), cesium  $D_2$  (852 nm) and cesium  $D_1$  (984 nm) absorption lines, with wavelength distributions much narrower than the Doppler-broadened absorption lines of the atomic vapor. These solid-state light sources have already been used for optical pumping of cesium and rubidium in both atomic beams [11-15] and ordinary optical absorption cells [16-18]. In these existing

light sources, the laser diode is tuned to the required wavelength by using a small resistance heater or Peltier cooler to adjust its temperature. For fine tuning, small temperature adjustments are made by varying the DC bias current to the diode. Because the diodes tune discontinuously with temperature, it is necessary to test more than one device before selecting one that tunes through the desired wavelength rather than skipping over it. However, the devices are inexpensive enough to make this approach viable.

This prior work clearly indicates the feasibility of laser pumping in the OIOPM. We can use laser pumping for cesium and rubidium by essentially copying the technology developed in prior work. An OIOPM based on cesium or rubidium would have sensitivity and heading errors comparable to those of existing cesium and rubidium OPMs.

As discussed in Secs. 6.1.1 and 6.1.3, an OIOPM based on potassium vapor would have greater sensitivity and lower heading errors than most previous OPMs. Our investigation indicates that laser pumping in potassium is possible, with a modest R&D effort to modify the characteristics of existing laser diodes. The key issue will be to shift the output wavelength of existing laser diodes to match the  $D_1$  absorption line of potassium (770 nm). Our best information in this area comes from Dr. Randy Klein at Spectra Diode Laboratories in the San Francisco Bay area. Laser diodes are already available at 780 nm. Our discussion with Dr. Klein brought out the following key points:

1. Tuning laser diodes to 770 nm is not a completely trivial matter, even though such devices are available commercially at 780 nm. Due to some fundamental limitations in the properties of the laser materials, the output power available from the laser diodes drops off rapidly as their doping is changed to produce wavelengths shorter than 780 nm. However, laser diodes at low powers have worked at wavelengths as short as 750 nm. Consequently, the required intensity of the pump light is crucial in determining the feasibility of laser pumping for potassium.

2. Fortunately, our power requirements are very modest. The peak optical power will depend on the number of photons required for repumping, and the time allotted to the repumping phase of the measurement cycle. During the repumping process, there will be roughly one pump-beam photon absorbed for each atom in the cell. We estimate that there will be roughly  $10^{12}$  or  $10^{13}$  atoms in the cell. Since only a fraction of the pump beam may be absorbed by the atoms, we assume that the laser diode needs to supply roughly  $10^{14}$  photons during the repumping phase. We would like the repumping time to consume no more than, say, ten percent of the measurement cycle. The length of the cycle will be comparable to the  $T_2$  of the alkali atoms, or roughly 100 milliseconds. Thus, we need a laser diode that produces  $10^{14}$  photons in  $10^{-2}$  seconds. Since each photon corresponds to roughly one electron volt of energy, the optical power in the pump beam comes to approximately 2 milliwatts. In comparison, Dr. Klein from SDL estimates that even the lowest-power laser diodes produce approximately 10 milliwatts.

These two points indicate that, because of our modest power requirement, it is feasible to develop laser diodes for optical pumping in potassium, in spite of the fundamental limitations on laser diode characteristics at the shorter wavelengths. Given this basic feasibility, we considered three strategies for obtaining an actual laser-diode source at 770 nm:

1. **Temperature tuning alone.** We considered the possibility of tuning laser diodes to 770 nm by simply cooling them. The output wavelengths of laser diodes vary with temperature, and it is a common practice to shorten the output wavelength of a laser diode by cooling it below room temperature. In fact, commercially available laser diodes often have small Peltier coolers incorporated in the device package. The availability of these simple, compact, inexpensive cooling systems makes temperature tuning an attractive possibility. However, temperature tuning alone will probably not produce the wavelength we require. The shortest-wavelength devices commercially available produce 780-nm light at 25 Celsius. Since the wavelength decreases by only 0.3 nm per degree Celsius, these devices would have to be cooled to -8 Celsius to produce light at 770 nm. Unfortunately, the Peltier coolers only reach -10 Celsius or so, and the cooler itself needs to be a few degrees colder than the laser die itself in order to conduct sufficient heat out of the diode. More elaborate coolers, such as closed-cycle refrigerators, would be too expensive, complicated, and unreliable.

2. **Temperature tuning with preselection.** Due to variations in fabrication, laser diodes have a statistical spread in their output wavelengths. We can take advantage of this variation to reach 770 nm with somewhat less cooling. One model from SDL has a nominal wavelength of 780 nm with a specified variation of +/- 5 nm. This specification translates into roughly a 2-nm standard deviation for the wavelength. If we select individual diodes that are at least one standard deviation below the mean, their wavelength will be only 778 nm at 25 Celsius, and they will reach 770 nm at -2 Celsius. This temperature is comfortably within the range of Peltier coolers. Because of discontinuous tuning, Dr. Klein estimated that only one third of the diodes selected would actually produce the specific wavelength required for pumping potassium.

3. **Temperature tuning plus redoping.** Pre-selecting laser diodes is probably an adequate approach for a research program that demonstrates the capabilities of the potassium-vapor OIOPM. However, to manufacture an instrument in quantity, we would want to change the wavelength distribution of the diodes themselves so that most of the devices could be tuned to 770 nm. With this modification, we would not have to test and reject many diodes in order to find a few that produced the desired light. The wavelength distribution can be shifted by altering the doping of the diodes, and Dr. Klein estimates that this change would require several person-months of labor. This analysis indicates that, with a reasonable investment in light-source development, we can develop and manufacture a potassium-vapor OPM with laser pumping.

In addition to obtaining laser diodes that can produce the right wavelength, we also need to stabilize the laser output at the atomic absorption line. In existing laser pumping systems for cesium and rubidium, coarse tuning is accomplished by controlling the temperature of the laser diode. (The temperature can be adjusted using one of the small resistance heating stages or thermoelectric coolers that are commonly used in temperature-sensitive electronics.) The wavelength is stabilized on the atomic absorption line by monitoring the wavelength, and using a feedback loop to adjust the bias current supplied to the laser diode. The existing laser pumping systems monitor the laser wavelength by passing a portion of the light through an optical interferometer or an auxiliary alkali-vapor cell. This approach requires a separate photodetector, vapor cell or interferometer, beam splitter, and other optics, all for the sole purpose of controlling the laser wavelength [11-18].

This basic wavelength-feedback system appears suitable for the OIOPM. However, we propose to simplify the tuning system somewhat by eliminating the auxiliary cell or interferometer. In our proposed system, the laser light passes first through a collimating lens and a circular polarizer, then through the alkali-vapor cell, and finally to a silicon photodetector. The photodetector monitors the absorption of the laser light by the alkali vapor, and this photoabsorption signal is used in a feedback loop to control the laser bias current, and keep the laser wavelength centered on the atomic absorption line.

In this wavelength control loop, the bias current is modulated rapidly, sweeping the laser wavelength over an interval comparable to the natural width of the atomic absorption line. The wavelength modulation produces an oscillating signal at the photodetector, reflecting the wavelength-dependent absorption of the laser light by the alkali vapor. If the wavelength modulation is exactly centered on the absorption line, this oscillating photodiode signal will contain only the even harmonics of the modulation frequency. However, if the wavelength sweep is not centered on the absorption line, the photodiode signal will contain a component at the sweep frequency. This first-harmonic component is used as an error signal to adjust the DC component of the bias current, centering the wavelength modulation with respect to the atomic absorption line.

#### **6.1.6 Fluorescence Detection and Laser Pumping**

*"To make use of laser diodes, we will evaluate an alternative method for monitoring the absorption of the pump beam. Since the light from the laser diode has a much broader spectral width than the absorption lines of potassium, a large amount of pump light will pass through the optical pumping cell without interacting with the potassium vapor. This additional light will add to the noise in measuring the transmission of the pump beam. However, instead of monitoring the transmitted beam, we can measure the pump-beam absorption by detecting the light reemitted by optically excited atoms. This fluorescence would be detected using photodiodes that were mounted at the sides of the optical pumping cell, out of the path of the transmitted pump beam."*

In our Phase-I statement of work, we proposed to evaluate fluorescence detection as a way of getting around the signal-to-noise problems associated with the use of a broad-line source in an optical absorption measurement. This plan was based on the assumption that laser diodes would produce linewidths too large for efficient optical measurements in the conventional transmitted-beam mode. However, our subsequent investigation indicates that this assumption was too pessimistic; laser diodes can in fact produce linewidths more than narrow enough for efficient optical transmission measurements. Consequently, fluorescence detection is not necessary as a way of accommodating the characteristics of laser diodes.

However, as discussed in Sec. 6.1.1.3, fluorescence detection does give us a way to improve the sensitivity of the optical measurements in unbuffered cells where the alkali atoms only absorb a small fraction of the pump beam. This approach may be useful in applications where the presence of large magnetic gradients makes it desirable to use unbuffered cells.

#### **6.1.7 Low-Power Operation of the OIOPM**

*"We will estimate of the power consumption of the instrument, including the light source, cell heaters, magnetic-field coils, and associated electronics."*

In some applications, such as floating sensor packages, remote sensor arrays, and hand-held instruments, the OIOPM will have to operate for long periods on battery power. Low power consumption will be important for these applications.

We modeled the power consumption of the OIOPM as part of our previous Navy sensor study (Appendix A3.2). We found a total power consumption of approximately 320 milliwatts, including less than 10 mW for heating the alkali-vapor cells, approximately 40 mW for the laser-diode light source, and approximately 265 mW for the measurements electronics. This power consumption corresponds to an operating life of approximately seven months with 5 kilograms of lithium-oxihalide batteries.

This preliminary analysis already indicates that the new OPM will be suitable for long periods of unattended operation. However, the power consumption of the instrument can be made much lower than this rather conservative analysis indicates. The main area for improvement is in the measurement electronics, which consume more than two-thirds of the power in our initial estimates. Our previous analysis was based on an electronic design that was not specifically engineered to reduce power consumption. This design included a digital frequency synthesizer (50 mW), several digital-to-analog convertors (80 mW total), and 12 operational amplifiers of standard (OP-21 and OP-97) design (60 mW total). We anticipate improving upon this initial design by replacing these standard components with specially designed low-power circuitry.

A second way to reduce the power requirements is to operate the OPM on a low duty cycle. To illustrate the possibilities, we can imagine an OIOPM that is mounted on a remote floating platform in order to monitor the movements of ships and submarines. This magnetometer would only need maximum time resolution when it was being used to characterize the dipole profile of a vehicle passing nearby. Most of the time, the magnetometer would either be watching for the approach of a distant vehicle, or waiting for a ready signal generated by other parts of the surveillance system. During these periods of reduced activity, we can greatly reduce the drain on the system's batteries by making measurements only as frequently as needed.

With these varied requirements in mind, we can define four different levels of activity, with correspondingly different power requirements:

1. **Quiescent.** In some cases, it may be desirable to turn off the magnetometer, and then activate it when needed. For this mode of operation, the key parameter is the time required for the instrument to start working normally after being turned back on. In the new OPM, the start-up time will probably be determined by the need to stabilize the alkali-vapor cells at their operating temperature of 60 to 70 degrees Celsius. We envision warm-up times of three to ten minutes, depending on the short-term power available for the heaters and the sophistication of the temperature control circuit used. A more detailed investigation of warm-up times may become appropriate during the latter part of Phase II.
2. **Ready.** With the exception of the alkali-vapor cells, most components in the OPM will have very short warm-up times. One possible mode of operation is a ready state, in which the alkali-vapor cells are maintained at their operating temperature, but the rest of the measurement electronics are turned off to save power. In this mode, the main power drain will be the cell heaters themselves. This power drain will be determined mainly by the thermal insulation around the cells. According to our recent OIOPM study, this loss can be less than 10 mW, if we insulate the cell oven using an evacuated enclosure, using aluminized mylar to minimize radiative heat transfer (Appendix A3.2.2).
3. **Threat Detection.** To detect approaching vehicles, the OPM would make measurements every several seconds. To achieve a sensitivity of roughly one picotesla or less, each measurement would require roughly one second, so that the full electronics package would be operating perhaps 10% of the time. In this mode, the total electric power would include approximately 10 to 30 mW for the measurement electronics, in addition to the power required by the cell heaters.
4. **Maximum Resolution.** To characterize a passing vehicle, the OPM would operate 100% of the time, measuring magnetic signals at frequencies of tens of hertz. In this mode, the instrument would consume 100 to 300 mW of power.

During Phase II, we plan to design a low-power electronics package for the new ground sensor. We will use this design to analyze in detail the power consumption of the electronics package. We will also reexamine the other subsystems including the cell heaters and laser light source. Based on this analysis, we will predict the power requirements of the new OPM at several different levels of activity.

### **6.1.8 Interfacing the OIOPM to a Sensor System**

In addition to the fundamental issues listed in our Phase-I statement of work, we have done some preliminary thinking about other issues that affect the way the OIOPM integrated with the rest of a sensor system. These issues include (1) compact, rugged packaging, (2) required supply voltages and currents, and (3) environmental considerations such as temperature limits and magnetic gradients.

#### **6.1.8.1 Rugged Packaging**

In some applications, it will be important that the OIOPM be able to withstand rough handling. With this requirement in mind, we note that our optical pumping technique involves no components that have to be maintained in a very precise alignment. Indeed, the new OPM will be less fragile than some sensors, such as hydrophones, that are already routinely used in air-dropped sonobuoys.

The packaging scheme for the OIOPM will have to meet three main criteria. First, it must avoid rupturing the alkali-vapor cells. At the same time, the alkali-vapor cells must be insulated thermally from their environment, so that they can be maintained at temperatures near 70 degrees Centigrade without excessive power consumption. The sensor package must also keep the optical system well enough aligned so that most of the pump light makes it through the absorption cell to the photodetector. However, no great geometrical accuracy is required, since the optical path is only a few centimeters long, and the capture area of the photodetector can be as large as one centimeter in diameter. The pump beam can therefore be misaligned by several degrees and still be collected by the detector.

In this design, the light source, optics, photodetector, and electronics are all packed together in a solid structure. All fragile components in the structure are potted in epoxy or some other suitable matrix for mechanical support. The alkali-vapor cell is supported by a semi-rigid foam which provides thermal insulation, mechanical support, and shock absorption. The foam packing entirely surrounds the cell, except for narrow openings at each end for the incoming and outgoing pump beam. The cell itself is made of a durable plastic that is transparent to the near-infrared pump beam. (We have had good results with plastic lenses in the cesium-vapor magnetometers that we previously manufactured for the Navy.)

### 6.1.8.2 Voltage Requirements

The new OPM will require no unusual electric supply voltages. All components of the system, including the laser diodes, cell heaters, photodetector, and measurement electronics, can operate at voltages in the range of  $\pm 5V$ .

### 6.1.8.3 Temperature Requirements

The new OPM will probably tolerate ambient temperatures as high as 60 degrees Celsius, and could in principle be designed to tolerate much higher temperatures. The most fundamental temperature restriction will arise from the need to control the density of the alkali atoms in the optical absorption cell. The vapor density is normally controlled by adjusting the temperature of a reservoir of the liquid alkali metal. In normal operation, we would control the reservoir temperature by varying the current in an electrical resistance heater. This approach works only if the ambient temperature is at least slightly below the desired reservoir temperature.

In our previous work with potassium-vapor magnetometers, we obtained the best signal-to-noise ratio at a potassium reservoir temperature of approximately 55 degrees Celsius. There are several possible ways to operate the OPM at higher temperatures. One approach would be to introduce another component into the alkali-metal reservoir, suppressing the vapor pressure of the alkali component. Another approach would be to use a buffer gas in the alkali-vapor cell, suppressing radiation trapping and allowing us to increase the density of atoms in the cell. We could also increase the atom density without using a buffer gas, as long as we used a narrower cell to raise the atom density required to produce radiation trapping. Doubling the density of the vapor in our previous experiments would have increased the optimum operating temperature by several tens of degrees.

### 6.1.8.4 Magnetic Environment

To exploit the high sensitivity of the OIOPM, it will be important to make sure that the rest of the sensor system does not itself generate excessive magnetic fields or field gradients. There will be two major engineering requirements:

First, fluctuating electric signals will need to be routed in twisted pairs or other geometries that avoid large open loops of current. The new OPM will detect fluctuating magnetic fields of order  $10^{-12}$  tesla, and fields of this magnitude can be produced by relatively small current loops. For example, a field of one picotesla corresponds to a current of 300 microamperes flowing in a loop one centimeter in diameter, at a distance of roughly one foot. Fortunately, the effects of repetitive fluctuating currents can often be filtered out of the data. In our previous studies with a potassium-vapor OPM, we made measurements at a sensitivity below one picotesla with 60-Hz background fields of 1000 to 10,000 picotesla.

Second, magnetic materials must be kept sufficiently far away from the OPM. Magnetic objects can produce fluctuating fields if they move or vibrate, as they might if the sensor package were buffeted by the wind. Magnetic materials can also distort magnetic fields originating in the environment, slightly altering the magnitude of the magnetic signal detected by the OPM. (A sphere of infinitely permeable material, one centimeter in diameter and ten centimeters from the OPM, would enhance or reduce the apparent size of an external magnetic signal by roughly 0.1%.) Magnetic materials can potentially produce magnetic gradients large enough to affect the linewidth of the atomic Larmor resonance, thus spoiling the operation of the OPM. However, OPMs are reasonably tolerant of such magnetic gradients, especially if they use unbuffered alkali-vapor cells. In our previous experiments with unbuffered cells, we found that a pair of steel pliers at a distance of several inches would only slightly affect the linewidth of the Larmor resonance.

Although sensitive magnetic measurements do involve careful engineering, the resulting design constraints are far from insurmountable. Sensitive OPMs are routinely flown in airplanes for applications such as antisubmarine warfare and mineral exploration. In our own experiments with the potassium-vapor OPM, we did not take extreme precautions to provide a magnetically clean environment. This instrument achieved noise levels below one picotesla per root hertz [8,9].

## 6.2 Design of Prototype Instrument

*"We will produce a conceptual design for a full-scale OIPM, specifying the overall configuration of the instrument, identifying the major system components and their performance requirements, and detailing the main engineering tradeoffs.*

Based on the engineering analysis presented above, we have developed a conceptual design for a full-scale OIOPM. We plan to use this design during Phase II in developing a prototype instrument. This conceptual design includes the overall geometry of the optical pumping unit and pump-beam optics, specifications for some key components, and a description of the electronics and measurement algorithms. Our intent in this design is to produce an instrument that is flexible enough for a variety of experiments, but also compact enough and simple enough to illustrate how a production model of the instrument might look.

In this spirit, we have chosen a special configuration for the applied-field coils, giving the optical pumping unit a geometry nearly as simple and compact as would be used in a production instrument. At the same time, we have designed the unit so that most major components can readily be modified or replaced. We have designed the pump-beam optics so that we can use either buffered or unbuffered alkali-vapor cells. We have also designed the instrument so that we can demonstrate a number of possible schemes for thermal insulation of the alkali-vapor cells. This flexibility will allow us to explore experimentally the tradeoffs between simplicity, ruggedness, and low power consumption for the cell heaters.

We have also used a flexible approach in designing the electronics and measurement algorithms for the OIOPM. We plan initially to control the experiment and record the magnetic-field measurements using a PC-compatible computer. This approach allows us to modify the measurement process at will. Later versions of the instrument will replace the computer by a microprocessor, or by a special low-power electronic system (Appendix A3.2.4).

The following subsections present, first, our mechanical design for the optical pumping unit, and then our conceptual design for the electronics and measurement algorithm.

### **6.2.1 Configuration of the Optical Pumping Unit.**

As shown in Fig. 8, the optical pumping unit for the OIOPM has a cylindrical geometry similar to those of existing hand-held cesium and rubidium magnetometers. The mechanical structure of the sensor consists of a central tube supporting the alkali-vapor cell and pump-beam optics, an outer shell including coil forms for the applied-field coils, and two end plates which support the photodetector and laser-diode light source.

The pump-beam optics are designed for the most straightforward optical detection technique, in which the photodiode simply monitors the transmitted intensity of the pump beam. The pump beam is produced by the laser diode (right-hand side of figure). The light is formed into a parallel beam by a Fresnel lens, and then circularly polarized using a linear polarizer followed by a quarter-wave plate. The circularly polarized beam then passes through the alkali-vapor cell, and is focused onto the photodiode by a second Fresnel lens.

In the figure, the alkali-vapor cell is cylindrical, and the optics are arranged to spread the pump beam evenly across the entire cross section of the cell. This arrangement allows us to use either buffered or unbuffered cells in the prototype instrument. In a buffered cell, where the atoms are essentially immobilized by the buffer gas, the broad pump beam is necessary to ensure that all the atoms are exposed to the probe beam. With the broad pump beam, the cylindrical cell becomes necessary to ensure that the optical thickness of the cell uniform across the entire cross-section of the pump beam. For an unbuffered cell, where the atoms move freely and rapidly sample all parts of the cell, we could use a narrow pump beam, and still expect that all the atoms would be exposed to the pump light for approximately the same amount of time. In this case, the ideal cell geometry might be a sphere, which provides the longest possible spin relaxation time in the regime where the limiting relaxation process is collisions with the cell wall. However, the difference will not be great, and we anticipate using the same cylindrical shape for both buffered and unbuffered cells.

To maintain the required density of alkali vapor, the cell is heated to a temperature of 50 to 60 Celsius, using phosphor-bronze resistance wires. Phosphor bronze is appropriate because it has a very low magnetic signature. Each heater wire is wound as a twisted pair, with identical currents flowing in opposite directions through the two elements. This bifilar winding minimizes any magnetic fields produced by the heater

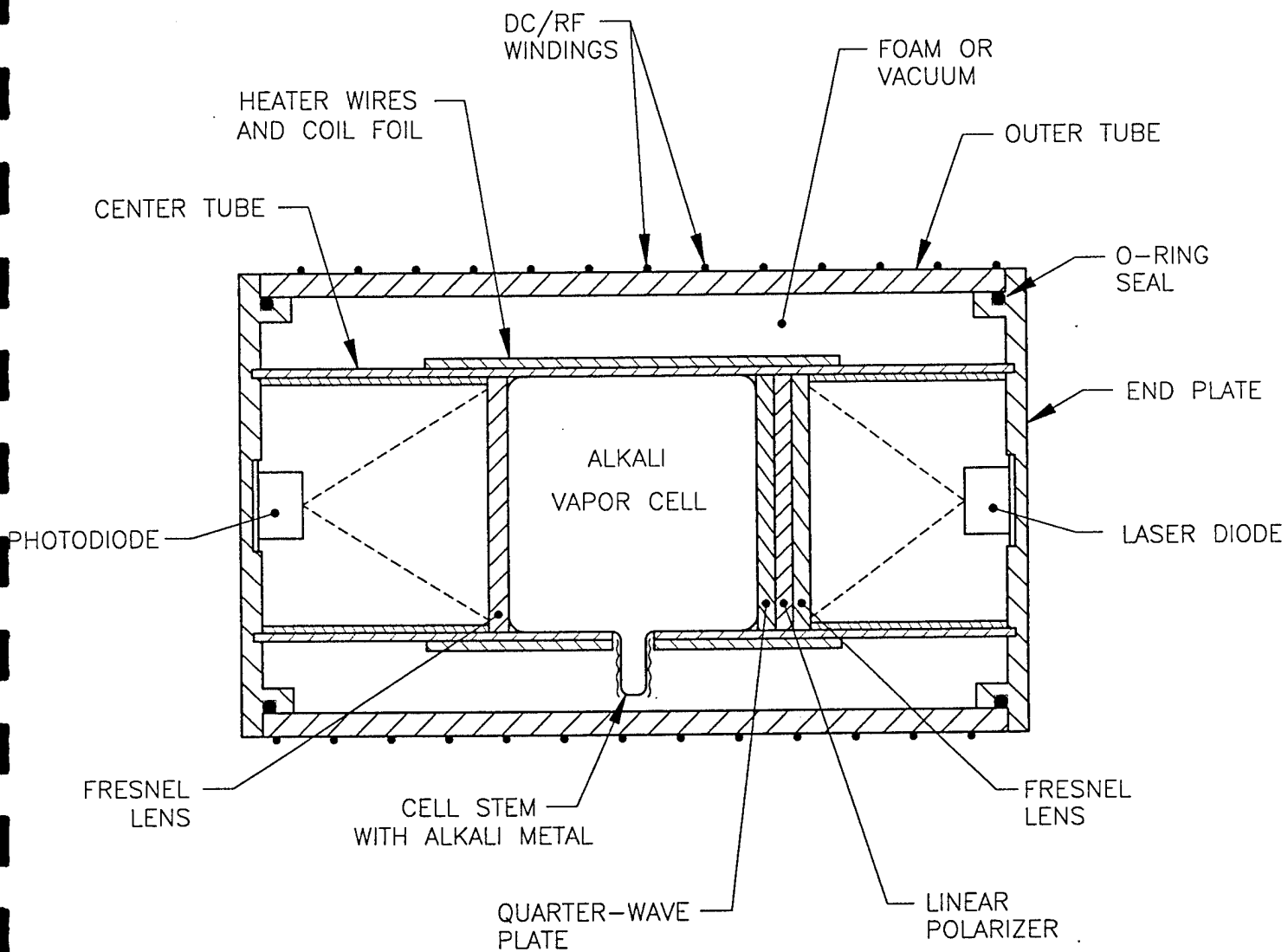


**Fig. 8. Optical pumping unit for Phase-II prototype.**

wires, so that we can keep the heaters on continuously during the measurements. We have used this approach successfully in our manufacture of cesium magnetometers. An alternative approach, which relieves any concerns about the geometry of the heater windings, is to switch the heaters off during the portion of the measurement cycle where the Larmor frequency is actually being measured. We used this approach in our previous work with potassium magnetometers.

To maintain a uniform temperature in the cell, we surround the cell with "coil foil", a composite structure made by laying parallel, insulated copper wires on a substrate of Kapton tape. This structure conducts heat well, but does not create eddy currents when the instrument is rocked back and forth in the presence of the earth's magnetic field. The lack of eddy currents removes one potential source of motional noise in the magnetometer. In our design, the coil foil is laid in two perpendicular directions on the outside of the central support tube that contains the optical cell.

The alkali vapor in the cells is provided by a small reservoir of the alkali metal. This reservoir is contained in a small tube which projects out from the side of the cell. This cell stem extends out beyond the main cell heater wires and coil foil wrapping, so that we can maintain it at a temperature slightly lower than that of the rest of the cell. This slightly lower reservoir temperature prevents the deposition of alkali metal on the cell walls.

To minimize the power required for the cell heaters, we need to insulate the cells from the surrounding environment. For thermal isolation, the central support tube is constructed of G-10 fiberglass, a good thermal insulator that is also light, strong, durable, non-magnetic, and electrically non-conductive. To prevent conductive heat loss to the environment, our design allows us either to surround the central tube with insulating material, or to evacuate the entire sensor package. To evacuate the package, we would use O-rings to seal the end plates of the enclosure to the outer shell. This design flexibility will allow us to demonstrate experimentally a number of thermal insulation schemes.

The key to our compact, cylindrical design is the arrangement of the coils that produce the RF and DC applied fields for the field-cycling experiment. In our previous laboratory experiments on optical pumping, we used Helmholtz coils to produce these fields. However, Helmholtz coils have to be much larger in diameter than the alkali vapor cells, in order to produce sufficiently uniform fields. For the prototype OIOPM, we plan to use a more compact arrangement that fits naturally into a cylindrical geometry. We would use three coils to produce the three independent components of the applied fields, using the same coils for both the RF and DC fields at different stages of the measurement process. One of the three coils would be a simple solenoid, wound in a spiral groove around the outer cylinder of the sensor unit. This solenoid would produce a field longitudinal to the pump beam. The other two coils, producing the two field components transverse to the pump beam, are laid in grooves that run axially

along the outer cylinder. These grooves are strategically placed around the periphery of the cylinder to null out the first few spatial derivatives of the magnetic field on the central axis of the sensor unit (Fig. 9).

We studied the design of similar transverse-field coils as part of a previous research program. In one simple case, which we could solve analytically, a system using a total of eight longitudinal wires (four loops) could be arranged to cancel all the second derivatives of the magnetic field at the central axis (Fig. 9). Higher-order schemes, cancelling higher derivatives of the field, could be designed by numerically solving a simple set of transcendental equations. Such higher-order coil sets would somewhat reduce the coil diameter required to produce a given field uniformity over a given cell volume.

### **6.2.2 Measurement Algorithm and Electronics for the OIOPM.**

As described in Sec. 2.3, the OIOPM measures the ambient magnetic field by a pulsed optical pumping experiment with adiabatic field cycling. In the first phase of the measurement cycle, we apply a magnetic field to the alkali-vapor cell, and turn on the pump beam to align the alkali atoms with this applied field. We then turn off the pump beam and adiabatically remove the applied field, leaving the atomic spins aligned with the ambient magnetic field. In the presence of the ambient field, we partially depolarize the spins by applying an RF field at approximately the Larmor frequency of the alkali atoms. To observe the result of this depolarization, we adiabatically restore the applied field, turn on the pump beam, and monitor the transmission of the pump beam as the atomic spins realign themselves with the applied field.

Within this measurement cycle, we use a feedback loop to make the RF frequency track the atomic Larmor frequency. During each pulse of the pump beam, we measure the transmission of the pump beam to determine the degree to which the RF field has depolarized the atomic spins. Using this information, we then calculate a new frequency for the next RF field pulse. We alternate between two different RF frequencies, one on either side of the Larmor resonance, on successive measurement cycles. Maintaining a constant separation between the two frequencies, we adjust the frequencies so that the spin depolarization is the same for both frequencies. This condition occurs when the two RF frequencies are equidistant from the peak of the Larmor resonance. We use this method of frequency measurement because it is unaffected, to first order, by drifts in the pump-beam intensity or alkali-vapor density.

In addition to this frequency-measurement loop, we also operate a second feedback loop that adjusts the pump-beam wavelength to match the absorption line of the alkali atoms. As described in Sec. 6.1.5, this loop rapidly modulates the bias current to the laser diode, sweeping the output wavelength over the absorption line. The resulting modulation of the optical absorption signal is used to adjust the DC component of the laser bias current, keeping the wavelength sweep centered on the atomic absorption line.

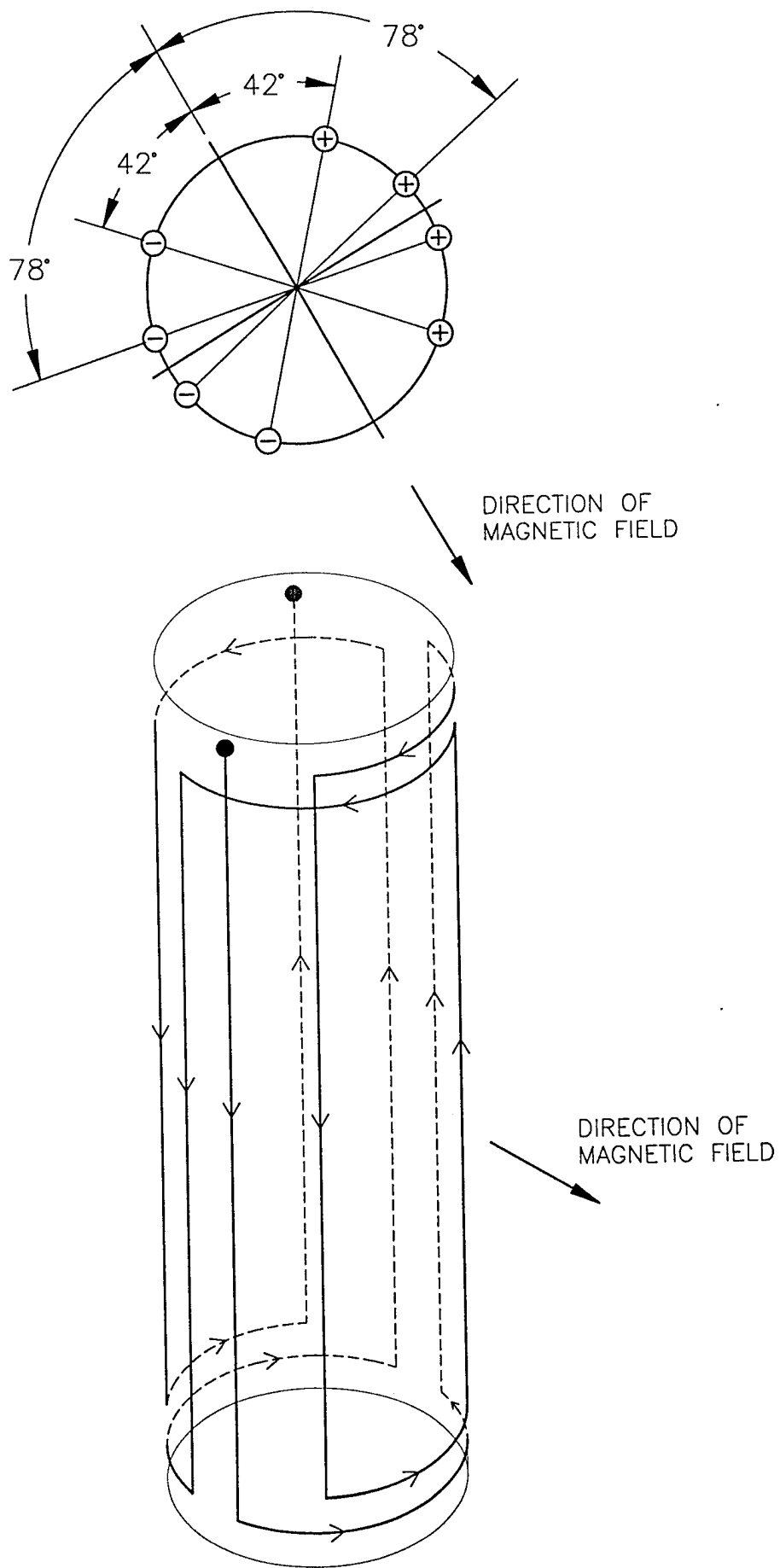


**Fig. 9. Longitudinal windings for producing homogeneous field transverse to cylinder axis.**

Fig. 10 shows schematically the electronic system that we will use at first to implement this measurement scheme. For maximum flexibility in optimizing the measurement process, the measurements are controlled using a PC-compatible computer. The computer monitors the photodiode signal that indicates the transmission of the pump beam, and corrects the RF frequency to track the atomic Larmor resonance. The RF frequency itself is generated by a digital frequency synthesizer, or direct digital synthesizer (DDS). The computer also controls the timing of the experiment, switching on and off the RF field, DC field, and pump beam. We plan to use a waveform-synthesizer board, controlled by the computer, to define the slew rate and functional form of the DC applied field as it is switched on and off. By adjusting the time dependence of the applied field, we hope to minimize the loss of spin polarization during field cycling. In addition to these computer-controlled functions, we will develop analog electronics to stabilize the temperature of the alkali-vapor cells, and adjust the wavelength of the pump beam.

Once the measurement process has been optimized, we plan to replace the computer-controlled system with specially designed, low-power analog and digital electronics.

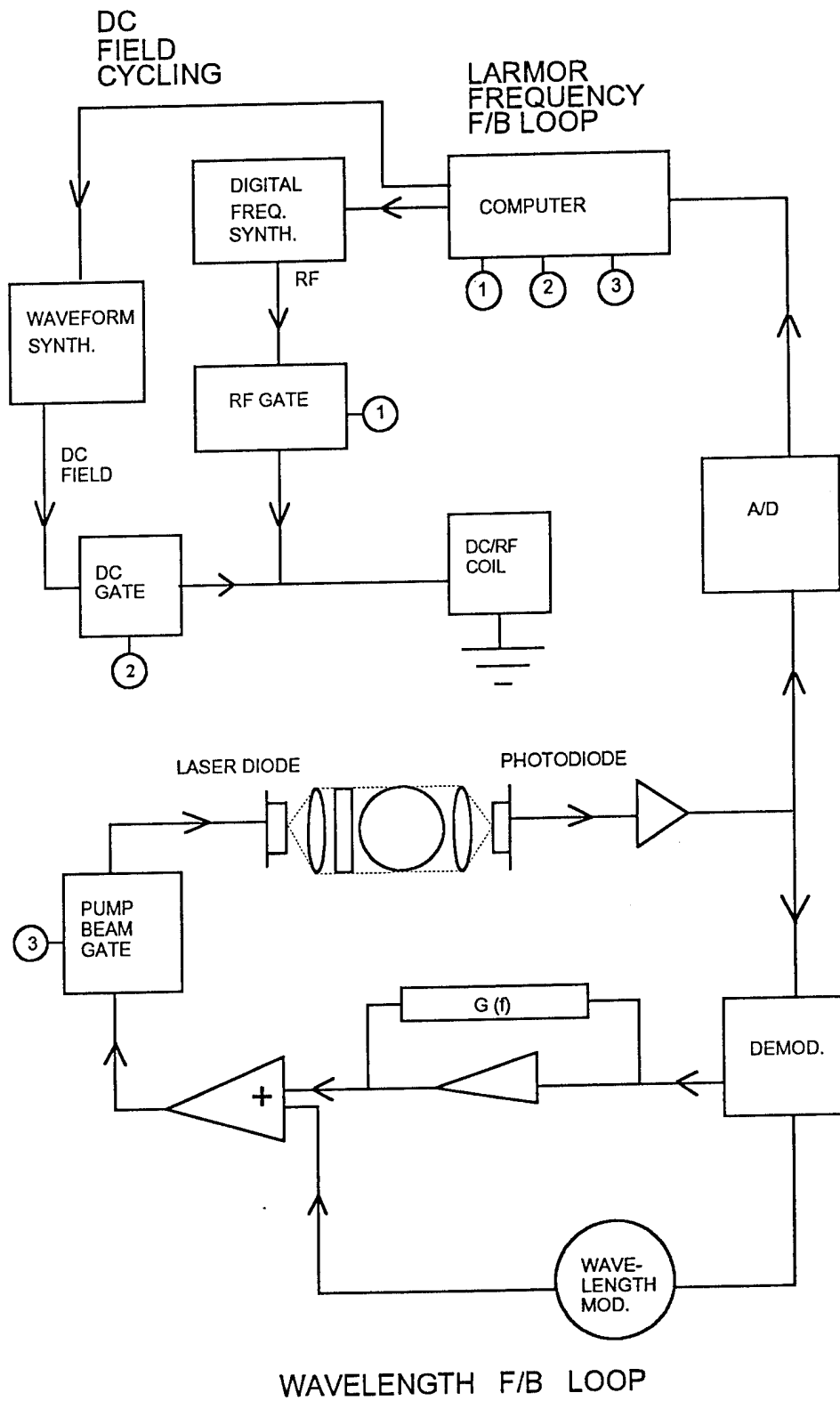


Fig. 10. Electronic feedback system for orientation-independent optically pumped magnetometer.

## 7 REFERENCES

1. E.B. Aleksandrov and V.A. Brunevich, "Optically Pumped Magnetometers After Three Decades", *Optical Engineering* 31, 711 (1992).
2. W. F. Stuart, "Earth's-Field Magnetometry", *Reports on Progress in Physics* 35, 803, (1972).
3. W. Happer, "Optical Pumping", *Rev. Mod. Phys.* 44, 169 (1972).
4. E.B. Aleksandrov, "Precision Atomic-Resonance Magnetometers for Geomagnetic Measurements", *Measurement Techniques* 28, 312 (1985).
5. M.S. Redford and J.S. Sumner, *Geophysics* 29, 482 (1964).
6. J.H. Allen, "Long-Term Stability of Self-Oscillating Rb Magnetometers", *J. Geomag. Geoelectr.* 20, 197 (1968).
7. W. Happer, "Improved Optically Pumped Magnetometers and Gradiometers", Report # STD-R-308, Applied Physics Laboratory, Johns Hopkins University, October, 1979.
8. W.F. Avrin and R.E. Sager, "An Optically Pumped Magnetic Detector with Submilli-gamma Resolution," Final Report, Contract # N00024-85-C-5374, Naval Sea Systems Command, August 1988.
9. W.F. Avrin and R.E. Sager, "An Optically Pumped Magnetic Sensor with Submilligamma Resolution", *IEEE. Trans. Mag.* 25, 3408 (1989).
10. A.D. Hibbs, W.F. Avrin, D.N. Shykind, and L.J. Burnett, "New Magnetic Sensors for Undersea Surveillance," Final Report, Contract No. N66001-92-C-6020, Naval Command, Control, and Ocean Surveillance Center, Quantum Magnetics, Inc., May 1993.
11. D.H. Yang and Y.Q. Wang, *Optics Communications* 73, 285 (1989).
12. D.H. Yang and Y.Q. Wang, *Optics Communications* 74, 54 (1989).
13. D.H. Yang and Y.Q. Wang, *Optics Communications* 80, 23 (1990).
14. P. Cerez, et al, *IEEE Trans. Instrum. Meas.* 40, 137 (1991).
15. R.E. Drullinger, et al, *IEEE Trans. Instrum. and Methods* 40, 162 (1991).
16. S. Yamaguchi, I. Matsuda, and M. Suzuki, *J. Quantum Electronics* 28, 2551 (1992).
17. A. Michaud, P. Tremblay, and M. Tetu, *IEEE Trans. Instrum. Meas.* 40, 170 (1991).
18. G.M. Saxena, A. Chatterjee, and B.S. Mathur, *Indian Journal of Pure and Applied Physics* 27, 791 (1989).

---

---

**Orientation-Independent Optically Pumped Magnetometers:  
Total Field Sensors Without Dead Zones**

---

APPENDIX A  
Final Report Excerpts  
Contract No. N660001-92-C-6020

Prepared For

Naval Command, Control and Ocean  
Surveillance Center  
RDT&E Division  
San Diego, California

May 31, 1993

This appendix presents an engineering analysis for the OIOPM, which we performed under a recent contract with the Naval Command, Control and Ocean Surveillance Center. As discussed in Sec. 6 above, this analysis was the foundation of our Phase-I design studies for a prototype instrument.



Quantum Magnetics, Inc.  
11578 Sorrento Valley Road  
San Diego, CA 92121

## A1 Work Statement for Evaluation of the OIOPM

Before presenting our performance analysis of the OIOPM, we first review the relevant portion of our work statement for Phase I. The work statement included two main tasks relating to the OIOPM. The first task addressed the fundamental performance characteristics of the instrument:

*Task 4a. Evaluate Measurement Technique. Assess the proposed method for measuring fields regardless of sensor orientation. Refine noise estimates. Select methods for improving sensitivity.*

We identified two specific issues to be included in this fundamental performance evaluation:

1. **Shot-noise limit of the OIOPM.** We proposed to evaluate possible improvements in our optical pumping techniques, so as to improve the basic shot-noise sensitivity limits of the OIOPM. Our analysis confirms that there are several possible methods for improving the sensitivity. However, we have concluded that the sensitivity required in the rapidly deployed sensor array can be achieved with no fundamental change in our optical pumping technique (Secs. A2.1 and A2.2).

2. **Low-frequency stability of the OIOPM.** We proposed to analyze the other factors affecting the low-frequency stability of the OIOPM. An important concern in this area was the required performance of the electronic subsystems responsible for maintaining constant conditions in the optical pumping measurements. As presented in Sec. A2.3, our refined analysis indicates that the OIOPM can achieve extremely good low-frequency performance, without exceptional stability in these electronic subsystems.

Our second main task addressed the practical characteristics of the OIOPM:

*Task 4b. Evaluate System Characteristics. Estimate size, weight, and power requirements. Identify methods for incorporating laser diodes and minimizing heater power.*

We proposed to investigate a number of specific practical issues:

1. **Laser light sources.** We proposed to investigate the feasibility of using laser diodes instead of vapor discharge lamps to produce the potassium D1 light required for optical pumping. The use of the laser diodes would reduce the power consumption of the OIOPM. However, we anticipated some difficulty in finding a source for laser diodes that produced the precise wavelength required for our experiments. It also appeared that our optical measurement techniques would have to be modified to allow for the very broad wavelength distribution produced by the laser diodes. During Phase I, we found that laser diodes could in fact be made to produce the required wavelength, and we identified at least two ways to deal with the broad laser line (Secs. A3.3 and A3.4).

2. **Power consumption of the OIOPM.** Since the rapidly deployed sensors will operate for long periods on battery power, power consumption is a crucial issue in evaluating each proposed sensor type. We proposed to estimate the power requirement of the OIOPM, taking into account the light source, cell heaters, magnetic-field coils, and associated electronics. Our preliminary analysis (Sec. A3.2) indicates that the OIOPM can operate with a total power less than one-half watt. Since this analysis is based on an electronic measurement scheme that is not designed to minimize power consumption, it appears likely that the OIOPM will ultimately consume less than 200 milliwatts.

3. **Size-sensitivity tradeoff.** We proposed to estimate the size and geometry of a practical OIOPM, taking into account the inherent tradeoff between the sensitivity of the magnetometer and the size of the potassium-vapor cell. Our analysis indicates that a sensitivity better than one picotesla per root hertz can be obtained with a sensor unit less than two inches in diameter and six to ten inches long (Secs. A2.1, A2.2, and A4).

4. **Practical sensor design.** We proposed to design an OIOPM that would meet the practical requirements of the rapidly deployed sensor array. Our design concept is described in Section A4.

In addition to the issues identified in the Phase-I proposal, we have also addressed two other instrumental characteristics of potential importance in a deployed sensor array:

1. **Motional noise.** If the rapidly deployed sensors are mounted on a platform that sways in response to waves and shifting currents, the rocking motion of the platform may produce noise in the magnetic measurements. Our analysis indicates that this rocking noise is much less of a problem for the OIOPM than for a major competing technology, the  $^3\text{He}$  nuclear magnetometer (Sec. 3.5).

2. **Gradient tolerance.** If the magnetometer is deployed on the ocean floor, magnetic rocks nearby may produce large magnetic-field gradients. Such gradients can disrupt the operation of an optically pumped magnetometer. Our analysis indicates that the OIOPM will tolerate much larger gradients than the  $^3\text{He}$  magnetometer (Sec. 3.1). This increased gradient tolerance may simplify the deployment of the magnetometer by eliminating the need for additional structures that hold the instrument up off the ocean floor.

In the next three sections, we present our fundamental analysis of long-term and short-term noise, our predictions of other, practical performance characteristics, and our conceptual design for the OIOPM.

## **A2 Sensitivity and Stability of the OIOPM**

The theoretical sensitivity limit of the OIOPM is close to the performance obtained in practice with SQUID magnetometers. In assessing this sensitivity limit, we consider both the fundamental sensitivity limit, which arises mainly from the shot noise in the optical measurements, and the long-term stability of the instrument, which is determined mainly by instrumental effects that perturb the precession of the potassium atoms.

### **A2.1 Shot-Noise Limits of the OIOPM**

On time scales ranging from a fraction of a second to several seconds, the sensitivity of the OIOPM is determined fundamentally by the shot-noise statistics involved in measuring the absorption of the pump beam [1,4,5]. To calculate this shot-noise sensitivity limit, we first identify the key steps in the magnetic measurement, and show how the sensitivity of the measurement is related to the linewidth of the atomic spin resonance and the signal-to-noise ratio in the optical absorption measurement. We next relate these two key factors to more fundamental parameters of the optical pumping experiment. We then produce reasonable estimates for these fundamental parameters, and use them to calculate the shot-noise limit of the OIOPM. Finally, we describe how the sensitivity limits would be affected by various changes in the design of the instrument.

#### **A2.1.1 Key Steps in the Magnetic Measurement**

As described in Sec. A1 above, the OIOPM uses a complex measurement process that achieves constant measurement sensitivity regardless of the instrument's orientation in the ambient magnetic field. For the purposes of our shot-noise analysis, this process is essentially equivalent to a simpler measurement cycle similar to that used in the traditional locked-oscillator magnetometer [2]. In this simplified analysis, we can assume that the polarization axis of the circularly polarized pump beam is aligned with the ambient magnetic field. At the beginning of this measurement cycle, the pump light aligns the atomic spins with the ambient magnetic field. Then an rf field pulse excites the Larmor resonance of the atoms, reducing their spin alignment with the ambient magnetic field. Finally, the pump light is again applied, re-aligning the atomic spins with the ambient field. During this optical repumping process, the pump-beam is absorbed strongly at first, because the atomic spins are only partially aligned with the polarization axis. The pump-beam absorption then decreases as the atoms become more strongly aligned with the axis of circular polarization.

In this measurement cycle, the initial absorption of the pump beam is a measure of the degree to which the rf field has depolarized the atomic spins. In turn, the degree of spin depolarization depends on the relationship between the rf frequency and the atomic Larmor resonance. As a result, we can determine the atomic Larmor frequency, and hence the ambient magnetic field, by monitoring the pump-beam absorption while adjusting the rf frequency.

The absorption of the pump beam will exhibit a peaked lineshape as a function of rf frequency. This lineshape is characterized by a maximum percentage absorption  $A_0$ , which occurs when the rf frequency is exactly in resonance with the atomic precession, and a linewidth  $\Delta f_{lw}$ , which is determined by the intensity of the rf field and the spin relaxation time of the potassium atoms.

In the simplest possible measurement scheme, we choose an rf frequency on one side of the absorption lineshape, near the point where the lineshape had its maximum slope. At this operating point, if the atomic precession frequency changes by an amount  $\delta f$ , the pump-beam absorption will change by an amount

$$\delta A = \delta f (dA/df) \cong \delta f (A_0/\Delta f_{lw}) , \quad (1)$$

where  $dA/df$  is the slope of the absorption lineshape at the rf frequency, and  $\Delta f_{lw}$  is the characteristic width of the atomic precession line. Using these changes in the pump-beam absorption, we can adjust the rf frequency to follow the variations of the atomic precession frequency in response to changes in ambient magnetic field.

Since a change in the pump-beam absorption is interpreted as a change in the atomic precession frequency, a fluctuation  $\delta A$  in the absorption measurement will produce a corresponding fluctuation in the magnetic-field measurement:

$$\delta B = \Gamma \delta f = \Gamma \frac{\delta A}{dA/df} \cong \Gamma \Delta f_{lw} \frac{\delta A}{A_0} , \quad (2)$$

where  $\Gamma$  is the gyromagnetic ratio of the atoms (in cycles per second per unit field).

### A2.1.2 Fundamental Parameters in the Sensitivity Calculation

Eq. (2) indicates that the noise in the precession frequency measurement is determined by the linewidth  $\Delta f_{lw}$  and by the signal-to-noise ratio ( $A_0/\delta A$ ) in our measurement of the pump-beam absorption.

The linewidth  $\Delta f_{lw}$  will be determined by the spin relaxation time of the potassium atoms, and by the intensity and duration of the rf pulse. If the rf pulse is too short and too intense, the linewidth will be unnecessarily long. However, if the rf pulse is too long, the spin population will decay excessively during the rf pulse, and the optical absorption signal will be diminished. The optimum compromise between linewidth and signal amplitude will be achieved when the length of the rf pulse is approximately equal to the spin relaxation time  $T_2$ . Under these conditions, the linewidth will be given roughly by

$$\Delta f_{\text{lw}} \sim 1/\pi T_2 . \quad (3)$$

The signal-to-noise ratio  $A_0/\delta A$  is limited fundamentally by the shot noise in the optical measurement: The optical absorption signal is essentially the total number of photons removed from the pump beam due to enhanced absorption during the repumping process, while the noise in the absorption measurement is equal to the statistical fluctuation in the total number of photons detected during this process.

To calculate both the signal and the noise, we first relate the photon flux reaching the photodetector to the orientation-dependent absorption cross-section of the potassium atoms. If we use potassium D1 light in the pump beam, the photon flux is given by

$$I_{pd} \cong I_0(1 - nL\sigma), \quad (4)$$

where

$$\sigma = \frac{\sigma_0}{2}(1 - \langle m_z \rangle).$$

In this expression,  $I_{pd}$  is the net current of photons reaching the photodetector,  $I_0$  is the photon current that reaches the detector when the potassium spins are fully polarized.  $n$  is the number density of the potassium vapor,  $L$  is the length of the potassium vapor cell, and  $\sigma_0$  is the absorption cross section for D1 light by potassium atoms with randomly oriented spins.  $m_z$  is the spin quantum number with respect to the direction of the ambient field.

In the particular expression given above, we have assumed that the potassium vapor cell is optically thin, that is, that  $nL\sigma \ll 1$ . As discussed below, this simplifying assumption can probably be relaxed without greatly affecting our sensitivity estimates for the OIOPM.

To calculate the optical absorption signal, we need to determine the magnitude and time dependence of the atomic spin  $\langle m_z \rangle$ . We first relate this quantity to the relative populations of the different atomic spin states:

$$\langle m_z \rangle = \sum_{m=-2}^2 m P_m(t) , \quad (5)$$

Immediately before the rf pulse, the atomic spin states have populations  $P_m^i$  determined by the balance between the pump light and a variety of spin-relaxing effects. The rf field then excites the uppermost atomic spin transition of the potassium atoms, transferring probability amplitude between the  $m=1$  and  $m=2$  spin states. We adjust the rf field so that, when the rf frequency is at the peak of the atomic spin resonance, the rf pulse will exactly exchange the populations of the two states. In addition to this

coherent transfer of probability amplitudes, the spin population relaxes toward thermal equilibrium through processes such as collisions between the potassium atoms and the walls of the potassium vapor cell.

After the rf pulse, the pump light is turned back on. The potassium atoms become re-aligned with the ambient field through a process that involves the repeated absorption and reemission of light. Each time an atom absorbs a photon from the circularly polarized pump beam, it acquires one quantum of angular momentum. The excited atom then decays by emitting another photon. However, the selection rules for photon emission permit the atom to emit a photon with a polarization different from that of the pump beam. On average, the atom acquires a net angular momentum in the direction of the pump beam each time it absorbs and reemits a photon. As a result, the potassium atoms gradually become aligned with the polarization axis of the pump light.

This repumping process occurs at a rate given by

$$\frac{d \langle m_z \rangle}{dt} = \frac{I_0 \sigma_0}{A b_r} (2 - \langle m_z \rangle) , \quad (6)$$

where  $A$  is the cross-sectional area of the potassium vapor cell.  $b_r$ , is the average number of circularly polarized photons that must be absorbed to pump an atom from the  $m=1$  state into the  $m=2$  state. This parameter, determined by the selection rules for the emission of light, is somewhat greater than 1.

Combining the effects of the rf pulse, the spin relaxation, and the repumping process, we expect the atomic spin to evolve during repumping according to the following expression:

$$2 - \langle m_z \rangle = m_0 e^{-t/\tau_r} , \quad (7)$$

where

$$\tau_r = \frac{A n_r}{I_0 \sigma_0} ,$$

and

$$m_0 = e^{-1} (P_2^0 - P_1^0) .$$

This expression applies to the case where the rf frequency coincides with the peak of the atomic spin resonance. In this equation, the factor of  $e^{-1}$  represents the decay of the non-equilibrium spin population due to relaxation during the rf pulse. We assume here that the assumption that the duration of the rf pulse is equal to the spin relaxation time  $T_{rel}$ .

The purpose of the optical absorption measurements is, in essence, to monitor the spin-depolarizing effect of the rf pulse by determining the number of photons removed from the pump beam during the repumping process. To obtain the required information, we integrate the photodetector current for a time  $T_f$ , starting at the beginning of the repumping period. The resulting optical absorption signal is given approximately by

$$\begin{aligned} N_{sig} &\cong (1/2)n_k\sigma_0 b_r m_0 L I_0 \int_0^{t_{int}} e^{-t/\tau_r} dt \\ &= (1/2) L A n_k m_0 b_r (1 - e^{-t_{int}/\tau_r}) \end{aligned} \quad (8)$$

This integrated optical signal is proportional to the total number of potassium atoms in the cell ( $L A n_k$ ), the degree of spin polarization ( $m_0$ ), and the number of photons required to repump each potassium atom ( $b_r$ ).

The fluctuation in the optical signal will be equal to the square root of the total number of photons collected during the integration period:

$$N_{noise} \cong (t_{int} I_0)^{1/2} = \left( \frac{A b_r}{\sigma_0} \right)^{1/2} \left( \frac{t_{int}}{\tau_r} \right)^{1/2} \quad (9)$$

Combining Eqs. (8) and (9), we calculate the signal-to-noise ratio in the optical absorption measurement:

$$\frac{N_{sig}}{N_{noise}} \cong (n_k m_0 L / 2) (A b_r \sigma_0)^{1/2} f(t_{int}/\tau_r) \quad (10)$$

where  $f(x) = x^{-1/2}(1 - e^{-x})$ .

The function  $f(x)$  in this equation has a maximum value of 0.638, which occurs when  $x$  is equal to 1.26.

Eq. (10) represents the statistical error in a single repetition of the optical measurement. We can improve upon this statistical error by averaging several measurements together. The amount of averaging that can be done will be determined mainly by the repetition rate of the measurement. This repetition rate is determined mainly by the length of the rf pulse, and by the time required for optical pumping. Although we can make the optical-pumping time short by supplying an intense pump beam, the length of the rf pulse is dictated by the spin relaxation time  $T_{rel}$ . As a result, the period of the measurement cycle will be roughly equal to the spin relaxation time. In a given measurement time  $T_{avg}$ , the total number of repetitions will be roughly

$$N_{avg} \cong \frac{T_{avg}}{T_{rel}} \cong \frac{\Delta f_{lw}}{\Delta f_{bw}}, \quad (11)$$

where  $\Delta f_{bw}$  is the bandwidth of the magnetic measurement.

Including the gain due to signal averaging, the overall signal-to-noise ratio of the optical measurement is

$$\frac{A_o}{\delta A} = N_{avg}^{1/2} \frac{N_{sig}}{N_{noise}} \cong \left( \frac{0.638}{2} \right) (n_k m_o L) (A b_r \sigma_o)^{1/2} \left( \frac{\Delta f_{lw}}{\Delta f_{bw}} \right)^{1/2} \quad (12)$$

Finally, from Eqs. (2), (3) and (12), the shot-noise fluctuation in the magnetic measurement is

$$\begin{aligned} \delta B &\cong \left( \frac{1}{0.319e} \right) \left( \frac{1}{\Gamma n_k L (P_2^o - P_1^o)} \right) \left( \frac{\Delta f_{bw}}{\pi T_{rel} A b_r \sigma_o} \right)^{1/2} \quad (13) \\ &= \left( \frac{0.649}{\Gamma n_k L (P_2^o - P_1^o)} \right) \left( \frac{\Delta f_{bw}}{T_{rel} A b_r \sigma_o} \right)^{1/2} \end{aligned}$$

### A2.1.3 Sensitivity Calculation for the OIOPM

To estimate the sensitivity limit of the OIOPM, we need specific values for each of parameters in Eq. (13). The cross section  $\sigma_o$  is approximately  $10^{11}$  cm<sup>2</sup> for the absorption of D1 spectral light by potassium atoms [6].  $b_r$ , the average number of photons required to pump an atom from the  $m=1$  state to the  $m=2$  state, could be obtained from the literature on optical pumping, or calculated from the selection rules regarding the absorption and reemission of light. For our purposes, however, it is more expedient simply to assume that  $b_r$  is equal to 1. Since  $b_r$  must be greater than 1, this approach will slightly overestimate the shot noise in the magnetic measurements.

The length  $L$  and cross-sectional area  $A$  of the potassium vapor cell will depend on the requirements of a given application. To achieve the greatest possible sensitivity, we would use a long, wide cell. However, for the rapidly deployed sensor array, our goal is to develop a compact instrument with a sensitivity better than one picotesla per root hertz. With this goal in mind, we base the following sensitivity estimate on a cylindrical cell with a length of 5 cm and a diameter of 2 cm.

The remaining two parameters, the potassium vapor density  $n_k$  and the state population difference  $(P_2^o - P_1^o)$ , can be estimated on the basis of our previous experiments with a potassium magnetometer [4,5]. This Free-Precession Magnetic Detector (FPMD)

uses a detection scheme different from that of the OIOPM, but the basic processes that determine the measurement sensitivity are essentially the same in both instruments. In particular, both instruments rely on a modulated optical absorption signal that is produced by stimulating the transition from the  $m=2$  state to the  $m=1$  state of the potassium atom. This signal in both cases is proportional to the population difference  $(P_2^0 - P_1^0)$ .

With the FPMD, we found that the optical absorption signal reached a maximum at a certain potassium vapor density, and then decreased at higher densities. We interpreted this trend as an indication that the population imbalance produced by optical pumping was being degraded at high vapor densities. Under the conditions corresponding to the largest signal amplitude, the potassium vapor density was approximately  $6 \times 10^9 \text{ cm}^{-3}$ , as determined by measuring the absorption of unpolarized potassium D1 light. Under these same conditions, we also determined the relative populations of the atomic spin states, using a special optical pumping experiment in which we compared the optical absorption signals that were produced by stimulating each of the spin transitions of the potassium atom. These experiments indicated that the pump beam placed approximately 50% of the potassium atoms were being pumped into the  $m=2$  state, and 25% of the atoms into the  $m=1$  state. For such a state distribution, the population difference  $(P_2^0 - P_1^0)$  is equal to 0.25.

Inserting all these values into Equation (13), we obtain a theoretical sensitivity of  $3 \times 10^{-14}$  tesla per root hertz for an OIOPM with a potassium vapor cell 5 cm long and 2 cm in diameter. This sensitivity is nearly as good as that obtained with Superconducting Quantum Interference Devices (SQUIDS).

#### **A2.1.4 Possible Improvements in the Sensitivity Limit**

The sensitivity calculation in the previous section is based on some specific assumptions about the key physical parameters of the instrument. In the next few paragraphs, we describe how some of these parameters could be varied, changing the balance between the sensitivity of the instrument and its other performance characteristics.

One basic change would be to increase the length of the potassium vapor cell. According to the analysis above, doubling the length of the cell would double the sensitivity of the instrument, at the cost of increasing its overall size and weight. In our calculations above, we assumed a cell length of only 5 cm in order to ensure that the magnetometer was as compact as possible, while still providing sensitivity adequate for the rapidly deployed gradiometer.

As second basic change would be to increase the density  $n_K$  of the potassium vapor, or improve the population difference ( $P_2^0 - P_1^0$ ) between the  $m=2$  and  $m=1$  states. In our previous experiments on the potassium free-precession magnetometer, we found that this population difference was degraded as the potassium density increased, so that the amplitude of the optical absorption signal reached a maximum at a vapor density of  $0.6 \times 10^{10} \text{ cm}^{-3}$ . The most likely cause for this degraded population difference was a process called photon trapping. In these previous experiments, the potassium vapor cells did not contain the inert background gas, or buffer gas, that is often used in optical pumping experiments. Under these conditions, essentially every potassium atom that absorbs a photon will subsequently release energy by emitting another photon of the same wavelength. If the potassium vapor is sufficiently dense, these reemitted photons can, be absorbed by other potassium atoms. Since the reemitted photons have random polarization, the reabsorption of these photons tends to spoil the spin-aligning effect of the circularly polarized pump beam.

One way to suppress radiation trapping is to introduce an inert buffer gas so that electronically excited atoms decay primarily through collisions, rather than reemission of radiation. With a buffer gas, we would expect the population difference ( $P_2^0 - P_1^0$ ) to increase from approximately 0.25 to nearly 1, at potassium vapor densities as high or higher than those used in our previous experiments. Since our analysis indicates that the sensitivity of the magnetometer is proportional to ( $P_2^0 - P_1^0$ ), this improved optical pumping would increase the sensitivity of the magnetometer by a factor of four.

The use of a buffer gas may not be appropriate for certain applications, where the magnetometer must operate in the presence of large magnetic-field gradients. In an unbuffered cell, the potassium atoms move very rapidly about the cell, usually traveling from one side of the cell to the other without suffering any collisions along the way. This rapid atomic motion averages out the effects of a magnetic-field gradient. In a buffer gas, however, the potassium atoms move only through the slow process of diffusion. As a result, the motional averaging is much less effective, and the magnetometer is much more susceptible to the effects of field gradients.

Even in an unbuffered cell, however, it may be possible to use potassium vapor densities higher than those assumed in our calculations above. The importance of radiation trapping will depend both on the density of the potassium vapor and on the average distance that a photon must travel through the vapor to escape the cell. In a long, narrow cell, this escape distance will be determined mainly by the diameter of the cell. Roughly speaking, if we cut the cell diameter in half, we would expect that twice the potassium density would be required to produce the same degree of photon trapping.

In our calculations above, we assumed a cell diameter of two centimeters, approximately half as great as that used in our previous experiments. With this smaller cell diameter, we could probably double the potassium density that was used in our previous experiments, without reducing the population differences produced by optical pumping.

### A2.1.5 Validity of Sensitivity Analysis for Optically Thick Cells

If we sufficiently increase the length of the cell or the density of the potassium vapor, it will no longer be strictly correct to assume, as we did in our sensitivity calculation, that the cell is optically thin. Nevertheless, the following qualitative reasoning suggests that our basic conclusions will remain valid even as this simplifying condition begins to break down:

The key quantity in our optical absorption measurements is the total number of photons removed from the pump beam during repumping, due to enhanced absorption by the depolarized atomic spins. To calculate this quantity, we assumed that the quantity  $n_K L \sigma$  was much smaller than 1, so that the intensity of the pump beam was virtually the same in every portion of the cell, at all times during the repumping process. Under this condition, the atomic polarization, and thus the absorption cross section, increased in a simple exponential fashion with time. Integrating this exponential function with respect to time, we found that the total number of photons removed was directly proportional to the total number of potassium atoms in the cell, and to the spin-state population difference created by the pump beam.

As we increase the potassium density and the cell length, we will eventually enter a regime where  $n_K L \sigma$  is no longer small compared with 1 at all times, in all portions of the potassium vapor cell. In this regime, the intensity of pump light reaching any part of the cell will vary according to the transparency of the potassium vapor through which the light has passed. At the same time, the transparency of the vapor will depend on the polarization of the atomic spins, which in turn will depend on the amount of pump light that has been absorbed since the beginning of the repumping process. Because of this relationship between the pump-light intensity and the absorption cross section, we expect the spin polarization of the potassium vapor to vary in a complex way with both time and location within the cell.

The absorption cross section for circularly polarized potassium D1 light goes to zero when the atomic spins are completely aligned with the polarization axis of the light. Consequently, we can imagine a regime in which the cell is optically thick when the spins are depolarized, but optically thin ( $n_K L \sigma \ll 1$ ) when the optical pumping process is complete. This situation can occur when the pump beam produces nearly complete spin alignment, as it would in the presence of a buffer gas, or in an unbuffered cell where the cell diameter and vapor density were low enough to avoid radiation trapping.

In this regime, the transmission of the pump beam will vary in a non-exponential manner with time. However, in the absence of processes that spoil the spin alignment produced by the pump beam, the only photons absorbed by the potassium vapor will be those that contribute to restoring the spin alignment of the potassium atoms. As a result, even if the pump-beam intensity has a complex time dependence, it will effectively obey a conservation law, in which the total number of photons removed from the beam during the repumping process will still be determined entirely by the number of potassium atoms in the cell, and the degree of spin depolarization produced by the rf pulse. The total time-integrated optical absorption signal will be just as large as that in our previous calculations, and the sensitivity limit of the magnetometer will be essentially the same as that previously estimated.

Our previous analysis will break down if the potassium vapor cell is optically thick and there are processes that spoil the spin alignment produced by the pump beam. Under these conditions, the potassium vapor will never be optically thin, even when the optical repumping has reached a steady state. As the pump beam passes through the highly absorptive cell, any signals imposed on the pump beam will be attenuated. This attenuation will apply to the optical absorption signal imposed on the pump beam by the repumping of potassium atoms in portions of the cell that are far upstream from the point where the pump beam exits the cell. The contribution of these atoms to the measured absorption signal will be less than the total number of photons that they remove from the pump beam during repumping. Consequently, for an optically thick cell with incomplete optical pumping, the net optical absorption signal will be less than that of an optically thin cell with the same number of potassium atoms. For such a cell, the sensitivity of the magnetometer will be less than that calculated in the previous section.

## **A2.2 Sensitivity Projections Based on Previous Measurements**

In addition to calculating the sensitivity limits from first principles, we can also project the performance of the OIOPM based on our previous experiments with the free-precession potassium magnetometer (FPPM). In this sensitivity projection, we use our theoretical model to account for changes in the dimensions of the optical pumping cell and the density of the potassium vapor.

Our previous results do not approach the theoretical sensitivity limits derived in the previous section. However, we did make measurements at a root-mean-square noise level of 0.6 picotesla. Since the free-precession instrument uses approximately the same basic physics as the OIOPM, this result indicates that the OIOPM can provide a sensitivity better than one picotesla, even without improving upon our previous techniques.

This conclusion is supported by a more detailed analysis, in which we use our theoretical sensitivity to correct our previous results for the slightly different experimental conditions that we would use in the OIOPM. One important set of corrections arises from differences in the size and shape of the optical-pumping cell. From the calculation in the previous section, the noise in the magnetic measurements is proportional to the quantity  $n_K T_2^{1/2} A^{1/2} L$ , where  $n_K$  is the density of the potassium vapor,  $T_2$  is the spin relaxation time, and  $A$  and  $L$  are the cross-sectional area and length of the optical-pumping cell. For a non-cylindrical cell, we can show that the factor  $A$  should be replaced by  $V/L$ , where  $V$  is the volume of the cell. Each of these factors is affected by the geometry of the optical pumping cell. The factors  $V$  and  $L$  can, of course, be calculated directly from the cell dimensions.

The other two parameters,  $n_K$  and  $T_2$ , are related to the cell dimensions in a subtler way. In an unbuffered potassium vapor cell, the spin-relaxation time  $T_2$  will be roughly proportional to the cell diameter, since it depends on the frequency with which the potassium atoms collide with the cell walls. At the same time, the optimum potassium density  $n_K$  will vary roughly as the inverse of the cell diameter, since it depends inversely on the average distance that reemitted light must travel to escape the cell.

In our previous experiments, we used spherical cells with a diameter of approximately 5 cm, while the OIOPM will probably use a cylindrical cell 10 cm long and 2 cm in diameter. Including the differences in cell length and volume, assuming that the spin relaxation time is proportional to cell diameter, and assuming that the potassium density is inversely proportional to diameter, we estimate that the geometrical scaling factors will improve the sensitivity of the OIOPM by a factor of 1.6 relative to that obtained in our previous experiments.

In addition to correcting for differences in the cell geometry, we also apply corrections for changes in the timing and signal-averaging statistics of the measurements. In our previous experiments, we obtained a sensitivity of 0.6 picotesla by averaging only two repetitions of the optical pumping cycle. During a measurement period of 0.3 seconds, which corresponds to a signal bandwidth of one hertz, we could actually repeat the measurement cycle three times instead of two. The increased number of repetitions would improve the measurement sensitivity by a factor of  $\sqrt{3/2}$ .

Our original noise measurements also involved taking the difference in signal between two identical magnetometers. Since this difference measurement involved two independent noise sources, the sensitivity for a single sensor would be better than that in the difference measurement by a factor of  $\sqrt{2}$ . However, the OIOPM will probably also subtract two optical pumping measurements, made at rf frequencies on either side of the atomic Larmor resonance, in order to determine the magnetic field. This difference measurement will reduce the overall sensitivity by a factor of two, since it both introduces

two independent noise sources and reduces by half the number of magnetic measurements that can be performed in a given time. Combining all these factors, we need to increase our noise estimate by a factor of  $\sqrt{2}$ .

Combining these corrections for cell geometry and experimental design, our scaling of previous results indicates that the OIOPM would have a sensitivity of approximately 0.4 picotesla per root hertz, using an optical pumping cell 10 cm long and 2 cm in diameter. This predicted sensitivity is, in itself, probably adequate for the rapidly deployed sensor array. If necessary, since this projection is far from the theoretical limit, there is also considerable room for technical improvements what would increase the sensitivity of the instrument.

### **A2.3 Long-Term Stability and Heading Error in the OIOPM.**

In addition to the shot noise inherent in the optical absorption measurement, errors in the magnetic measurements will also arise from processes that perturb the measured precession frequency of the potassium atoms. Such processes will determine the heading error of the OIOPM, as well as its stability of the OIOPM over periods of minutes and hours. In predicting these drifts and heading errors, we are concerned mainly with two types of perturbations.

One important perturbation is that caused by collisions between potassium atoms. This effect has been considered previously by Happer [3]. According to Happer's analysis, the shift in the atomic precession frequency is proportional to the frequency of collisions between potassium atoms, and hence to the density of the potassium vapor. At a density of  $6 \times 10^9 \text{ cm}^{-3}$ , a value consistent with our shot-noise calculations in the previous section, the total shift of the precession frequency would be equivalent to a change of 5 picotesla in the absolute value of the magnetic field. In most applications, we will be concerned, not with the absolute value of the field, but in the measurement fluctuations associated with fluctuations in the potassium vapor density. To keep these measurement fluctuations below  $10^{-13}$  tesla, we would have to keep the potassium density constant to approximately 2%. We could control the potassium density to the required precision by maintaining a reservoir of liquid potassium at a temperature that varied by less than 0.3K.

The second source of drift and heading error is the perturbation of the atomic spin states by the radio-frequency tipping field. In order to measure the atomic precession frequency, we apply an rf field that resonantly excites the quantum-mechanical transition between the  $m=2$  and  $m=1$  spin states within the  $F=2$  hyperfine manifold of the potassium atom. This resonant excitation transfers probability amplitude from the  $m=2$  state to the  $m=1$  state, reducing the spin polarization of the atoms. This spin polarization depends on the rf frequency, and is maximized when the rf frequency exactly matches the resonant frequency of the transition.

in addition to this resonant excitation, the rf field also weakly and non-resonantly mixes the  $m=1$  and  $m=0$  states. This mixing in effect shifts the energy of the  $m=1$  state slightly, thus perturbing the resonance frequency of the transition between the  $m=2$  and  $m=1$  states. This shift of the resonant frequency is equivalent to a slight offset in the magnetic field measurement.

To estimate the magnitude this perturbing effect, we have used time-dependent perturbation theory to calculate the shift in the energy of the  $m=1$  state. This energy shift is given by  $\hbar\delta\omega_{12}$ , where

$$\delta\omega_{12} \cong -\frac{3\Omega_{rf}^2}{8\omega_{12}} \quad (14)$$

where

$$\Omega_{rf} = 2\pi\Gamma B_{rf} .$$

In this equation,  $\omega_{12}$  is the difference in angular frequency between the  $m=2/m=1$  transition and the  $m=1/m=0$  transition in an unperturbed potassium atom.  $B_{rf}$  is the magnitude of the rf field. This perturbative analysis is valid when  $\Omega_{rf}/\omega_{12} \ll 1$ .

(In defining the rf field amplitude  $B_{rf}$ , we consider the component of the applied rf field in the plane perpendicular to the ambient dc field. We represent this transverse rf field as the sum of two vector components which rotate in opposite directions about the ambient dc field.  $B_{rf}$  is the magnitude of the component that rotates in the same direction as the atomic precession. If the rf field were applied in the usual manner, with a constant direction and a sinusoidally varying magnitude,  $B_{rf}$  would be half the amplitude of the transverse component of this linearly polarized, sinusoidal rf field.)

Corresponding to the shift in the energy of the  $m=1$  state, there is a change of  $\delta\omega_{12}$  in the frequency of the  $m=2/m=1$  transition, and an offset  $\delta B_{rf} = \delta\omega_{12}/2\pi\Gamma$  in the measured magnetic field.

To estimate this measurement offset, we need to know both the splitting of the spin transitions,  $\omega_{12}$ , and the spin rotation rate produced by the rf field,  $\Omega_{rf}$ . The splitting frequency, in units of radians per second, is approximately  $6 \times 10^3 \text{ sec}^{-1}$  for the isotope potassium-41. Based on our shot-noise analysis in Sec. A2.1, we would expect to choose the rf field so that the spin-rotation rate  $\Omega_{rf}$  was approximately equal to  $10 \text{ sec}^{-1}$ . Such a spin-rotation rate would transfer all the probability amplitude from the  $m=2$  state into the  $m=1$  state during a time equal to the spin relaxation time of the potassium atoms.

Using these values of  $\Omega_{rf}$  and  $\omega_{12}$ , we estimate that the rf field will offset the magnetic measurement by approximately  $10^{-12}$  tesla.

Since this measurement offset depends on the amplitude of the rf field, variations in the rf power may produce drifts in the magnetic measurements. However, these drifts will be less than  $10^{-13}$  tesla if we keep the rf power constant to within 10%.

The rf-induced offset can also produce heading error, or variation of the magnetic measurement as a function of the orientation of the instrument with respect to the ambient earth's field. As discussed above, the effect of the rf field depends, not on the magnitude of the total rf field, but on a specific rotating component of the rf field transverse to the ambient dc field. If the rf field were produced by a single coil whose orientation varied with respect to the ambient field, this transverse rf field component would vary, producing variations in the magnetic measurement. As the instrument was rotated through all possible orientations, the maximum variation of the magnetic measurement would be comparable to the total measurement offset calculated above. That is, without active measures to maintain a constant transverse rf field, the total heading error of the OIOPM would be in the neighborhood of  $10^{-12}$  tesla. This heading error is already much smaller than that of conventional magnetometers based on cesium, rubidium, or metastable helium-4.

However, the OIOPM can potentially provide even lower heading errors. In the OIOPM, we plan to use a set of three orthogonal coils to maintain an rf field whose component transverse to the ambient field is constant. If the field component  $B_{rf}$  is maintained constant to within 10%, the total heading error of the OIOPM will be only  $10^{-13}$  tesla.

Still lower motional errors may be useful in a magnetic gradiometer, where two or more sensors are compared to determine the spatial gradients of the magnetic field. Gradiometric measurements are often limited by sensor noise, rather than ambient magnetic noise, because they depend on the resolution of small differences between the two magnetic measurements. If we mount two OIOPM cells in a rigid structure, so that they experience the same rocking motions, we might reduce the heading error in the magnetic difference measurement by a factor of 10, that is, to  $10^{-14}$  tesla. We might also achieve heading errors of this magnitude by maintaining the transverse rf field constant to within 1%.

#### **A2.4 Summary: Sensitivity and Frequency response of the OIOPM.**

The OIOPM will provide high sensitivity over a wide range of signal frequencies. The analysis above indicates that the low-frequency response of the OIOPM will be extremely good. By controlling the rf field to 10% and the cell temperature to 0.1K, we could keep the measurement drifts below  $10^{-13}$  tesla over periods of hours or days.

The maximum signal frequency for the OIOPM will be half the repetition rate of the measurement cycle. As discussed earlier, the OIOPM will achieve its maximum sensitivity if the period of the measurement cycle is comparable to the relaxation time of the atomic spins. This criterion would dictate a repetition rate of approximately 10 hertz. If higher-frequency measurements were required, we could increase the repetition rate at a small cost in sensitivity. Our earlier analysis of shot noise indicates that the noise floor of the instrument will increase roughly as the square root of the repetition rate.

Our analysis, including both shot noise and long-term drifts, indicates that the OIOPM will have an intrinsic noise limit of roughly  $2 \times 10^{-14}$  tesla per root hertz. The total heading error will be less than  $10^{-13}$  tesla for a single cell, and roughly  $10^{-14}$  tesla for a magnetic gradiometer involving two cells mounted in a rigid structure. Thus, the OPIM can potentially compete with SQUID magnetometers in sensitivity.

## A3 Other Performance Characteristics of the OIOPM

In this section, we analyze a variety of key performance characteristics affecting the practical utility of the OIOPM.

### A3.1 Tolerance for Magnetic-Field Gradients

If a magnetic sensor is placed near the bottom of the ocean, it may be subjected to magnetic-field gradients due to the proximity of magnetic rocks on the ocean floor. Sufficiently large field gradients will interfere with the operation of an optically pumped magnetometer by reducing the spin-relaxation time of the precessing atomic or nuclear spins. This problem of field gradients is important enough that, when helium-3 nuclear magnetometers are deployed on the ocean bottom, special precautions are taken to place the sensor a few feet above the bottom itself.

Because it operates in an inherently different physical regime, we believe that the OIOPM will be able to tolerate much larger magnetic-field gradients than the helium-3 magnetometer. This gradient tolerance may simplify the deployment of a sensor array by making possible to lay the magnetometers directly on the ocean floor.

In this section, we estimate in an approximate way the maximum field gradients in which optically pumped magnetometers will operate. We first consider the gradient tolerance of an OIOPM in which the motion of the potassium atoms is suppressed by a buffer gas. We then develop a simple model that takes into account the gradient-averaging effect of atomic motion. We apply this model to an OIOPM that eliminates the buffer gas in order to maximize this motional averaging. We also use this model to compare the gradient tolerance of the OIOPM to that of the helium-3 nuclear magnetometer.

In a non-uniform magnetic field, the atomic or nuclear spins precess at different rates in different parts of the optical pumping cell. As this differential precession continues, the precessing spins get progressively farther out of phase with each other, and the net polarization of the spins decays. The field inhomogeneity thus decreases the relaxation time  $T_2$  of the precessing spins. The reduction in  $T_2$  increases the linewidth of the nuclear precession, reducing the sensitivity of the optically pumped magnetometer.

To assess the importance of this inhomogeneous-field effect, we need to estimate the rate of increase in the phase dispersion  $\delta\phi$ . We define this quantity by

$$\delta\phi^2 = \langle (\phi - \bar{\phi})^2 \rangle , \quad (15)$$

where  $\phi$  is the phase associated with the precession of any given spin, and  $\bar{\phi}$  is the average of the phase over the entire ensemble of spins. The angular brackets here represent a thermal ensemble average over the possible arrangements of the atomic spins. Our main

concern below will be to estimate the time required for  $\delta\phi$  to increase to approximately one radian. This dephasing time is a measure of the rate at which the spin polarization decays due to the dephasing of the precessing spins.

For an OIOPM that uses a buffer gas in the optical pumping cell, we assume that the precessing species diffuse only an insignificant distance during the characteristic relaxation time of the spins. Under these conditions, the phase dispersion will increase linearly with time:

$$\frac{d(\delta\phi)}{dt} \sim 2\pi\Gamma L \frac{dB}{dx}, \quad (16)$$

where  $\Gamma$  is the gyromagnetic ratio of the spins (in cycles per second per unit field),  $dB/dx$  is the magnitude of the field gradient, and  $L$  is the length of the optical pumping cell in the direction of the field gradient.

The linewidth of the spin precession, and hence the sensitivity of the magnetometer will be significantly reduced at a field gradient large enough to make  $\delta\phi$  increase by one radian in a time comparable to the intrinsic spin relaxation time  $T_2$ . That is, the maximum tolerable field gradient is given roughly by

$$\left. \frac{dB}{dx} \right|_{\max} \sim \frac{1}{2\pi\Gamma L T_2}. \quad (17)$$

For a potassium magnetometer using a buffered cell, with a cell length  $L$  of 5 cm, the maximum tolerable gradient is approximately 5 nanotesla per meter, or 1.5 nanotesla per foot.

This gradient tolerance can be improved by eliminating the buffer gas. The density of potassium atoms is low enough so that, in the absence of a buffer gas, a potassium atom will usually travel from one side of the cell to the other without experiencing a collision along the way. Each atom effectively explores all parts of the cell, so that each atom effectively experiences an average of the magnetic field over the volume of the cell. To the extent that this averaged field is the same for all the atoms, this motional averaging will reduce the dispersion in spin precession rates produced by the inhomogeneity of the magnetic field.

To estimate the effectiveness of the motional averaging, we need a model that accounts for the statistical variation in the time-averaged fields experienced by the population of potassium atoms. To derive this model, we assume that the optical pumping cell is long and narrow, with its long axis in the  $x$  direction. We concentrate on describing the motion of the atoms along the  $x$  axis, since field gradients in this direction will have the greatest

effect on the dephasing time of the atomic spins. Within this one-dimensional description, we express the phase dispersion in terms of a correlation function describing the statistical motion of the spins:

$$\begin{aligned}
 \langle \delta\phi^2 \rangle &= \left\langle \left( 2\pi\Gamma \int dt {}_0^t B(x(t)) - \bar{B} \right)^2 \right\rangle \quad (18) \\
 &\cong (2\pi\Gamma)^2 t \left\langle \int_{-\infty}^{\infty} d\tau (B(x(0)) - \bar{B})(B(x(\tau)) - \bar{B}) \right\rangle \\
 &= \frac{(2\pi\Gamma)^2 t}{L} \int_0^L dx (B(x) - \bar{B}) \int_{-\infty}^{\infty} d\tau \int_0^L dx' P(x' - x, \tau) (B(x') - \bar{B}) .
 \end{aligned}$$

In these equations,  $x(t)$  is the position of a given atom as a function of time,  $L$  is the length of the cell in the  $x$  direction,  $B(x)$  is the magnetic field at the position  $x$ , and  $\bar{B}$  is the average of the field over the length of the cell.  $P(x' - x, \tau)$  is the probability of finding an atom at the position  $x'$  at the time  $\tau$ , given that it was at the position  $x$  at time zero.

The main approximation made in going from part (a) to part (b) of this equation is that the time  $t$  is long compared with the characteristic decay time of the correlation function on the right hand side. Since we will be using this analysis to estimate the phase dispersion at times comparable to the spin relaxation time  $T_2$ , this approximation will be valid when the characteristic correlation time is short compared with  $T_2$ .

In calculating the position-time correlation function  $P(x, \tau)$ , we have to take account of the fact that the atoms are confined by the ends of the cell to the interval  $0 < x < L$ . To avoid the inconvenience of incorporating this boundary condition, we note that, in terms of the time-dependent magnetic fields experienced by the atoms, our problem is equivalent to that of a population of atoms that moves freely along the entire  $x$  axis, where the position-dependent field  $B(x)$  is replaced by a suitable periodic function. This function has a period of  $2L$ , agrees with the actual field distribution within the interval  $0 < x < L$ , and is symmetric about the point  $X = 0$ . If the magnetic field within this interval is a linear ramp, the appropriate periodic function is a triangular wave with period  $2L$ .

Having eliminated the cell boundaries and replaced  $B(x)$  by its periodic equivalent, we can now use a position-time correlation function

$P(x, \tau)$

appropriate for unrestricted motion along the entire  $x$  axis:

$$\langle \delta\phi^2 \rangle = \quad (19)$$

$$\frac{(2\pi\Gamma)^2 t}{L} \int_0^L dx (B(x) - \bar{B}) \int_{-\infty}^{\infty} d\tau \int_{-\infty}^{\infty} dx' P(x-x', \tau) (B(x') - \bar{B}) ,$$

where 
$$P(x' - x, \tau) = \frac{1}{\sqrt{4\pi D\tau}} \exp\left(-\frac{(x' - x)^2}{4D\tau}\right) .$$

Here,  $D$  is an effective diffusion coefficient describing the statistical motion of the atoms along the  $x$  axis.

To evaluate Eq. (19), we represent the periodic triangle wave  $B(x)$  by its Fourier series:

$$B(x) - \bar{B} = \sum_{n=1}^{\infty} B_n \cos(n\pi x/L) , \quad (20)$$

where 
$$B_n = \frac{4L}{(n\pi)^2} \left( \frac{dB}{dx} \right) .$$

The summation here includes only odd values of  $n$ .

Inserting Eq. (20) into Eq. (19), and evaluating the resulting integrals, we have

$$\langle \delta\phi^2 \rangle \cong \frac{64\Gamma^2 L^4 t}{\pi^4 D} \left( \frac{dB}{dx} \right)^2 \sum_{n=1}^{\infty} \frac{1}{n^6} . \quad (21)$$

Here, as in the previous equation, the summation includes only odd values of  $n$ . Only the first term in the summation makes a significant contribution to the result.

As in the case of the potassium vapor cell with buffer gas, the maximum tolerable field gradient for the unbuffered cell is that which causes the phase dispersion to increase to approximately one radian in a time  $T_2$ . That is,

$$\left( \frac{dB}{dx} \right)_{\max}^2 \cong \frac{\pi^4 D}{64\Gamma^2 L^4 T_2} . \quad (22)$$

To estimate the maximum field gradient, we need values for the gyromagnetic ratio  $\Gamma$ , the spin relaxation time  $T_2$ , the cell length  $L$ , and the effective diffusion coefficient  $D$ . The gyromagnetic ratio for potassium atoms is approximately 700 kHz per gauss. From our previous experiments with potassium optical pumping, a typical  $T_2$  is approximately 0.1 sec. In keeping with our shot-noise sensitivity estimate from Sec. A2.1, we choose a cell length  $L$  of 5 cm.

To derive a reasonable value for the effective diffusion coefficient, we start with a formula from the kinetic theory of gases [7]:

$$D = \frac{1}{3} \bar{v} l, \quad (23)$$

where  $\bar{v}$  is the mean thermal velocity of the potassium atoms, and  $l$  is their mean free path. In ordinary diffusion within a gas,  $l$  is the average distance an atom travels before its velocity and direction are changed by a collision with another gas molecule. In the unbuffered potassium vapor cell, the atoms travel freely from one side of the cell to the other, changing their direction and velocity when they collide with the walls of the cell. In this case, roughly speaking,  $l$  is the average distance the atoms travel between collisions with the cell walls. This distance will be comparable to the diameter of the cell. Using an  $l$  of 2 cm, we obtain a  $D$  of approximately  $1.4 \text{ m}^2/\text{sec}$ .

Inserting all of these parameters into Eq. (22), we estimate that the maximum tolerable field gradient is roughly  $260 \text{ nT/m}$  ( $86 \text{ nT/ft}$ ), for an OIOPM with an unbuffered potassium vapor cell, with a cell length of 5 cm and a cell diameter of 2 cm. Comparing this result with that obtained for the buffered cell, we find that, with the cell dimensions considered here, the motional averaging in the unbuffered cell increases the gradient tolerance of the magnetometer by nearly a factor of 100. Since the maximum gradient scales differently with cell dimensions in the two cases, the relative advantage of motional averaging will decrease somewhat as the cell length increases.

This ability to operate in large field gradients is potentially an important advantage for the OIOPM over other types of optically pumped magnetometer. Although we are not aware of any published information on the gradient tolerance of these other instruments, we can make reasonable inferences about their performance using the models derived above. Most cesium and rubidium magnetometers will use buffered cells, with cell dimensions,  $T_2$ s and gyromagnetic ratios similar to those assumed in our calculations for the OIOPM. These instruments will have gradient tolerances in the neighborhood of  $5 \text{ nT/m}$ , in keeping with our estimates for the OIOPM with the buffered potassium vapor cell. The helium-4 magnetometer, with a gyromagnetic ratio of  $2.8 \text{ MHz per gauss}$  and a  $T_2$  in the vicinity of one millisecond, will probably tolerate field gradients of  $100 \text{ nT/m}$  or greater.

Of all the current types of optically pumped magnetometer, the helium-3 nuclear magnetometer is probably the most sensitive to magnetic-field gradients. The gradient sensitivity of this instrument arises from its unique measurement process, which relies on the exceptionally long spin relaxation time of helium-3 nuclei. The measurement cycle includes an initial optical pumping phase and a long period of free nuclear precession. During the optical pumping phase, an electrical discharge places some of the helium atoms into a metastable, electronically excited state that has a nonzero electronic spin. Optical pumping

aligns these metastable electronic spins with the ambient magnetic field, and a collisional process transfers this spin alignment to the helium-3 nuclear spins. The electrical discharge and pump light are then turned off, and an rf field stimulates the nuclei to precess synchronously about the ambient magnetic field. During the free-precession period, the nuclei continue to precess about the ambient field. This precession is observed, using induction coils to detect the oscillating nuclear magnetic moment, and the precession frequency is monitored in order to determine the intensity of the ambient magnetic field. In a typical helium-3 magnetometer, the optical pumping process might require several minutes, and the free nuclear precession might last as long as a day.

In this measurement scheme, the sensitivity of the magnetic measurements will be seriously degraded if the spin relaxation time drops much below the interval between optical pumping phases. Consequently, the measurement interval will help to determine the tolerance of the helium-3 magnetometer for magnetic-field gradients. The measurement period can be undoubtedly be adjusted according to the field gradients expected in a given application. However, a long measurement cycle is presumably desirable, both to minimize the dead time and power consumption associated with the optical pumping phase. In our estimates of the tolerable field gradient, we will consider measurement times of  $10^5$  seconds, or roughly one day, and  $10^3$  seconds, or 16 minutes. Based on our limited information about the helium-3 magnetometer, we believe that this longer interval is close to that used in conventional helium-3 magnetometers. In order to reduce the measurement period to  $10^3$  seconds, it will presumably be necessary to reduce significantly the time and power consumption required for the optical pumping phase.

For any reasonable measurement interval, the spin relaxation time will be much longer than the time required for a helium atom to diffuse across the optical pumping cell. As a result, motional averaging will significantly reduce the spin-dephasing effects of field gradients. We therefore use Eq. (22), rather than Eq. (16), to estimate the maximum field gradient for the helium-3 magnetometer. In this formula, we assume a cell length  $L$  of 5 cm. We insert the gyromagnetic ratio of helium-3 nuclei, 3.2 kHz per gauss. For the helium-3 magnetometer, the effective diffusion constant  $D$  is the actual self-diffusion coefficient of the helium-3 atoms within the cell. We assume  $D$  is equal to  $0.01 \text{ m}^2/\text{sec}$ , which corresponds to a pressure of 10 torr in the helium-3 cell. The information available to us indicates that this helium pressure is typical for the helium-3 nuclear magnetometer.

With these parameters, we estimate a maximum field gradient for the helium-3 magnetometer is  $4.9 \text{ nT/m}$  with a  $T_2$  of  $10^5$  seconds, or  $49 \text{ nT/m}$  with a  $T_2$  of  $10^3$  seconds. This estimate suggests that, even with a measurement cycle 100 times shorter than that used in conventional instruments, the gradient tolerance of the helium-3 magnetometer will be many times less than that of the OIOPM.

### A3.2 Power Requirements of the OIOPM

In a rapidly deployed sensor array, OIOPM will be required to operate for long periods on battery power. It will therefore be important to minimize power consumption of instrument.

Our initial analysis indicates that the OIOPM can operate on a total power of roughly 320 milliwatt. This analysis is very conservative in that it is based on a electronic measurement scheme that was not originally conceived to minimize power consumption. It seems likely that, with a revised electronic design, the power consumption of the OIOPM can be reduced below 200 milliwatts.

In estimating the power requirements of the OIOPM, we have analyzed all of the major subsystems in the instrument. According to the detailed analysis below, the estimated power consumption for these subsystems is as follows:

- (1) Losses in the rf and dc field coils: less than one mW.
- (2) The oven that keeps the potassium vapor cell at its operating temperature: less than 10 mW.
- (3) Laser diodes to produce potassium spectral light: approximately 40 mW.
- (4) Electronics to control the instrument and measure the precession frequency of the potassium atoms: approximately 265 mW.

Adding up the power requirements for all these subsystems, we estimate a total power budget of 316 mW.

#### A3.2.1 Power Requirements of the RF and DC Field Coils

The OIOPM applies its own dc and rf fields during the optical pumping process. In this section, we verify that the field coils do not require excessive amounts of power.

For the dc field coils, our main concern is the ohmic loss in the coil windings. This loss is determined mainly by the required magnetic field, the overall size and shape of the field coils, the electrical conductivity of the windings, and the total cross-sectional area of conductor in the windings. To get a rough idea of the power requirements, we consider a simple cylindrical solenoid with a length  $l$  of 5 cm and a diameter  $d$  of 2 cm. To produce a field  $B_{dc}$ , the solenoid windings must carry a current given by

$$I = \frac{B_{dc} l}{\mu_0 N}, \quad (24)$$

where  $\mu_0$  is the permeability constant and  $N$  is the number of windings in the solenoid. This total current must pass through the resistance of the windings, which is given by

$$R = \frac{\rho \pi d N^2}{l t} , \quad (25)$$

where  $\rho$  is the resistivity of the windings, and where the total cross-sectional area of the windings is equivalent to that of a layer of material with thickness  $t$  covering the circumference of the solenoid. The ohmic loss in the windings is given by

$$P_{ohmic} = I^2 R = \frac{\rho B^2 l \pi d}{\mu_0^2 t} . \quad (26)$$

The dc coils need to produce a field of approximately one gauss ( $10^{-4}$  tesla) in order to cancel the earth's magnetic field and apply a field of comparable magnitude along the axis of the pump beam. If we use copper windings, and if the winding thickness  $t$  is one millimeter, the length  $l$  is 5 centimeters, and the coil diameter  $d$  is 2 centimeters, producing such a field will entail an ohmic power loss of less than one half milliwatt.

The actual coil configuration in the OIOPM will undoubtedly be different from the simple solenoid assumed here. However, the results of this preliminary calculation clearly indicate that the dc field coils will not require any substantial fraction of our one-watt total power budget.

In addition to the dc field coils, we have also estimated the power required to produce the rf fields required by the OIOPM. Based on the gyromagnetic ratio of the potassium atom, we estimate that an rf field amplitude of several microgauss will be required to produce a 90-degree spin rotation during the typical rf pulse length of 0.1 second. With this small field, the ohmic losses in the rf coils will be even smaller than those in the dc coils.

Depending on the details of the rf drive circuit, some energy may also be consumed as the field is alternately created and destroyed with each period of the rf oscillation. To estimate the maximum power that would be dissipated in this way, we calculated the total energy associated with a field of 3.7 microgauss in a cylindrical volume 5 centimeters long and 2 centimeters in diameter. We then assumed that this energy was completely dissipated each time the rf field went from its maximum value to zero. At an rf frequency of one megahertz, corresponding to the precession frequency of potassium atoms in an ambient earth's field greater than one gauss, the total power consumed in this way was only 20 picowatts. This calculation confirms that the rf field coils will represent a negligible contribution to the total power budget of the OIOPM.

### A3.2.2 Power Requirement of the Cell Oven

The OIOPM must keep its optical pumping cell at a somewhat elevated temperature in order to maintain a suitable vapor pressure of potassium. One of our main tasks in this engineering study was to verify that we could maintain the required cell temperature within our desired power budget.

To minimize the heating requirements, we plan to use a design borrowed from liquid-helium dewars. We will surround the potassium vapor cell with a thermally insulating vacuum jacket which uses several layers of aluminized mylar "superinsulation" to minimize radiative heat transfer. A fiberglass spacer material will keep the layers from touching, thus minimizing the conductive heat transfer through the superinsulation.

The heat flow through this layered superinsulation is given by

$$Q = \frac{k_a A (T_2 - T_1)}{t}, \quad (27)$$

$$\text{where } k_a = \left( \frac{1}{N/\Delta x} \right) \left\{ h_s + \left( \frac{\sigma \epsilon T_2^3}{2 - \epsilon} \right) \left( 1 + \left( \frac{T_1}{T_2} \right)^2 \right) \left( 1 + \frac{T_1}{T_2} \right) \right\}.$$

In these equations,  $T_2$  and  $T_1$  are the temperature of the inner and outer walls of the vacuum jacket,  $A$  and  $t$  are the area and thickness of the insulating jacket,  $N/\Delta x$  is the number of insulating layers per unit thickness,  $h_s$  is the conductance per unit area of the spacer material between the layers,  $\sigma$  is the Stephan-Boltzmann constant, and  $\epsilon$  is the emissivity of the aluminized mylar.

For our heat-flow calculation, we use  $N/\Delta x = 3000$  layers per meter,  $h_s = 0.085 \text{ W/m}^2 \text{ K}$ , and  $\epsilon = 0.05$ . These values are typical for aluminized mylar with fiberglass spacer material. We take  $T_1 = 298 \text{ K}$  ( $25^\circ \text{C}$ ) and  $T_2 = 333 \text{ K}$  ( $60^\circ \text{C}$ ). This upper value is the cell temperature that gave us the optimum signal-to-noise ratio in our previous experiments with potassium-vapor magnetometers.

To determine reasonable values of the jacket area  $A$  and jacket thickness  $t$ , we consider a cylindrical dewar with an inner diameter of 2.5 cm, an outer diameter of 4.5 cm, and an overall length of 10 cm. Eq. (27) has actually been derived for a planar geometry, in which both the inner and outer walls of the vacuum jacket have the same area. For our cylindrical dewar, the appropriate value of  $A$  in Eq. (27) is somewhere between the areas of the inner and outer walls. However, to put an upper bound on the heat flow, we choose  $A = 0.02 \text{ m}^2$ , which is approximately the area of the outer wall of the cylindrical dewar.

With these reasonable values of the parameters, we find a total heat leak 6.3 mW from the potassium vapor cell to the environment through the superinsulated vacuum jacket. This calculation indicates that only a very small portion of the total power budget will be required to maintain the potassium vapor cell at its optimum temperature.

### **A3.2.3 Power Requirement of the Potassium D1 Light Sources**

In the previous two subsections, we have shown that neither the cell oven, nor the rf and dc field coils, contributes more than a few milliwatts to the power consumption of the OIOPM. A somewhat more significant contribution comes from the lamps that supply the potassium D1 light for optical pumping.

In our previous experiments with potassium-vapor magnetometers, we produced the potassium spectral light using electrodeless discharge lamps containing potassium vapor. An advantage of these lamps was that they automatically produced light at precisely the spectral wavelengths of potassium, with linewidths nearly as narrow as the absorption bands of the potassium vapor in the optical pumping cells. However, the radio-frequency oscillators that excited the lamps consumed several watts of electric power.

In the OIOPM, we plan to use laser diodes to produce the required spectral light with much lower power consumption. The feasibility of using laser diodes is established in a separate section below.

To predict the power consumption of the laser diodes, we first estimate the total number of D1 photons that must be passed through the optical-pumping cell during the optical repumping phase. In our previous experiments with potassium optical pumping, we found that a pump-beam photocurrent of one microampere produced a repumping time constant of approximately 0.1 second. Integrated over one repumping time constant, this pump-beam current corresponds to a total of approximately  $10^{12}$  D1 photons. To derive a conservative power estimate, we assume that the pump light is actually left on for ten time constants, so that roughly  $10^{13}$  D1 photons would be required each time the optical pumping is repeated.

Now, since the output specifications of laser diodes are given in terms of optical power, rather than photon flux, we need to convert the required number of photons into its energy equivalent. Given the wavelength of the potassium d1 light (770 nanometers), we know that each photon carries approximately  $3 \times 10^{-19}$  joules of energy. Therefore, the number of photons required for repumping is equivalent to  $3 \times 10^{-6}$  joules of optical energy from the laser diode.

One representative laser diode (Sharp Corp. Model # LT024) produces 30 mW of optical energy at a wavelength of approximately 780 nanometers, while consuming 100 mW of input power. (We assume that the same laser diode technology could be used

to produce approximately the same output with the same efficiency at 770 nanometers.) However, the output linewidth of this laser diode is approximately one nanometer, while the Doppler-broadened linewidth of the potassium absorption line is only 1/400 of one nanometer. Consequently, this laser diode will actually provide only  $30 \text{ mW}/400 = 0.075 \text{ mW}$  of optical power within the optical absorption band of the potassium vapor. At this power level, the laser would be pulsed for 40 milliseconds in order to produce the required 3 microwatt-seconds of optical energy within the d1 absorption line of potassium. The total input energy consumed during this pulse would be  $40 \text{ msec} \times 100 \text{ mW} = 4 \text{ millijoules}$ .

The repumping process would be repeated roughly ten times per second, or once for each cycle of our pulsed measurement scheme. Thus, the average power consumption of the laser diode would be roughly  $4 \text{ millijoules} \times 10 \text{ Hz} = 40 \text{ milliwatts}$ .

### **A3.2.4 Power Requirements for the Electronics**

The largest single contribution to the power consumption of the OIOPM will probably be the electronics used to measure the precession frequency of the optically pumped atoms. To place an upper bound on the power requirements for the electronics, we started with a block diagram for the electronics system, and then identified specific devices for performing each function. We assumed a specific measurement scheme, in which a direct digital synthesizer (DDS) was used to generate the frequency of the rf field. Since the DDS is designed for speed, precision, and flexibility, rather than low power consumption, this approach is clearly not the optimum one for low-power operation. Even with the DDS, however, we find that the total power consumption of the electronics system is roughly 300 milliwatts. We anticipate that a different electronic design could bring the total power consumption well below 200 milliwatts.

In addition to the main function of frequency measurement, our preliminary block diagram also includes such functions as maintaining the temperature of the potassium-vapor cells and controlling the currents in the dc field coils. The major electronic components in this design include (1) the logic used to process the photodiode signals and control the DDS, (2) the operational amplifiers used as buffers and drivers throughout the system, (3) the crystal oscillator that provides the frequency reference for the precession-frequency measurement, (4) the analog-to-digital convertors that convert the photodiode signal to digital form, (5) the digital-to-analog convertor that converts the output of the DDS into an analog rf signal, and (6) the DDS itself.

#### **A3.2.4.1 CMOS Logic Types**

The CMOS logic that would be used in a project such as this comes in two types of integrated packages, the 4000 series and the newer 74Hc series. The 4000 series uses approximately 4 microamps at 5 volts per MHz per complex package. The

more versatile 74HC series may consume as much as 5 times more current. The current consumed by these logic elements will depend somewhat on loading conditions and clocking speed. However, at the 2-MHz clocking speed used in the OIOPM, most CMOS logic will operate at a current only slightly greater than the specified quiescent package current.

We anticipate using a mixture of these two logic families. Considering the slow sample rate of the magnetometer (10 samples per second) the 4000 series would be more compatible with our low power requirements. We would reserve the 74HC family for either logic functions not served by the 4000 series or direct interfacing with VLSI components such as the DDS. With these considerations in mind, we conservatively estimate an average current consumption of 10 microamperes for each complex package. We anticipate using roughly 20 logic packages, for a total current drain of 200 microamperes, and a total power consumption of approximately one milliwatt. This result implies that the logic functions will not be a major factor in the total power consumption of the electronics system.

#### **A3.2.4.2 Operational Amplifiers**

Our block diagram uses 12 op amps to perform a variety of functions, such as driving the rf and dc coils, driving the heaters for the potassium vapor cells, amplifying the outputs of the Hall sensors used to monitor the approximate direction of the ambient field, and buffering the output of the photodetector. In our initial power estimates, we have assumed the use of standard operational amplifiers (OP-21 and OP-97), which have a power consumption of approximately 5mW per amplifier, or a total power consumption of 60 mW for all 12 amplifiers. This figure could be reduced considerably using micro-power operational amplifiers.

#### **A3.2.4.3 Temperature Compensated Crystal Oscillator**

Our initial block diagram uses a temperature-compensated crystal oscillator (TCXO) as a time base for measuring the atomic precession frequency. Most TCXOs presently available from reputable firms offer about the same stabilities or aging characteristics. Typical drift specifications are:

Per year  $1E-7$  over the temperature range of 0 to 50 degrees C.

Per Day  $3E-9$  average.

Per second  $1E-9$  under constant conditions.

Power consumption 50 milliwatts max. 30 milliwatts typical.

A frequency drift of  $3E-9$  per day corresponds to an error of only 0.3 picotesla in the magnetic measurement. Even better performance can be obtained at an increased current.

The above specifications apply in particular to the model number C0252B17 presently manufactured by Vectron Laboratories Inc., of Norwalk, Connecticut.

#### **A3.2.4.4 Analog to Digital Converters**

Our initial block diagram uses five analog-to-digital (A-D) converters, one 12-bit A-D for the signal from the photodiode, and 8-bit A-Ds for the signals from one thermometer and three Hall sensors. We considered several types of A-D convertor. The most ideal unit would be one which embodies the following characteristics; CMOS, 12 bit, parallel output, contains internal reference, operates from a single supply, and can provide 50 conversions per second.

Current specifications for A-D convertors can be misleading. The lowest-current A-D convertors tend to have serial data outputs and, in some cases, require an external voltage reference. Serial data output adds to the power requirements of the electronics because a register is required to hold the value yielded of each conversion. The requirement for an external reference also adds to the overall power requirements, since the voltage reference is the most current-consuming portion of an A-D convertor.

Based on these considerations, we selected an A-D convertor which is self contained, requires a single power source, has a power consumption of 1mW, and a provides 12-bit parallel data output. The specific unit identified is a Datal ADC-HS12B, an "industry standard". Other A-Ds of the same type are available from both Analog Devices and Maxim. The same device would serve well both as the 12-bit convertor for the photodiode output, and the 8-bit A-D for the Hall sensors and thermometer.

This analysis indicates that the total power consumption for the A-D convertors will be 5 mW or less.

#### **A3.2.4.5 Digital to Analog Converters**

One significant component in the power requirement of the electronics is the Digital-to-Analog (D-A) convertor that takes the output of the DDS and produces an analog waveform for the rf coils. Our initial calculations are based on the 12-bit PMI DAC 8012. This device, together with its external voltage reference, would consume approximately 50 milliwatts at a clock speed of 2 MHz.

Our preliminary design also uses three 8-bit D-A convertors to drive the dc bias coils, and an additional 8-bit convertor to drive the heater for the potassium vapor cell. A suitable D-A for these requirements is National Semiconductor DAC-0830, which consumes 2 milliamperes at 5 volts. The power requirement for three convertors could be reduced using a three-output D-A, which uses the same voltage reference for all three output channels.

The total power consumption for D-A convertors is 80 milliwatts in our initial block diagram.

#### **A3.2.4.6 Direct Digital Synthesizer**

The recommended DDS for this project is the TRW TMC 2340. Its power consumption at a reduced clock frequency (2 MHz) is approximately 10 milliamperes at 5 volts, which is about typical for other DDS devices presently on the market. The TDC 2340 controls frequency through a 32 bit parallel port. Normally, at a 20 MHz clock rate the least-significant control bit corresponds to a frequency increment of 0.005 Hz. However, however by reducing the clock speed by a factor of 10 the frequency resolution improves to 0.0005 Hz to an maximum output frequency of 1 MHz.

#### **A3.2.4.7 Total Power for the Electronics Package**

The total power estimate for the electronics package is 265 milliwatts, including the specific items discussed above, plus an additional 40 milliwatts for power conditioning and miscellaneous voltage references.

### **A3.3 Feasibility of Using Laser-Diode Light Sources**

In order to establish that the OIOPM can operate with a minimum power consumption, we need to show that laser diodes, rather than electrodeless discharge lamps, can be used to produce the potassium D1 light required for optical pumping. In our previous study of potassium-vapor magnetometers, we found two main obstacles to this use of laser diodes.

First, it was not entirely clear that we could obtain laser diodes that would produce the precise 770-nanometer wavelength required for potassium optical pumping. Laser diodes were available at a wavelength of 780 nanometers, and it was known that the output wavelength could be shortened by cooling the laser diode below room temperature. However, the amount of cooling required to reach 770 nanometers would have slightly exceeded the normally specified temperature range for these devices. In addition, the output wavelength for these devices varied discontinuously with temperature, so that there was no guarantee that any individual device could be made to produce the desired wavelength.

The second problem was that the output linewidth of the laser diodes was much broader than the absorption line of the potassium vapor. Because of this broad linewidth, a large amount of light from the laser diode would pass through the optical-pumping cell without interacting with the potassium vapor. In the usual detection scheme, where we determine the absorption of the pump light by monitoring the current in the transmitted beam, this additional light would greatly increase the shot noise in the optical absorption measurement.

The technology of laser diodes has been advancing since our previous study, and it appears that both of these problems can be solved. One way to achieve both continuous tuning and a narrow linewidth is to place the diode in an external laser cavity with an adjustable mirror position. New Focus, Inc., has used this principle to develop a diode laser that will provide any wavelength within a 16-nanometer range surrounding a center frequency near 780 nanometers. The center frequency can be selected so that this tuning range includes the 769.9-nanometer D1 line of potassium. The output linewidth is roughly  $4 \times 10^{-6}$  nanometers, many times smaller than the absorption linewidth of potassium vapor, and the output power within this output line is approximately 5 mW. The narrow linewidth and precise tuning of this laser would be ideal for perform optical pumping measurements, with transmission detection, on potassium vapor.

(In tuning over the entire wavelength range, this laser will at some points hop from one cavity mode to another. However, the modes overlap in wavelength, so that any desired wavelength within the tuning range can be produced. The manufacturers report that the laser operates stably on a single mode even at wavelengths where two modes overlap.)

The New-Focus laser is a laboratory instrument, designed for very precise measurements over a range of wavelengths. It has a retail price of \$16,500, and includes an electronics package that takes up a full standard-sized rack-mount chassis. This high price and bulky packaging are not directly suitable for a compact magnetometer that would be deployed in the field. However, the existence of this instrument clearly demonstrate that diode lasers can produce the wavelength and linewidth required for optical pumping of potassium vapor.

Presumably, the basic external-cavity approach can be adapted to a compact, suitably priced laser light source for the OIOPM. This compact laser would only need to produce a single wavelength, and would not need the extremely narrow linewidth achieved by the New Focus instrument.

As an alternative to developing a compact, narrow-line diode laser, it may be possible to use more conventional, broad-line laser diodes. We would start with the laser diodes now available with nominal center wavelengths of 780 nanometers. These diodes have a statistical distribution of center wavelengths, with a standard deviation in the vicinity of 5 nanometers. From this spectrum, we would select devices whose center wavelengths were as close as possible to 770 nanometers. We would then use temperature tuning or external optics to produce the precise wavelength required. We would overcome the problem of discontinuous tuning by simply selecting those individual diodes that could be made to produce the required wavelength.

This approach would produce an output linewidth of approximately one nanometer, roughly 400 times greater than the absorption linewidth of the potassium atoms. For transmission detection, we would use an external filter, such as a Fabry-Perot interferometer, to block the unwanted light that fell outside of the potassium absorption line.

### A3.4 Fluorescence Detection with Laser-Diode Pump Light

In our Phase-I statement of work, we proposed to investigate another possible detection scheme, fluorescence detection, which would allow us to use the laser diodes without special means for narrowing the output line. In fluorescence detection, we would surround the optical pumping cell with photodetectors, and detect the photons reemitted by atoms that had absorbed light from the pump beam. As long as the photodetectors were not in the path of the pump beam, and there were no excessive reflections of pump light into the detectors, we would detect roughly one fluorescence photon for each pump-beam photon that was absorbed by the potassium vapor. With fluorescence detection, unlike transmission detection, the shot noise in the optical measurement would not be affected by the large amount of pump light that passed unabsorbed through the optical-pumping cell.

One potential problem with fluorescence detection is the dark current in the photodetectors. Photodiodes produce a certain amount of output current even when they are not exposed to light. This dark current is especially important in fluorescence detection because of the large detector area required. If the dark current is much larger than the current produced by fluorescence photons, the signal-to-noise ratio of the optical measurements will be compromised.

However, photodetectors are available with dark currents is low enough for efficient fluorescence detection in the OIOPM. One example of these devices is the Model SD-444 silicon photodiode produced by Silicon Detector Corporation. Because our optical measurements do not require particularly short response times, we would operate the photodiode at a low bias voltage in order to minimize the dark current. At a bias of one volt, the SD-444 has a response time less than 1.1 microseconds, and a dark current of approximately 7 nanoamperes per square centimeter of active area. We would require approximately 60 square centimeters of detector to surround our optical pumping cell, so that the total dark current would be approximately 400 nanoamperes.

Based on our calculations of the photon flux from a broad-line photodiode (see previous section), we estimate that the repumping process will take place with a time constant of at most a few milliseconds. If we, therefore, assume that most of the fluorescence signal is collected during the first ten milliseconds of repumping, the dark current during that collection time will be equivalent to  $2.5 \times 10^{10}$  fluorescence photons. This dark-current background signal is approximately equal to the total number of fluorescence photons that we expect to collect during this signal integration time. (We estimate this total fluorescence signal using the same basic model that we developed for predicting the shot-noise sensitivity limit of the instrument.)

This analysis indicates that we can, in principle use fluorescence detection to achieve roughly the same signal-to-noise ratio that we would achieve with transmission detection under conditions where a significant fraction of the pump beam was absorbed by the potassium vapor.

In addition to this concern with dark currents, fluorescence detection would probably introduce some problems in the practical engineering of the optical-pumping cell. One problem is that of obtaining sufficient detector area in a reasonably simple package. The largest individual photodiodes that can be manufactured with reasonable yield have an active area of approximately one square centimeter. To surround the optical-pumping cell, we would probably mount a large number of individual photodiodes on a printed-circuit board. Representatives from Silicon Detector Corp. have told us that this kind of packaging is a routine process for them.

An additional problem with fluorescence detection is that of providing thermal insulation for the optical pumping cell, while allowing the fluorescence light to reach the photodetectors. One possible solution would be to mount the photodiodes within the cell oven. However, this approach may increase the dark current in the photodetectors. Another possible approach would be to enclose the cell in a transparent vacuum jacket. Since this approach would eliminate the use of aluminized-mylar radiation barriers, it might increase the power required to maintain the cell at its elevated temperature.

To minimize the complexity of the OIOPM, we prefer to use transmission detection rather than fluorescence detection, using post-filtering or an external-cavity laser to narrow the output line of the laser diode. However, fluorescence detection is a viable alternative strategy in case unforeseen problems arise in obtaining the necessary narrow-line light sources. The problems this strategy presents are those of engineering complexity rather than fundamental limits.

### **A3.5 Noise Due to Rocking Motions**

If a magnetometer is deployed on a floating platform, it will be subject to a rocking motion due to waves and currents. This rocking motion may produce two kinds of noise in the magnetic measurements. First, as discussed in Sec. A2.3 above, the magnetic measurements may vary somewhat according to the orientation of the instrument with respect to the earth's magnetic field. This heading error is very low in the OIOPM because of the special design of the optical pumping cycle.

In addition to this heading error, optically pumped magnetometers are also subject to gyroscopic errors, which are proportional to the rotation rate of the platform. As the instrument rocks back and forth, its rotation rate adds to or subtracts from the apparent precession frequency of the optically pumped atoms or nuclei in the ambient magnetic field. Since the apparent intensity of the magnetic field is directly proportional to this measured precession frequency, the rocking motion directly affects the magnetic measurement.

In the most unfavorably geometry, where the platform rotates about an axis parallel to the ambient magnetic field, the gyroscopic error in the magnetic measurement is given by

$$\delta B = \delta\omega / 2\pi\Gamma , \quad (28)$$

where  $\delta\omega$  is the rotation rate of the platform and  $\Gamma$  is the gyromagnetic ratio of the precessing species in cycles per second per unit field. For potassium atoms, the gyromagnetic ratio is approximately  $7 \times 10^9$  hertz per tesla, and the corresponding rocking error is approximately 23 picotesla per radian per second. If the platform rocks with an amplitude of one degree and a period of ten seconds, the magnetic measurements of the OIOPM will vary with an amplitude of approximately 0.25 picotesla.

The OIOPM is 200 times less sensitive to gyroscopic errors than the helium-3 nuclear magnetometer, since the potassium atom has a gyromagnetic ratio 200 times greater than that of the helium-3 nucleus. With a rocking amplitude of one degree and a rocking period of ten seconds, the helium-3 magnetometer would have a gyroscopic error of approximately 50 picotesla.

## A4 Design for a Practical Magnetometer

Our design concept for the OIOPM is based on the results of our engineering analysis, together with our previous research and manufacturing experience with alkali-vapor magnetometers. The OIOPM would consist of a sensor head connected through a flexible cable to an electronics package. Each package would be roughly 5cm (2 inches) in diameter, and 25 cm (10 inches) in length. The entire system would weigh 2 to 5 kg (1 to 2 pounds), and consume 200 to 500 milliwatts of battery power.

The sensor unit would contain the optical-pumping cell, the laser-diode light source, the photodetector, and the three orthogonal coils for the rf and dc applied fields. Based on our fundamental sensitivity analysis, the optical pumping cell would be approximately 2 cm in diameter, and 5 to 10 cm long. The cell would contain no buffer gas, so that the effects of external magnetic fields would be greatly reduced by motional averaging. To establish an optimum density of potassium vapor, electrical resistance heaters would be used to maintain the cell at a temperature close to 330K (60 degrees Celsius). To minimize the required heater power, the optical-pumping cell would be enclosed in an evacuated dewar flask, similar to those used in liquid-helium experiments, with several layers of aluminized mylar to minimize radiative heat transfer.

Surrounding the cell oven would be the three sets of rf/dc field coils. One of these coils would be a simple cylindrical solenoid, coaxial with the optical pumping cell. This solenoid would produce rf and dc fields along the axis of the pump beam. To produce fields orthogonal to the pump beam, the other two coils would consist of a series of straight conductors parallel to the axis of the optical pumping cell. These transverse-field windings would lie on a cylindrical surface coaxial with the cell, and would be placed strategically around the circumference of the cylinder in order to produce a field of sufficient homogeneity within the optical-pumping cell. We have previously designed similar transverse coil arrangements for producing the rf fields in nuclear magnetic resonance.

In addition to the applied-field coils, the sensor unit would include the light source, optics, and photodetector for optical pumping and optical absorption measurements. To minimize the power consumption of the OIOPM, we would use laser diodes, rather than electrodeless discharge lamps, to produce the potassium d1 light for optical pumping. To minimize the complexity of the mechanical design, we would probably use transmission detection, rather than fluorescence detection, to measure the absorption of the pump beam. In this detection scheme, the light from the laser diode would first pass through a collimating lens and a circular polarizer, and then traverse the length of the potassium-vapor cell. The transmitted light would then be focused onto a silicon photodiode which would monitor the total current in the transmitted beam. For efficient transmission detection, we would place the laser diode in an external laser cavity, or pass its output light through a Fabry-Perot interferometer, to produce a spectral linewidth at least as narrow as the absorption band of the potassium vapor.

This design would provide a balance of performance characteristics well suited to the rapidly deployed sensor array. These characteristics would include a sensitivity better than one picotesla per root hertz, long-term drifts and heading errors of approximately 0.1 picotesla, rocking noise less than 25 picotesla per radian per second, and the ability to operate in magnetic-field gradients of several hundred nanotesla per meter. At the same time, this instrument would easily meet the size, weight, and electric-power constraints of the rapidly deployed sensor array.

## A5 References

1. W. Happer, *Rev. Mod. Phys.* **44**, 169 (1972).
2. E.B. Aleksandrov and V.A. Brunevich, "Optically Pumped Magnetometers after Three Decades", *Optical Engineering* **31**, 711 (1992).
3. W. Happer, "Improved Optically Pumped Magnetometers and Gradiometers", Report # STD-R-308, Applied Physics Laboratory, Johns Hopkins University, October, 1979.
4. W.F. Avrin and R.E. Sager, "An Optically Pumped Magnetic Detector with Submilli-gamma Resolution," Final Report, Contract # N00024-85-C-5374, Naval Sea Systems Command, August 1988.
5. W.F. Avrin and R.E. Sager, *IEEE. Trans. Mag.* **25**, 3408 (1989).
6. J.B. Marling, J. Nilsen, L.C. West, and L.L. Wood, *J. Appl. Phys.* **50**, 610 (1992).
7. F. Reif, *Fundamentals of Statistical and Thermal Physics*, McGraw-Hill, Inc., New York, 1965.